

PDF hosted at the Radboud Repository of the Radboud University Nijmegen

The following full text is a publisher's version.

For additional information about this publication click this link.

<http://hdl.handle.net/2066/113919>

Please be advised that this information was generated on 2017-03-14 and may be subject to change.

410g

**SUBMILLIMETER SPECTROSCOPY OF
MOLECULAR COMPLEXES AND IONS**

Erik Zwart

SUBMILLIMETER SPECTROSCOPY OF MOLECULAR COMPLEXES AND IONS



Print: Haveka B.V., Alblasserdam, The Netherlands.

SUBMILLIMETER SPECTROSCOPY OF MOLECULAR COMPLEXES AND IONS

**EEN WETENSCHAPPELIJKE PROEVE OP HET GEBIED VAN
DE NATUURWETENSCHAPPEN**

PROEFSCHRIFT

**TER VERKRIJGING VAN DE GRAAD VAN DOCTOR
AAN DE KATHOLIEKE UNIVERSITEIT TE NIJMEGEN,
VOLGENS BESLUIT VAN HET COLLEGE VAN DECANEN
IN HET OPENBAAR TE VERDEDIGEN
OP DONDERDAG 10 JANUARI 1991,
DES NAMIDDAGS TE 3.30 UUR**

door

HENRICUS JOHANNES MARIA ANTONIUS ZWART

geboren op 1 april 1963
te Helden-Panningen

Promotor : Prof. Dr. J. Reuss
Co-promotores : Dr. W.L. Meerts
: Dr. J.J. ter Meulen

Dankwoord

Op deze plaats wil ik iedereen bedanken die een bijdrage heeft geleverd tot het gereedkomen van dit boekje. Met name zou ik willen bedanken :

- Alle mensen die de laatste paar jaren op de afdeling Molekuul- en Laserfysica hebben gewerkt voor de fijne werksfeer.
- Leo Meerts, Hans ter Meulen en Prof. Reuss, die me begeleid hebben en het onderzoek op belangrijke momenten in de goede richting hebben geleid. O.a. de beslissing om een angstwekkend grote pomp te kopen heeft veel invloed gehad.
- Peter Verhoeve, die me de FIR opstelling heeft leren kennen; bedankt voor de goede samenwerking.
- Marcel Drabbels en Harold Linnartz, die bij enkele experimenten meegewerkt hebben; Marcel bij de experimenten aan ionen en Harold bij de laatste metingen aan complexen.
- Prof. van der Avoird, John van Bladel en Paul Wormer van de Theoretische Chemie afdeling voor de goede samenwerking.
- Paul Uijt de Haag en Johannes Heinze voor de prettige sfeer op de zitkamer en voor hulp bij fysische problemen.
- Annet van der Heijden voor hulp en advies en voor het maken van de meest ingewikkelde tabel uit dit boekje.
- Eugène van Leeuwen die een onmisbare bijdrage heeft geleverd op technisch gebied; ook bedankt voor de hulp bij de nachtelijke metingen met de "bijna ontploffende" magneet.
- John Holtkamp, Frans van Rijn en Cor Sikkens voor hun technische bijdragen.
- Alle dienstverlenende afdelingen van de faculteit.
- Jeroen Oomen voor de laatste Engelscorrecties.
- Martina Havenith, wier aandeel niet alleen beperkt is tot het laten slagen van het dipoolmomentexperiment; haar enthousiasme en steun zijn ook onmisbaar geweest bij de metingen aan complexen.
- Jon Hougen, die me zo vaak heeft verteld dat het water dimeer interessant is en dat ik daar ook aan zou moeten werken, dat ik uiteindelijk de meting geprobeerd heb.
- Laurent Coudert and Jerry Fraser who made a major contribution to this "boekje"; thanks for the great "bitnet-cooperation".
- Tot slot wil ik mijn ouders bedanken die me altijd gesteund hebben.

Contents

1	Introduction	9
1.1	General	9
1.2	The spectrometer	10
1.3	Investigated molecules	13
2	Direct absorption spectroscopy of molecular ions	16
2.1	Introduction	16
2.2	D_2H^+ and H_2D^+	16
2.3	KrH^+ and KrD^+	17
3	Determination of the electric dipole moment of HN_2^+	19
3.1	Abstract	19
3.2	Introduction	19
3.3	Experimental	21
3.4	Results	24
4	The $K_a = 0 \rightarrow 1$ submillimeter rotation-tunneling spectrum of the water dimer	32
4.1	Abstract	32
4.2	Introduction	32
4.3	Experiment and Results	33
5	The submillimeter rotation-tunneling spectrum of the water dimer	38
5.1	Abstract	38
5.2	Introduction	38
5.3	Experimental	40
5.4	Results	41
	5.4.1 ($K_a=0$,lower) \rightarrow ($K_a=1$,upper)	44
	5.4.2 ($K_a=1$.lower) \rightarrow ($K_a=2$,upper)	45
5.5	Analysis	46
5.6	Discussion	51
6	The submillimeter rotation-tunneling spectrum of $(D_2O)_2$	53
6.1	Abstract	53
6.2	Introduction	53
6.3	Experimental	55
6.4	Results	55
6.5	Discussion	58

7	Unassigned bands of $(\text{NH}_3)_2$	64
7.1	Introduction	64
7.2	Results	64
7.3	Discussion	65
8	The submillimeter rotation-tunneling spectrum of Ar-D_2O and Ar-NH_3	69
8.1	Abstract	69
8.2	Introduction	69
8.3	Experiment	70
8.4	Theoretical	71
8.5	Results	77
	8.5.1 Ar- D_2O	77
	8.5.2 Ar- NH_3	79
8.6	Discussion	83
9	Microwave and submillimeter spectroscopy of Ar-NH_3 states correlating with Ar + $\text{NH}_3(j=1, k =1)$	89
9.1	Abstract	89
9.2	Introduction	90
9.3	Experiment	91
9.4	Results	92
9.5	Dynamical model	98
9.6	Determination of the potential energy surface	103
9.7	Discussion	107
9.8	Conclusion	107

Chapter 1

Introduction

1.1 General

Spectroscopy of molecules in the gas phase has been used for a long time to investigate the properties of molecules. Molecules exert motions like a rotation or a vibration at very specific frequencies. These frequencies are reflected in spectra, since the spectra consist of transitions between well defined (e.g. rotational) states. Many properties of molecules can be extracted from their spectra. As a result of the strength of the spectroscopic technique, it is possible to go further than the investigation of single molecules. As an example the reaction of single molecules in the gas phase or the forces that act between two molecules which are very close together can be investigated. This work leads to an understanding on a fundamental level of chemical reactions and the condensation process, respectively. Besides theoretical interest, there are many practical applications. The spectrum of a molecule is its 'fingerprint' and is important in areas as air pollution, combustion processes and interstellar chemistry.

The frequency range of the electromagnetic spectrum which is investigated in this thesis is called the submillimeter or far infrared region. A typical wavelength is 0.5 mm. In this frequency region rotations of molecules and vibrations of weakly bound molecules can be studied. The applied technique is direct absorption of tunable narrowband radiation.

The investigated molecules are ions and complexes. Under normal conditions these species live very short and therefore have to be produced during the experiments. Molecular ions, i.e. charged molecules, turned out to be important in the chemistry of interstellar space. The ions emit radiation in the microwave and submillimeter range which is detected on earth. By producing the ions in a laboratory and by detecting the observed emission transitions in absorption, it is possible to determine which ions are present in interstellar space and what their abundances are. However, it is usually very difficult to produce the ions in amounts large enough to become spectroscopically (i.e. state-sensitively) detectable. We succeeded in doing so in specially designed discharges which are excited in the absorption cell. Another interesting kind of molecule is a complex. Molecular complexes consist of two or more single molecules bound by Van der Waals forces. An example is the complex of two water molecules, $(\text{H}_2\text{O})_2$. At very low temperatures two water molecules can stick together. Because the bond between the water molecules is very weak, very interesting internal motions occur within the complex. By measuring spectra e.g. of the $(\text{H}_2\text{O})_2$ molecule, insight into these internal motions and into the forces which act between two water molecules at a close distance can be gained. Fortunately it is easier to produce complexes than it is to produce ions. One produces a molecular jet by expansion of gas at about one atmosphere into vacuum through a narrow nozzle. During this process cooling takes place that leads

to the formation of complexes. We have measured the absorption of radiation by molecular jets.

1.2 The spectrometer

The submillimeter region can be defined by the boundaries 300 GHz and 3000 GHz (or $10\text{-}100\text{ cm}^{-1}$ or $1000\text{-}100\text{ }\mu\text{m}$). The frequently used term ‘far infrared’ usually defines a frequency region which lies somewhat higher. As a lower boundary 600 GHz can be taken. The upper boundary lies higher than 3000 GHz. Though the term submillimeter is more appropriate to cover the whole frequency range in this thesis, both submillimeter and far infrared will be used. The methods which are used for spectroscopy in the above defined frequency regions have been discussed in several previous theses [1, 2] and here we will only discuss the set up used in the present work.

The spectrometer consists of the far infrared laser sideband spectrometer, recently described by Verhoeve et al. [3]. The first version of this apparatus was built more than 10 years ago by Bicanic et al. [4]. It has been continually improved during the past decade. Fig. 1 shows a scheme of its present form. The principle of the laser sideband system is the following. In the far infrared region no tunable narrowband ($< 0.1\text{ MHz}$) lasers exist at this time. There are however fixed frequency far infrared lasers and tunable microwave sources. By mixing fixed frequency far infrared laser radiation (typically 1000 GHz) with tunable microwave radiation (typically 100 GHz), tunable sum and difference frequencies, sidebands, are generated. The sidebands are applied in spectroscopy.

The far infrared laser is a 4 m long waveguide laser (home-built) filled with a gas at a low pressure, which is pumped by a 100 W CO_2 laser (Apollo 150). Approximately 30 strong (50 mW) far infrared laser oscillations can be obtained. The tunable microwave radiation is supplied by klystrons (Oki and Varian) in the 50-114 GHz range.

The far infrared laser radiation (f_L in Fig. 1) and the microwave klystron radiation (f_K in Fig. 1) are mixed in the open mixer. The laser radiation propagates through free space to the mixer. The microwave radiation is guided by a waveguide. The nonlinear element is a Schottky barrier diode. We use diodes from Farran Technology (SD-018) and from the Semiconductor Device Laboratory of the University of Virginia (1I7). The diode is soldered to a gold pin, which passes through the waveguide. The pin in the waveguide receives the microwave radiation. A 2 mm long antenna in free space, which is placed on the diode chip, acts as an antenna for the far infrared radiation. The antenna pattern is improved by a movable corner reflector. The tunable sidebands ($f_L \pm f_K$ in Fig. 1) are radiated into free space by the antenna.

One of the difficulties of this technique is that the power of the sidebands is approximately 4 orders of magnitude less than that of the laser radiation. The laser radiation is partly reflected at the mixer and the radiation which comes back from the mixer consists only for a small part of sideband radiation. To separate the sidebands from the laser radiation a polarizing interferometer and a monochromator are used. The radiation passes through an absorption chamber and is detected by a 1.5 K Si bolometer (Infrared Laboratories).

The polarizing interferometer [5, 6] is not the one described in Ref. [3]. Here a non-polarizing interferometer, which contains a Mylar beamsplitter, was applied. The beamsplitter of the polarizing interferometer (home-built) is a grid of parallel metal wires of 5

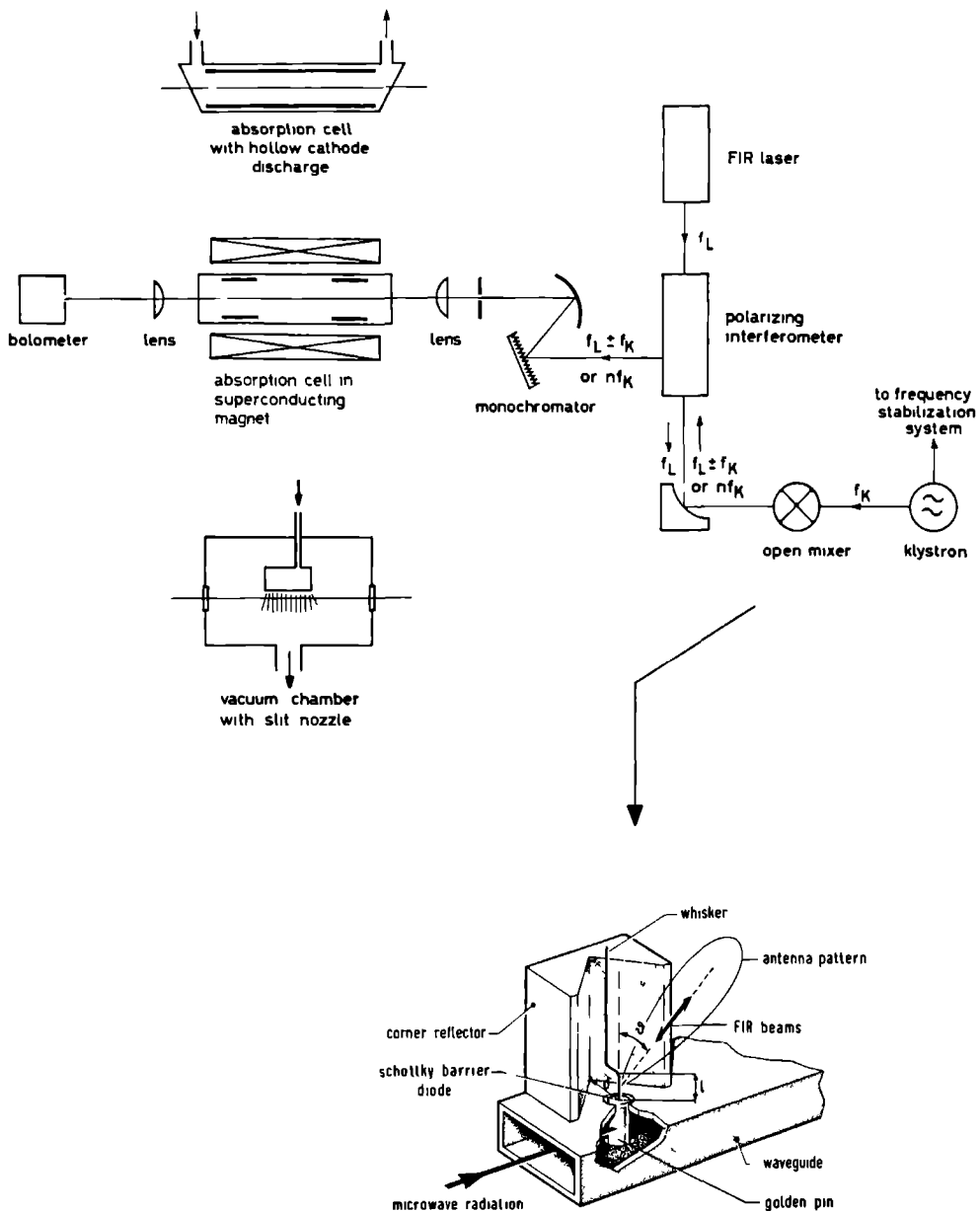


Figure 1 Scheme of the spectrometer

μm diameter at a distance of $25 \mu\text{m}$ (Specac). The polarizing interferometer serves several purposes. The polarization of the laser radiation has to be oriented parallel to the antenna; the sideband radiation should not be reflected back into the laser and has to be deflected; the laser radiation which is reflected at the mixer must be separated from the sidebands. The overall performance of the polarizing interferometer is not better than that of the previous non-polarizing one. In both cases the monochromator is needed to filter out the laser radiation which is still more powerful than the sidebands even after the polarizing interferometer. The major advantage of the new polarizing interferometer is its ease of operation. It operates at all submillimeter frequencies without replacing the beamsplitters and newly aligning the optical system. Another advantage is that the laser radiation can be oriented parallel to the antenna of the mixer. In the old set up the polarization had to be rotated with three extra mirrors. A disadvantage, also connected with the polarization of the radiation, is that in the old set up the polarization of the sidebands was always perpendicular to the grooves of the grating. In the new set up the polarization of the sidebands relative to the grooves depends on the laser line. The grating is, unfortunately, less efficient if the sidebands are polarized parallel to the grooves. Extra mirrors are sometimes used to rotate the polarization of the radiation.

The main part of this thesis consists of measurements done applying the spectrometer for harmonic generation. Harmonic generation of microwaves is an old technique, developed in the fifties by Gordy and coworkers [7]. It is a very convenient way to produce radiation in the low frequency region between 200 and 500 GHz. In our spectrometer the frequency below which harmonic generation and above which laser sideband generation yields better results lies somewhere between 400 and 500 GHz. An advantage of harmonic generation which is true for all frequencies is that the frequency of the harmonics is precisely known since the driving microwave sources are phase-locked to a frequency standard. The frequency uncertainty of the laser sidebands is determined by the frequency uncertainty of the laser, which is approximately 1 MHz at 600 GHz and 2 MHz at 1500 GHz.

In case of harmonic generation the laser is not used. The gold pin in the waveguide again receives the microwave radiation. The harmonics (nf_K in Fig. 1) of the microwave radiation are generated in the Schottky barrier diode and are radiated into free space by the 2 mm long antenna which is placed on top of the diode chip. The diode is the same as that used for laser sideband generation. The harmonics pass the polarizing interferometer and the monochromator and are then detected. The polarizing interferometer is not necessary in these experiments, but it is useful to check the frequency of the radiation.

The monochromator is the frequency selective element. The selection of only one harmonic makes it possible to optimize the whole set up on this particular harmonic. In particular the bias voltage on the diode and the position of the corner reflector influence the radiated harmonic power drastically. The optima are different for different harmonics. In the first measurements a Fabry-Perot (home-built) with meshes of 10 wires/mm (Buckbee-Mears) was used to separate the different harmonics, because the grating (3 grooves/mm, 30° blaze angle) did not operate below 550 GHz. The selection of a harmonic with a Fabry-Perot is, however, rather difficult compared with the selection with a grating. A new grating with 1.33 grooves/mm, 30° blaze angle was purchased from Hyperfine. Later a grating with 0.83 grooves/mm, 30° blaze angle was manufactured in the local workshop. Using these gratings, frequencies below 200 GHz can be reached.

To produce a large harmonic intensity, it is necessary to use as much microwave power as possible. For most experiments our two strongest klystrons were used. These are a 60 GHz Oki klystron (60V10) and a 70 GHz Varian klystron (VRE-2103B8). The powers of the two klystrons are comparable, but difficult to specify quantitatively. The Oki datasheet specifies 200 mW and the Varian datasheet 400 mW as maximum power. However, the klystrons are 25 and 15 years old, respectively, and their performance is expected to be somewhat degraded. The 70 GHz Varian klystron produces enough power to burn a diode contact.

The harmonic is guided by lenses and mirrors to a detector. At first a 1.5 K Si bolometer was used, but later this was replaced by a 4 K InSb hot-electron bolometer (Infrared Laboratories). The InSb bolometer is easier to handle, since it can be operated at 4 K instead of 1.5 K. The final sensitivity of the spectrometer is comparable with both detectors.

Usually a different technique is used to produce harmonics. Instead of the open multiplier which is described here, a multiplier with crossed waveguides is used [7, 8]. An antenna goes through both waveguides and contacts a diode in one of the waveguides. One of the waveguides is relatively wide and through this waveguide the fundamental microwave frequency propagates. The second waveguide is narrower (0.5 mm diameter circular waveguide in. [8]) The harmonics are emitted into this narrow waveguide and they are passed into free space by means of a horn. We were not able to compare the crossed waveguide technique with the technique described in this thesis.

1.3 Investigated molecules

Peter Verhoeve, who was the previous 'promovendus' on the far infrared apparatus, used the spectrometer mainly to study ions with a hollow-cathode discharge. As mentioned above, spectroscopy of ions is partly motivated by the connection with the study of interstellar chemistry. Further ions are often interesting from a theoretical point of view, like H_3O^+ (see [9] and references therein), which shows an inversion motion similar to that of NH_3 . Following this line of work we have tried to detect several more ion transitions. (Chapter 2).

A different experiment on ions is described in Chapter 3. The electric-dipole moment of the molecular ion HN_2^+ was determined by studying the Zeeman effect of several isotopomers of this ion. This technique, which is known from old microwave spectroscopy, is much less accurate than the technique based on the Stark effect. It is, however, impossible to determine the Stark effect for ions, since these will be accelerated in an electric field. The method was first applied to ions by Laughlin et al. [10]. Due to experimental difficulties, two repeated measurements resulted in two different values for the dipole moment of ArH^+ . We have improved the method of Laughlin et al. by employing a superconducting magnet, which produces a high constant field. This work was done together with M. Havenith who also initiated this project.

The major part of this thesis consists of measurements on molecular complexes. Molecular complexes consist of two or more molecules which are weakly bound together. The weak bonding gives us the opportunity to learn more about the forces that act between the two molecules which are close together. Spectroscopy has proved to be an excellent method to study these complexes. Interest in molecular complexes is very strong at the moment and it still seems to be growing. In all frequency regions spectroscopic work is progressing, with

many different methods. The submillimeter or far infrared region is of importance since rotations of complexes and vibrations between the constituents of a complex occur in this region and since excitation of complexes does not lead to dissociation, i.e. destruction. Two different production methods are in use. Complexes are studied either in a static gas cell or in a jet. Static gas cells are used in the group of Krupnov at Gorki together with a submillimeter BWO and photoacoustic detection. Recently $(\text{HF})_2$ has been studied [11]. Further static gas cells are used together with Fourier transform spectrometers. For example in the group of Quack $(\text{HF})_2$ has been observed [12]. The drawback of static gas cells is that often complexes are not formed in sufficient amounts. The molecular jet method is used by many groups and in the far infrared by the group of Saykally in Berkeley. To overcome the small absorption length in the jet, they use a slit nozzle of 4 cm long and 25 μm wide. This slit nozzle expansion is used together with a laser sideband spectrometer. With a jet, many different kinds of complexes can be formed. A disadvantage of a slit of 4 cm long and 25 μm wide (1 mm^2 in total) is the high consumption of gas and the large pumps necessary to keep the background pressure in the vacuum chamber below 0.1 mbar.

For our work we have chosen the same technique that Saykally and coworkers apply. We have constructed a slit nozzle similar to that described in [13]. Three pumps are used in series: two mechanical booster pumps, Edwards EH4200 and EH1200, and a rotary pump, Edwards E1M80. The total pumping speed at 0.1 mbar is approximately 4000 m^3/h . The vacuum chamber is placed directly on top of the largest booster pump. Due to the large wavelength of the radiation vibrations caused by the pump do not disturb experiments. After the first measurements it was realized that several molecular complexes had been investigated below 100 GHz, in the microwave range, or above 500 GHz, by groups with a laser sideband spectrometer in the USA. In the region in between, which can be reached with harmonic generation as discussed above, no spectra of complexes in a beam had been recorded. Interesting new information has been obtained for several complexes.

As an example the water dimer may serve. This complex possesses a well defined equilibrium structure. However, the potential barriers between two equivalent configurations of the water dimer are so low that tunneling splittings occur. From the magnitude of the tunneling splittings it is possible to derive information about the height of the potential barriers. Theory has not yet developed far enough to determine the complete potential energy surface. In Chapters 4, 5 and 6 submillimeter spectra of the water dimer are presented. These spectra yield new information on the tunneling splittings in this complex. Chapter 5 contains a theoretical analysis by L.H. Coudert.

A complex with a difficult spectrum is $(\text{NH}_3)_2$. Attempts have been made to explain the observed microwave and far infrared spectra with the same model as $(\text{H}_2\text{O})_2$ (see [14] and references therein). However, it is not yet certain if this approach is valid. In Chapter 7 additional submillimeter spectra of $(\text{NH}_3)_2$ are presented. Also these spectra do not yield decisive information about the internal motions within this complex.

Complexes of a molecule with an Ar atom form another interesting species. Since the Ar atom has no permanent electric-dipole moment, the bond in such a complex is relatively weak. The molecule can rotate nearly freely within the complex and it probes a large part of the intermolecular potential. Based upon a potential model, the measured transition frequencies can be reproduced by adjusting the potential parameters. This has been successfully applied to Ar-HCl and Ar-HF and work is now in progress on Ar- H_2O and Ar- NH_3 .

Many theoreticians and experimentalists are working on Ar-H₂O and Ar-NH₃ at this moment. In Chapter 8 we present submillimeter spectra of Ar-D₂O and Ar-NH₃. These spectra are explained with the model of nearly free rotation. In Chapter 9 spectra of Ar-NH₃ in which NH₃ inversion is visible are presented. This last chapter includes microwave results from other authors (G.T. Fraser, D.D. Nelson Jr. and W. Klemperer) and an analysis of the potential energy surface by G.T. Fraser.

References

- [1] K.B. Laughlin, thesis, University of California, Berkeley (1988).
- [2] P. Verhoeve, thesis, University of Nijmegen (1989).
- [3] P. Verhoeve, E. Zwart, M. Versluis, M. Drabbels, J.J. ter Meulen, W.L. Meerts, A. Dymanus and D.B. McLay, *Rev. Sci. Instrum.* 61, 1612 (1990).
- [4] D.D. Bicanic, B.F.J. Zuidberg and A. Dymanus, *Appl. Phys. Lett.* 32, 367 (1978).
- [5] D.H. Martin and E. Puplett, *Infrared Phys.* 10, 105 (1970).
- [6] J. Farhoomand, G.A. Blake, M.A. Frerking and H.M. Pickett, *J. Appl. Phys.* 57, 1763 (1984).
- [7] O.R. Gilliam, C.M. Johnson and W. Gordy, *Phys. Rev.* 78, 140 (1950).
- [8] P. Helminger, J.K. Messner and F.C. de Lucia, *Appl. Phys. Lett.* 42, 309 (1983).
- [9] P. Verhoeve, M. Versluis, J.J. ter Meulen, W.L. Meerts and A. Dymanus, *Chem. Phys. Lett.* 161, 195 (1989).
- [10] K.B. Laughlin, G.A. Blake, R.C. Cohen and R.J. Saykally, *J. Chem. Phys.* 90, 1358 (1989).
- [11] S.P. Belov, E.N. Karyakin, I.N. Kozin, A.F. Krupnov, O.L. Polyansky, M.Yu. Tretyakov, N.F. Zobov, R.D. Suenram and W.J. Lafferty, *J. Mol. Spectrosc.* 141, 204 (1990).
- [12] K. von Puttkamer, M. Quack and M.A. Suhm, *Mol. Phys.* 65, 1025 (1988).
- [13] K.L. Busarow, G.A. Blake, K.B. Laughlin, R.C. Cohen, Y.T. Lee and R.J. Saykally, *J. Chem. Phys.* 89, 1268 (1988).
- [14] M. Havenith, thesis, University of Bonn (1990).

Chapter 2

Direct absorption spectroscopy of molecular ions

2.1 Introduction

Direct absorption spectroscopy of molecular ions in the submillimeter or far infrared frequency regions is usually performed with the use of a hollow-cathode discharge cell [1] or a cell with a magnetically extended negative glow [2]. In both cases, the larger part of the discharge consists of a negative glow, which is an ion-rich discharge region. In Nijmegen traditionally a hollow-cathode discharge cell has been used. N_2H^+ [1, 3], HCO^- [1], CO^+ [1], OH^+ [4], OD^+ [5], NH^+ [6] and H_3O^+ [7, 8] were investigated.

Following this line of research we have performed measurements on D_2H^+ , H_2D^+ , KrH^- and KrD^+ . The experimental details of the discharge cell can be found in the above mentioned papers. For D_2H^+ and H_2D^+ we used a 1:1 mixture of H_2 and D_2 and for KrH^+ (KrD^+) a 1:1 mixture of Kr and H_2 (D_2). In both cases the cathode was cooled with liquid nitrogen.

2.2 D_2H^+ and H_2D^+

H_3^+ was first spectroscopically detected by Oka [9] in the infrared region. Because of the symmetry of H_3^+ , the ion has no permanent electric-dipole moment. As a result pure-rotational transitions are electric-dipole forbidden and H_3^+ cannot be detected in interstellar space from submillimeter emission.

The isotopomers D_2H^+ and H_2D^+ possess, however, a permanent electric-dipole moment. A submillimeter transition of H_2D^+ has been observed by Bogey et al. [10] and by Warner et al. [11] and a microwave transition of the same ion by Saito et al. [12]. The constants of D_2H^+ and H_2D^+ obtained from infrared spectroscopy (see [13] and references therein) did not result in accurate predictions of far infrared transitions. The ab initio calculations of Miller et al. [14] yielded approximately the same uncertainty in the predictions, i.e. approximately 1 GHz. Recently, Kozin et al. [15] made new fits of the ν_1 fundamental of both D_2H^+ and H_2D^+ . The use of a Padé model and the correction of several earlier assignment errors provided a better prediction of far infrared transitions. The results for D_2H^+ could be further improved by Polyansky et al. [16] by reexamining also the ν_2 and ν_3 bands.

We tried to detect several far infrared transitions at a time when the latest results of Polyansky et al. were not yet available. Due to the weakness of the lines and the uncertainty of the frequency predictions we were able to observe only few transitions. The observed transition frequencies are listed in Table 1. Evenson et al. turned out to be working on the same problem, a fact which we were not aware of at the time of our first measurements. The relatively strong D_2H^+ transition at 1476 GHz, reported by Evenson in [16], was detected

Table 1. Observed transitions. All frequencies are in GHz.

Ion	Transition	Frequency
H_2D^+	$0_{00} \rightarrow 1_{01}^{\text{a})}$	1370.086(2)
D_2H^+	$2_{11} \rightarrow 2_{20}^{\text{a})}$	1370.054(2)
D_2H^+	$0_{00} \rightarrow 1_{11}$	1476.606(2)
KrH^+	$J=0 \rightarrow 1$	494.5143(10)
KrH^+	$J=2 \rightarrow 3$	1482.464(2)
KrD^+	$J=1 \rightarrow 2$	503.0203(10)

^{a)} First observed by Evenson et al. [14]

independently in our lab. The two transitions at 1370 GHz were first observed by Evenson et al. and were published in Ref. [14]. We found out that the frequencies of [14] are approximately 60 MHz too high. In Ref. [16] a corrected value for the D_2H^+ line was then reported.

2.3 KrH^+ and KrD^+

The ion KrH^+ is an interesting candidate for electric-dipole moment determination [17, 18]. A value of 1.944 D was determined from theoretical calculations of Rosmus and coworkers [19]. To determine the production efficiency we have tried to detect this ion in the hollow-cathode discharge. The transition frequencies of both KrH^+ and KrD^+ can be very accurately calculated with the Dunham coefficients obtained from infrared emission work of Johns [20] and microwave work of Warner et al. [21]. The observed frequencies are listed in Table 1. The measured frequencies agreed within 1 or 2 MHz with the calculated ones.

The KrH^+ $J=2 \rightarrow 3$ transition at 1482 GHz is very strong, even stronger than transitions of the well known ‘strong absorbers’ N_2H^+ and HCO^+ . The KrH^+ $J=0 \rightarrow 1$ transition is weaker. Assuming Doppler broadening and a rotational temperature of 150 K, the calculated ratio of the peak absorptions at 1500 and 500 GHz, respectively, amounts to approximately 5.

Regarding the strength of the lines and the fact that it is possible to detect KrH^+ and KrD^+ with harmonic generation around 500 GHz, KrH^+ is a good candidate for a determination of its electric-dipole moment.

References

- [1] F.C. van den Heuvel and A. Dymanus, Chem. Phys. Lett. 92, 219 (1982).
- [2] F.C. de Lucia, E. Herbst, G.M. Plummer and G.A. Blake, J. Chem. Phys. 78, 2312 (1983).

- [3] P. Verhoeve, E. Zwart, M. Versluis, M. Drabbels, J.J. ter Meulen, W.L. Meerts, A. Dymanus and D.B. McLay, *Rev. Sci. Instrum.* 61, 1612 (1990).
- [4] J.P. Bekooy, P. Verhoeve, W.L. Meerts and A. Dymanus, *J. Chem. Phys.* 82, 3868 (1985).
- [5] P. Verhoeve, J.P. Bekooy, W.L. Meerts, J.J. ter Meulen and A. Dymanus, *Chem. Phys. Lett.* 125, 286 (1986).
- [6] P. Verhoeve, J.J. ter Meulen, W.L. Meerts and A. Dymanus, *Chem. Phys. Lett.* 132, 213 (1986).
- [7] P. Verhoeve, J.J. ter Meulen, W.L. Meerts and A. Dymanus, *Chem. Phys. Lett.* 143, 501 (1988).
- [8] P. Verhoeve, M. Versluis, J.J. ter Meulen, W.L. Meerts and A. Dymanus, *Chem. Phys. Lett.* 161, 195 (1989).
- [9] T. Oka, *Phys. Rev. Lett.* 45, 531 (1980).
- [10] M. Bogey, C. Demuyne, J.L. Destombes and B. Lemoine, *Astron. Astrophys.* 137, L15 (1984).
- [11] H.E. Warner, W.T. Connor, R.H. Petrmichl and R.C. Woods, *J. Chem. Phys.* 81, 2514 (1984).
- [12] S. Saito, K. Kawaguchi and E. Hirota, *J. Chem. Phys.* 82, 45 (1985).
- [13] S.C. Foster, A.R.W. McKellar and J.K.G. Watson, *J. Chem. Phys.* 85, 664 (1986).
- [14] S. Miller, J. Tennyson and B.T. Sutcliffe, *Mol. Phys.* 66, 429 (1989).
- [15] I.N. Kozin, O.L. Polyansky and N.F. Zobov, *J. Mol. Spectrosc.* 128, 126 (1988).
- [16] O.L. Polyansky and A.R.W. McKellar, *J. Chem. Phys.* 92, 4039 (1990).
- [17] K.B. Laughlin, G.A. Blake, R.C. Cohen and R.J. Saykally, *J. Chem. Phys.* 90, 1358 (1989).
- [18] M. Havenith, E. Zwart, W.L. Meerts and J.J. ter Meulen, accepted for publication in *J. Chem. Phys.*
- [19] P. Rosmus and E.A. Reinsch, *Z. Naturforsch. Teil A* 35, 1066 (1980).
- [20] J.W.C. Johns, *J. Mol. Spectrosc.* 106, 124 (1984).
- [21] H.E. Warner, W.T. Connor and R.C. Woods, *J. Chem. Phys.* 81, 5413 (1984).

Chapter 3

Determination of the electric dipole moment of HN_2^+

M. Havenith

Institut für Angewandte Physik, Wegelerstr.8,
5300 Bonn 1, West Germany

E. Zwart, W. Leo Meerts and J.J. ter Meulen

Physics Laboratory, University of Nijmegen, Toernooiveld,
6525 ED Nijmegen, The Netherlands

3.1 Abstract

The electric dipole moment of the linear molecular ion HN_2^+ was determined by measuring the isotope shifts of the rotational g factors of different isotopic species. We studied the Zeeman effect of the $R(6)$ rotational transition at 650 GHz. In a magnetic field of 5.4 T the rotational transition split into two components, separated by 2.2-2.5 MHz. The g_R factors were determined for $\text{H}^{14}\text{N}^{14}\text{N}^+$, $\text{H}^{14}\text{N}^{15}\text{N}^+$ and $\text{H}^{15}\text{N}^{14}\text{N}^+$. The dipole moment for $\text{H}^{14}\text{N}^{14}\text{N}^+$ was determined as (3.4 ± 0.2) D, which is in excellent agreement with the theoretical value. The transitions were observed by direct absorption spectroscopy with a tunable FIR sideband spectrometer. The ions were generated in a modified anomalous discharge placed in a superconducting magnet.

3.2 Introduction

The permanent electric dipole moment of a molecule is a fundamental quantity reflecting its electronic structure. Knowledge of the electric dipole moment is essential for the calculation of rotational absorption intensities and radiative lifetimes. For neutral molecules Stark spectroscopy allows the determination of the electric dipole moment. Such measurements cannot be made for ions, because the electric field accelerates the ions towards the wall of the discharge tube. The lack of experimental data is confronted with a high number of theoretical data obtained by ab initio calculations.

The first direct measurement of an electric dipole moment for an ion was carried out by Laughlin et al. for ArH^+ . The dipole moment was determined from the measurement of the rotational Zeeman effect by FIR laser spectroscopy. In subsequent measurements [1, 2, 3] the dipole moment of ArH^+ was determined as (1.4 ± 0.4) D, (1.6 ± 0.4) D and (3.0 ± 0.6) D, whereas a theoretical value of 2.2 D was obtained by Rosmus [4]. Their

experiments were based on theoretical considerations by Townes et al. [5], who showed that the knowledge of the experimentally determinable rotational magnetic g_R factor for two different isotopic species allows the calculation of the electric dipole moment. The dipole moment was calculated with the following expression

$$\mu = -\frac{eh}{16\pi^2 M_p \Delta z} (g'_R/B' - g_R/B) + 1/2(Qe\Delta z) \quad (3.1)$$

where μ , g_R , B , Δz are the electric dipole moment, the rotational g factor, the rotational constant of the isotopic species (a), and the shift in the center of mass upon isotopic substitution, respectively. The primed quantities are the corresponding quantities of the isotopically substituted species (b). Q is the net charge of the molecule. This expression was first applied to determine the sign of the electric dipole moment of CO [6], which cannot be obtained by Stark spectroscopy.

Because the electric dipole moment is proportional to the difference between two nearly equal quantities g'_R/B' and g_R/B it is necessary to measure these ratios with a very high precision in order to obtain an acceptable error for μ . The result is quite sensitive even to small systematic errors. This was discussed after the third measurement by Laughlin et al. [3], where ‘systematic errors present in the previous data have been discovered and eliminated’.

The application of Eq. 1 is based on the following assumptions

1. The structure of the molecule remains constant upon isotopic substitution.
2. The validity of first order perturbation theory.

The first assumption implies that only the distance between the center of mass and each atom is changed, while the distance between the atoms is kept constant. This is generally not the case, mainly due to the effects of the zero point vibrations, which are different for distinct isotopic species. It is possible to correct for this by extrapolating all measured rotational factors $g_R(r')$ to a common equilibrium value $g_R(r_e)$ for all isotopic species (r' : value of r for $v=0$). This was discussed in detail in Ref. [3], where various methods for an extrapolation of $g_R(r)$ have been proposed. For comparison the dipole moment was calculated from

1. ground state g factors without any extrapolation, yielding 2.85 D ;
2. extrapolated equilibrium g factors based on the analogy with HF using a Dunham expansion, which resulted in a dipole moment of 3.35 D ;
3. extrapolation using a vibrationally corrected g_R factor, calculated by a method developed by Gruebele et al. [7], where the vibrational correction is determined from a fit of high resolution experimental data to a potential surface, yielding a dipole moment of 2.95 D.

Another ab initio study of Geertsen and Scuseria [8] presented more theoretical evidence supporting a dipole moment of 2.1 D. They pointed out that the use of a Dunham expression leads in general to unsatisfactorily large errors. They believe that using a Dunham expansion

can be the source of discrepancy between theoretical and experimental dipole moments. The lack of experimental vibrational corrections to the g factors is also considered by Laughlin et al. as an uncertainty in their data.

Our experimental setup is based on a FIR laser sideband spectrometer equipped for Zeeman measurements. The main features of the instrument and analysis are

1. The incorporation of a superconducting magnet, which allowed the measurements in high magnetic fields. For this purpose a modified discharge cell suitable for measurements in magnetic fields of 5 Tesla was developed.
2. The measurements were carried out at a fixed magnetic field. The consequences are discussed in the experimental section.
3. The lines were fitted to a Voigt instead of a Lorentzian line profile. It will be shown that this is essential in the analysis of the present data.

As long as only g_R factors for $v=0$ can be determined, it is important to restrict the isotopic substitution to the heavy nucleus. Since in the present work only the N atoms were substituted, the change in the reduced mass and hence the change of the zero point vibration is negligible. Therefore there is no need to extrapolate the rotational g factors for HN_2^+ .

In this work the first determination of the dipole moment of the astrophysically important ion HN_2^+ is reported. The ion was first observed in interstellar space [9] and later in the laboratory, in the microwave [10], infrared [11] and in the FIR [12] region. HN_2^+ was found to occur in a large number of interstellar sources, where the wide distribution of HN_2^+ supported the ion-molecule theory of interstellar chemistry. Molecular abundances in radioastronomy are determined from rotational emission intensities. Therefore an experimental determination of the electric dipole moment with high accuracy would allow a test of the high precision ab initio result obtained by Botschwina [13] as well as furthering the knowledge of interstellar cloud chemistry.

3.3 Experimental

Because the electric dipole moment μ is proportional to the difference between two nearly equal quantities g'_R/B' and g_R/B , an error of 1% in g_R will result in an error of 10% in μ for HN_2^+ . Whereas the rotational constants B and B' are normally well known from microwave measurements, g_R and g'_R have to be measured. In order to determine g_R the Zeeman splittings of pure rotational transitions in high magnetic fields were measured. According to the expression $E = g_R \beta_I M_J H$ (H : magnetic field, β_I : nuclear magneton), which describes the Zeeman energy for a linear $^1\Sigma$ molecule, pure rotational transitions split in a magnetic field, perpendicular to the polarisation of the laser, as $\nu = \nu_0 \pm \beta_I g_R H$, where ν_0 is the transition frequency for zero magnetic field and the + or - signs correspond to allowed $\Delta M = \pm 1$ transitions, respectively. This means that two separate transitions can be observed, split by $\Delta\nu = 2g_R \beta_I H$. The accuracy of the frequency and the magnetic field contribute equally to the final uncertainty of g_R . If measurements for the two isotopically

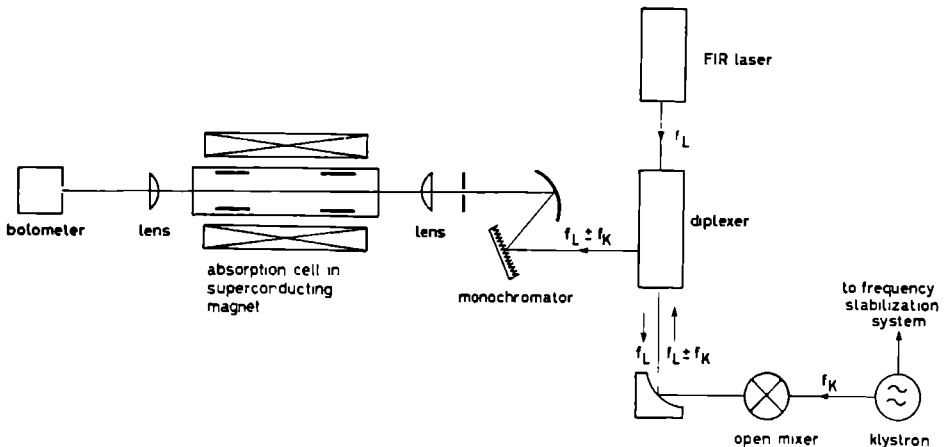


Figure 1. Experimental setup.

substituted species are made in the same magnetic field, Eq. 1 can be modified to

$$\mu = -\frac{eh}{16\pi^2 M_p \Delta z 2\beta_I H} (\Delta\nu'/B' - \Delta\nu/B) + 1/2(Qe\Delta z) \quad (3.2)$$

with $\Delta\nu$ and $\Delta\nu'$ being the Zeeman splittings of the two species.

The accuracy of the magnetic field measurement in our experiment was limited to 0.1% by the homogeneity of the magnetic field. The contribution of this error to the determination of μ was negligible compared with other errors. A superconducting magnet which allowed separate measurements at a constant magnetic field was chosen to avoid measurements at different magnetic fields, which would require very precise absolute magnetic field measurements for each magnetic field. The superconducting magnet had the advantage of providing a large magnetic field combined with a high field stability (fluctuating less than 0.05%). The uncertainty in the frequency determination completely dominated the error in μ .

The lines were recorded in the far infrared (FIR), where the linewidth, determined by Doppler and pressure broadening, was sufficiently small. A low pressure (less than 100 mT) in the ion generating gas discharge was chosen in order to suppress additional pressure broadening. The resulting linewidth was 2.6 MHz (FWHM). The spectra were taken with the tunable far infrared spectrometer in Nijmegen, which will be described in detail elsewhere [14]. The overall setup is displayed in Fig. 1. The tunable FIR radiation was generated by mixing tunable microwaves with a CO_2 pumped FIR laser on a Schottky diode. The laser line used in the course of the experiment was the 716.1568 GHz line of formic acid (HCOOH). The spectra were recorded with frequency modulation of the microwave source (klystrons) and lock-in detection at $2f$ with a 1.5 K Si bolometer.

The ions were observed with the use of a liquid nitrogen cooled discharge cell with a mixture of H_2 and N_2 . The diameter of the discharge cell was 2.6 cm, adapted to the

discharge tube

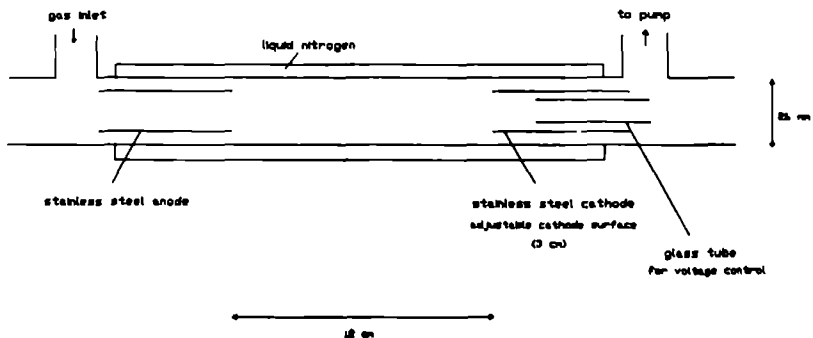


Figure 2. Modified discharge for measurements in high magnetic field.

diameter of the magnet. In order to achieve a high accuracy in the frequency measurement, a production method with a high signal to noise ratio at low pressures was required. This could be accomplished by using an anomalous discharge. We used a setup similar to the one described by de Lucia et al. [15], except that ours was modified for operation in high magnetic fields. De Lucia et al. applied a magnetic field of 300-400 G to extend the negative glow over the entire length of the discharge tube, thus increasing the ion density by two orders of magnitude. However, they found that the signal strength decreased after an optimum magnetic field of 300-400 G towards higher magnetic fields. This observation was reproduced in the present experiment. Furthermore, it was found that the decrease of the signal is accompanied by a decrease of the discharge voltage. For sufficiently high magnetic fields the discharge voltage became too low to maintain a negative glow. Since for an anomalous discharge the current is proportional to the voltage, the maximum current for which an anomalous discharge could be observed decreased with increasing magnetic field. In order to allow measurements at high magnetic fields (5.5 T) the superconducting magnet provided the field for the negative glow extension as well as for the Zeeman spectroscopy – we used a modified cathode design, shown in Fig. 2. The adjustable cathode surface allowed the discharge voltage to be controlled and hence kept large enough at higher magnetic fields. This technique was first applied by Bohle et al. [16] at higher pressures (ca. 2 Torr), where a special cathode design was indispensable. In the present work, the cathode surface was altered by sliding a glass tube inside the cathode, as can be seen in Fig. 2. Maximum signal to noise ratios were achieved with a uncovered cathode length of about 3 cm, which yielded a discharge current of 4 mA at a voltage of 1.2 kV.

Signals of the isotopic species $\text{H}^{14}\text{N}^{15}\text{N}^+$ and $\text{H}^{15}\text{N}^{14}\text{N}^+$ were generated with a mixture of equal amounts of $^{14}\text{N}^{14}\text{N}$ and $^{15}\text{N}^{15}\text{N}$. With this mixture, all four species $\text{H}^{14}\text{N}^{15}\text{N}^+$,

Table 1. Zero field transition frequencies for the $R(6)$ transitions of HN_2^+ and Zeeman splittings at 5.444 T of the different isotopic species.

	Zero field frequency	Zeeman splitting
$\text{H}^{14}\text{N}^{15}\text{N}^+$	631.735 GHz	2562(10) kHz
$\text{H}^{15}\text{N}^{14}\text{N}^+$	638.327 GHz	2203(10) kHz
$\text{H}^{14}\text{N}^{14}\text{N}^+$	652.095 GHz	2434(20) kHz

$\text{H}^{15}\text{N}^{14}\text{N}^+$, $\text{H}^{14}\text{N}^{14}\text{N}^+$ and $\text{H}^{15}\text{N}^{15}\text{N}^+$ were produced in equal amounts. This indicates that N_2 is completely dissociated in an anomalous discharge before recombination occurs. For the production of $\text{H}^{14}\text{N}^{14}\text{N}^+$ a mixture of H_2 and $^{14}\text{N}^{14}\text{N}$ was used.

3.4 Results

The Zeeman splittings of the $R(6)$ transitions of the three isotopic species $\text{H}^{14}\text{N}^{15}\text{N}^+$, $\text{H}^{15}\text{N}^{14}\text{N}^+$ and $\text{H}^{14}\text{N}^{14}\text{N}^+$ were recorded in a magnetic field of $B = 5.444$ T. The zero field transitions were found within 20 MHz of the frequencies predicted by the constants obtained by previous measurements from Szanto et al. [17] and Sastry et al. [18]. The zero field transitions are given in Table 1. The measured rotational transitions split by the Zeeman effect are shown in Figs. 3-5. The spectra were digitized and a curve fitting with approximately 170 points per spectrum was carried out. Each Zeeman component was fitted to a Voigt profile determined by four parameters: the height, the transition frequency and the two widths of the Lorentzian and the Gaussian part, respectively. The linewidth was assumed to be the same for both Zeeman components of the same isotopic species, whereas the height and the transition frequencies of the two components were fitted independently. The intensity ratio of the two components is determined by the ratio of the right to left handed circularly polarized component of the incident radiation. This ratio can differ from 1, due to the various optical components in the spectrometer. The baseline was fitted to a first degree polynomial. In total we fitted 8 parameters. The result of the curve fits is shown in Figs. 3-5. If 80 instead of 170 data points were used the resulting Zeeman splitting changed by less than 5 kHz. The results from two successive scans of the same isotopic species deviated by less than 5 kHz. Based on these considerations we estimate that the frequency precisions in the splittings of $\text{H}^{14}\text{N}^{15}\text{N}^+$ and $\text{H}^{15}\text{N}^{14}\text{N}^+$ were 10 kHz. The residuals (observed minus calculated line profiles) for all three isotopic species are given in Figs. 6-8.

The scan of the $\text{H}^{14}\text{N}^{14}\text{N}^-$ spectrum showed a considerable, but reproducible baseline offset (see Fig. 6), which resulted in a least-square deviation four times larger than that of the other two isotopic species. This baseline offset is limited to a small part of the scan and is probably caused by fluctuations of the microwave power. A second fit, where this part of the scan was neglected, was performed (see Figs. 9 and 10). The Zeeman splittings obtained for the different fits changed by up to 20 kHz. Hence the overall error in $\Delta\nu$ for

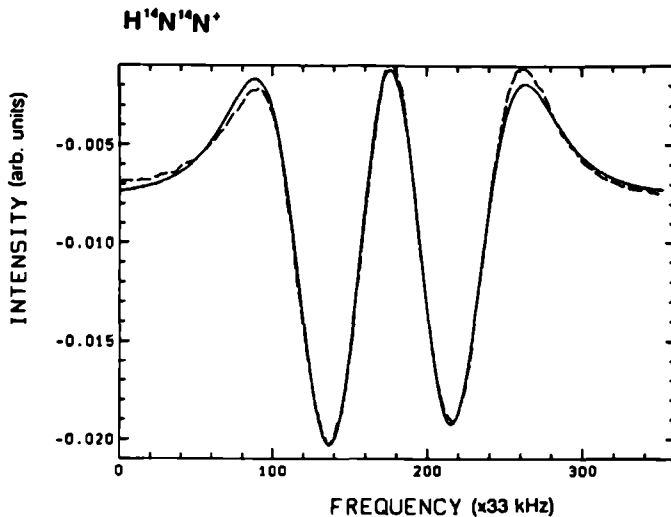


Figure 3. Experimental (dotted) and fitted (solid) line profile for H¹⁴N¹⁴N⁺, showing the Zeeman splitting at 5.444 T.

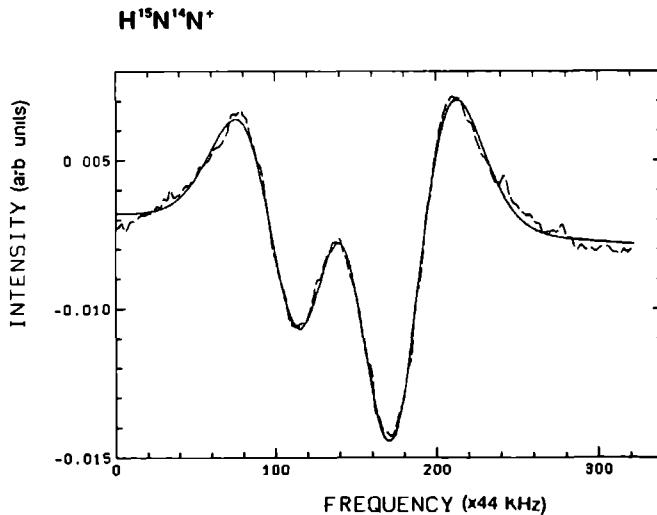


Figure 4. Experimental (dotted) and fitted (solid) line profile for H¹⁵N¹⁴N⁺, showing the Zeeman splitting at 5.444 T.

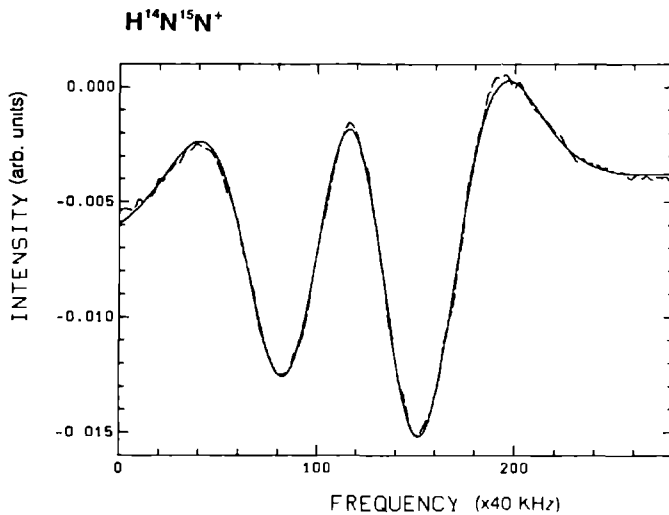


Figure 5. Experimental (dotted) and fitted (solid) line profile for $H^{14}N^{15}N^+$, showing the Zeeman splitting at 5.444 T.

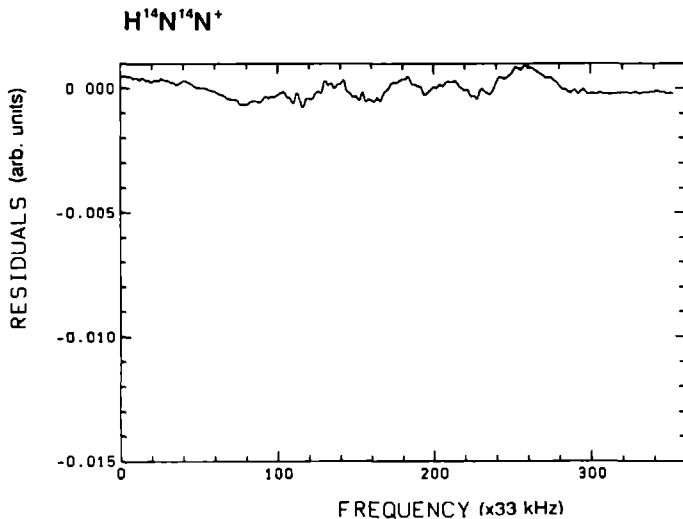


Figure 6. Residual (experimental minus fitted line profile) for $H^{14}N^{14}N^+$ corresponding to Fig. 3.

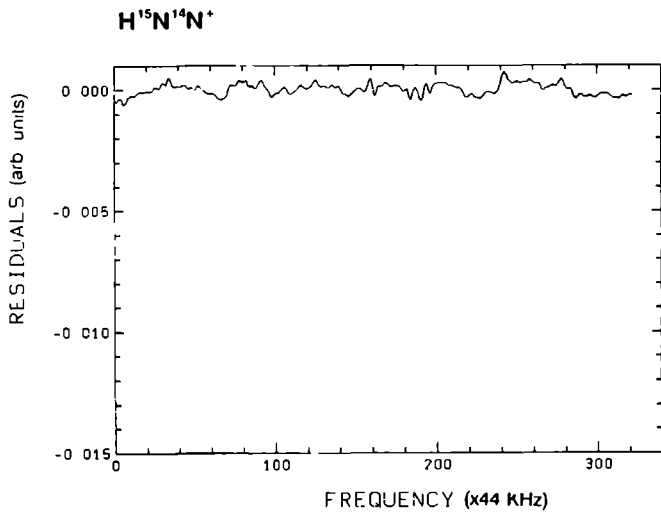


Figure 7. Residual for H¹⁵N¹⁴N⁺ corresponding to Fig. 4.

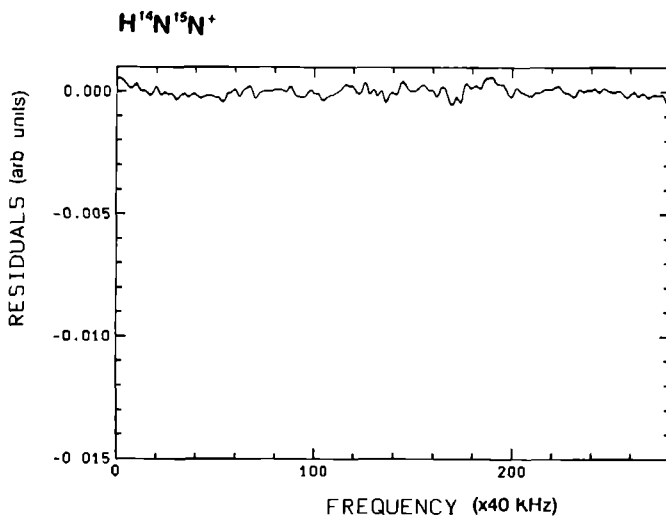


Figure 8. Residual for H¹⁴N¹⁵N⁺ corresponding to Fig. 5.

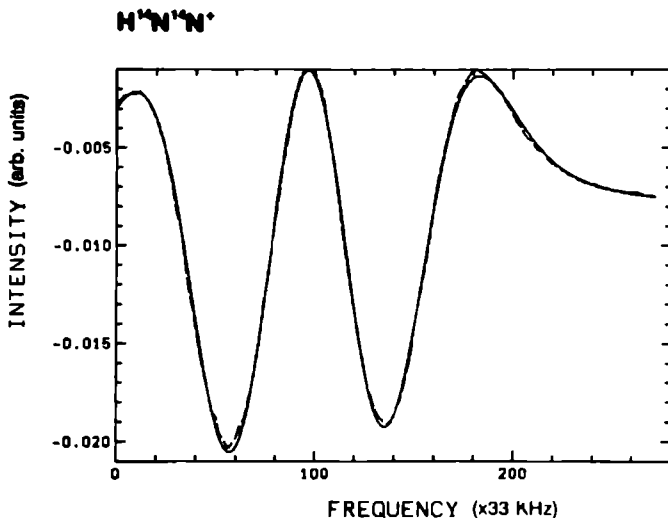


Figure 9. Experimental and fitted line profile for $\text{H}^{14}\text{N}^{14}\text{N}^+$, leaving out the parts affected by a base line shift.

$\text{H}^{14}\text{N}^{14}\text{N}^+$ was assumed to be 20 kHz. For the determination of the electric dipole moment, the Zeeman splitting was used as obtained from the second fit (Fig. 9).

The final Zeeman splittings for all isotopomers are listed in Table 1. Using Eq. 2 the dipole moments of the different isotopic species for all data sets were calculated. The rotational constant B as well as the equilibrium geometry were taken from Ref. [17]. The uncertainties in these numbers can be neglected compared with the estimated frequency errors. The results are given in Table 2. The resulting dipole moment changed by 0.4 D if a curve fitting with a Gaussian profile instead of a Voigt profile was performed (with a Lorentzian profile by up to 1.0 D). Because the pressure broadening contributed 1/3 of the overall linewidth, the application of the Gaussian profile resulted in a least-square deviation, which was twice that obtained with a Voigt profile. This showed, that the use of a Voigt profile is essential at the level of accuracy required in our work.

Combining the rotational g_R factors of two isotopic species the dipole moment of both isotopic species in the center of mass can be found. The difference between the dipole moments of the isotopomers is given by the shift in the center of mass multiplied by the net charge of the ion, which gives the dipole moment of all isotopic species,

$$\mu - \mu' = eQ\Delta z, \quad (3.3)$$

where Q is the net charge and Δz the shift of the center of mass. Hence three different values for each isotopic species can be derived.

If we compare the dipole moments given in Table 2, it can be seen that they agree very well within their estimated uncertainties. The weighted mean value for the electric dipole

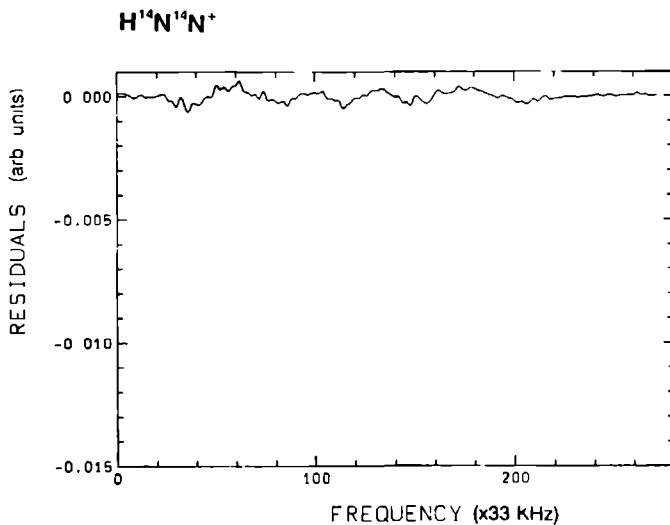


Figure 10. Residual for $\text{H}^{14}\text{N}^{14}\text{N}^+$ corresponding to Fig. 9.

Table 2. Dipole moments (in Debye units) derived from Zeeman splittings for different pairs of isotopic species.

	$\text{H}^{14}\text{N}^{15}\text{N}^+$	$\text{H}^{15}\text{N}^{14}\text{N}^+$	$\text{H}^{14}\text{N}^{14}\text{N}^+$
$\text{H}^{15}\text{N}^{14}\text{N}^+$ and $\text{H}^{14}\text{N}^{15}\text{N}^+$	3.46(15)	3.29(15)	3.37(15)
$\text{H}^{14}\text{N}^{14}\text{N}^+$ and $\text{H}^{14}\text{N}^{15}\text{N}^+$	3.3(6)	3.2(6)	3.2(6)
$\text{H}^{14}\text{N}^{14}\text{N}^+$ and $\text{H}^{15}\text{N}^{14}\text{N}^+$	3.6(4)	3.5(4)	3.5(4)

moment of $\text{H}^{14}\text{N}^{14}\text{N}^+$ (3.4 ± 0.2) D is in excellent agreement with the theoretical value obtained by Botschwina et al. (3.37 D) [13]. The reliability of our data is supported by the fact that dipole moments determined in independent measurements agree with each other. This confirms the assumption of Eq. 2 for the determination of the electric dipole moment in case of a restricted isotopic substitution (only the N atoms were substituted). In this context it would be interesting to compare these results with ab initio calculations of the functions $g_R(r)$, which are not yet available.

Acknowledgement

The authors wish to express their gratitude to Mr. E. van Leeuwen and Mr. J. Holtkamp for excellent technical assistance. This work has profited very much from helpful advice by Dr. W. Bohle. We would also like to thank Prof. W. Urban and Prof. J. Reuss for their support. This work has been supported by the Dutch Organisation for Scientific Research (FOM/ZWO) and by the Deutsche Forschungsgemeinschaft through Sonderforschungsbereich 334.

References

- [1] K.B. Laughlin, G.A. Blake, R.C. Cohen, D.C. Hovde and R.J. Saykally, *Phys. Rev. Lett.* 58, 996 (1987).
- [2] K.B. Laughlin, G.A. Blake, R.C. Cohen, D.C. Hovde and R.J. Saykally, *Trans. R. Soc. London A* 324, 109 (1988).
- [3] K.B. Laughlin, G.A. Blake, R.C. Cohen and R.J. Saykally, *J. Chem. Phys.* 90, 1358 (1989).
- [4] P. Rosmus, *Theor. Chim. Acta* 51, 359 (1979).
- [5] C.H. Townes, G.C. Dousmanis, R.L. White and R.F. Schwarz, *Discuss. Faraday Soc.* 19, 56 (1955).
- [6] B. Rosenblum, A.H. Nethercot Jr. and C.H. Townes, *Phys. Rev.* 109, 400 (1958).
- [7] M. Gruebele, E. Keim, A. Stein and R.J. Saykally, *J. Mol. Spectrosc.* 131, 343 (1988).
- [8] J. Geertson and G.E. Scuseria, *J. Chem. Phys.* 90, 6486 (1989).
- [9] B.E. Turner, *Astrophys. J.* 193, L83 (1974).
- [10] R.J. Saykally, T.A. Dixon, T.G. Anderson, P.G. Szanto and R.C. Woods, *Astrophys. J.* 205, L101 (1976).
- [11] C.S. Gudemann, M.H. Begemann, J. Pfaff and R.J. Saykally, *J. Chem. Phys.* 78, 5837 (1983).
- [12] F.C. van den Heuvel and A. Dymanus, *Chem. Phys. Lett.* 92, 219 (1982).

- [13] P. Botschwina, Chem. Phys. Lett. 107, 535 (1984).
- [14] P. Verhoeve, E. Zwart, M. Versluis, M. Drabbels, J.J. ter Meulen, W. Leo Meerts, A. Dymanus and D.B. McLay, Rev. Sci. Instrum. 61, 1612 (1990).
- [15] F.C. De Lucia, E. Herbst, G. Plummer and G. Blake, J. Chem. Phys. 78, 2312 (1983).
- [16] W. Bohle, J. Werner, D. Zeitz, A. Hinz and W. Urban, Mol. Phys. 58, 85 (1986).
- [17] G. Szanto, T.G. Anderson, R.J. Saykally, N.D. Piltch, T.A. Dixon and R.C. Woods, J. Chem. Phys. 75, 4261 (1981).
- [18] K.V.L.N. Sastry, P. Helminger, E. Herbst and F.C. De Lucia, Chem. Phys. Lett. 84, 286 (1981).

Chapter 4

The $K_a = 0 \rightarrow 1$ submillimeter rotation-tunneling spectrum of the water dimer

E. Zwart, J.J. ter Meulen and W. Leo Meerts

Fysisch laboratorium, University of Nijmegen,
Toernooiveld, 6525 ED Nijmegen, The Netherlands.

4.1 Abstract

The ($K_a=0 \rightarrow 1$) submillimeter rotation-tunneling transitions of the water dimer have been observed. The (H_2O)₂ clusters were produced in a slit nozzle arrangement and the transitions were detected by direct absorption of the submillimeter radiation. A number of lines in the allowed subbranches ($K_a=0, E^\pm \rightarrow K_a=1, E^\pm$), ($K_a=0, A_1 \rightarrow K_a=1, A_1^\pm$) and ($K_a=0, A_1^\pm \rightarrow K_a=1, A_1$) have been studied. Combination differences with the use of microwave transitions within the ($K_a=0$) and ($K_a=1$) states allowed an unambiguous assignment of the lines. The present results allow a more accurate determination of the A -rotational constant and the tunneling splittings of ($K_a=0$) and ($K_a=1$). Furthermore they show that the K -type doubling constant has a different sign for the lower and upper tunneling states in ($K_a=1$).

4.2 Introduction

The knowledge of the structure and the dynamics of the water dimer (H_2O)₂ has greatly developed since the early Molecular Beam Electric Resonance measurements of Dyke and co-workers [1]. In a series of experiments employing various different techniques from microwave [2], microwave double resonance [3], far infrared laser sideband [4] to electric-resonance optothermal spectroscopy [5, 6] a large body of experimental data has become available on the ground vibrational state of the water dimer. The basis for the understanding of the complicated spectrum of this dimer was laid by Dyke [7] followed by several other papers culminating in a theoretical paper by Coudert and Hougen [8]. In this last reference a global analysis has been made of the 173 transitions which had been observed up till then fitted to a model which describes the various possible tunneling motions of the water dimer. A complete list of references to experimental and theoretical work on (H_2O)₂ can be found in [8].

Pictures of the relevant tunneling motions in (H_2O)₂ and the corresponding energy level diagram can be found in [2]. The largest tunneling splitting is due to the tunneling motion which corresponds to a 180° rotation of the acceptor monomer about its two-fold axis of

symmetry during which the hydrogen atom in the hydrogen bond is not changed. This splits each K_a -level in lower and upper separated by approximately 200 GHz. The A -rotational constant in $(\text{H}_2\text{O})_2$ happens to be also about 200 GHz. Consequently the $(K_a=0,\text{upper})$ and $(K_a=1,\text{lower})$ level have almost equal energy. Most of the observed transitions are within either the lower or upper tunneling level of a given K_a -state. Only two sets of data connect levels with different K_a : the far infrared [4] ($K_a=1,\text{lower} \rightarrow K_a=2,\text{upper}$) and the microwave transitions [5, 6] ($K_a=0,\text{upper} \rightarrow K_a=1,\text{lower}$). As a consequence the A -rotational constant and the largest tunneling splitting in the $(K_a=0)$ and the $(K_a=1)$ states cannot be determined independently. The second largest tunneling splitting is due to a 90° geared rotation of each monomer about its two-fold axis of symmetry as a result of which the acceptor monomer becomes the donor monomer and vice versa. This motion causes a splitting of the lower and upper levels within an given K_a in 3 sublevels. These three sublevels are shifted again by all other possible tunneling motions in the water dimer. No microwave transitions have been observed within $(K_a=1,\text{upper})$ that determine these tunneling splittings. A measurement of the $(K_a=0,\text{lower} \rightarrow K_a=1,\text{upper})$ transition will largely remove the above-mentioned ambiguities.

The present paper reports the $(K_a=0 \rightarrow 1)$ c -type rotation-tunneling spectrum of the water dimer. The transitions are in the submillimeter region between 350 and 500 GHz. The observed transition frequencies are given in Table 1. Three different subbranches have been studied: the strongest $(K_a=0, E^+ \rightarrow K_a=1, E^\mp)$ branch and the two weaker $(K_a=0, A_1^- \rightarrow K_a=1, A_1^+)$ and $(K_a=0, A_1^+ \rightarrow K_a=1, A_1^-)$ branches. The present results will provide a better determination of the model constants used by Coudert and Hougen [8]. The most important improvements will be obtained for the A -rotational constant, the largest tunneling splitting in $(K_a=0)$ and $(K_a=1)$ as well as the smaller second largest tunneling splitting within $(K_a=1,\text{upper})$. Furthermore it was found that the sign of the K -type doubling constant is different between $(K_a=1,\text{lower})$ and $(K_a=1,\text{upper})$. This changes the assignment of the microwave transitions in $(K_a=1,\text{upper})$ from Fraser et al. [5]. In a forthcoming paper these results will be discussed as well as the strengths and weaknesses of the model [8] used to analyze the water dimer

4.3 Experiment and Results

The experimentally observed transition frequencies have been obtained by direct absorption of the submillimeter radiation passing through a molecular beam of water dimer clusters. The dimers were formed in a cw supersonic expansion through a slit nozzle similar to the one used by Busarow et al. [9, 10]. Room temperature water mixed with 400 mbar of argon was expanded through a $50 \mu\text{m}$ wide and 40 mm long slit into a vacuum chamber. This chamber was pumped by two mechanical booster pumps and one roughing pump connected in series. The effective pumping speed of the vacuum system was $4000 \text{ m}^3/\text{h}$. The pressure in the vacuum chamber behind the nozzle was approximately 10^{-1} mbar.

The submillimeter radiation has been obtained by generating harmonics of a series of klystrons around 100 GHz. The typical fundamental power was 100 mW. The 3rd, 4th or 5th harmonic were generated in a GaAs Schottky barrier diode, which is mounted in an open-structure multiplier. The harmonic generated was radiated into free space by an antenna. Optimized coupling was provided by a corner reflector. The basic part of this arrangement

Table 1. Observed transition frequencies (in MHz) of the ($K_a=0\rightarrow 1$) subband in the vibrational ground state of the water dimer. The transitions are labeled by the rotation-tunneling state and symmetry of the lowest state. The experimental uncertainties in the transition frequencies are 0.1 MHz.

Assignment	Observed value	Assignment	Observed value
$P(3)A_1^-$	372 784.99 ^{a)}	$P(5)E^-$	367 308.53 ^{a)}
$Q(1)A_1^-$	409 708.10	$P(4)E^+$	379 590.38 ^{a)}
$Q(3)A_1^-$	409 815.62	$P(3)E^-$	391 883.86 ^{a)}
$Q(5)A_1^-$	410 008.91	$P(2)E^+$	404 187.79 ^{a)}
$Q(7)A_1^-$	410 287.20	$Q(1)E^-$	428 833.58 ^{a)}
$R(1)A_1^-$	434 361.24 ^{a)}	$Q(2)E^+$	428 857.38 ^{a)}
$R(3)A_1^-$	459 083.49	$Q(3)E^-$	428 892.98 ^{a)}
		$Q(4)E^+$	428 940.45 ^{a)}
$P(4)A_1^+$	404 054.90	$Q(5)E^-$	428 999.90
$P(2)A_1^+$	428 731.67 ^{a)}	$Q(6)E^+$	429 071.26
$Q(2)A_1^+$	453 392.61 ^{b)}	$Q(7)E^-$	429 154.64
$Q(4)A_1^+$	453 395.29 ^{b)}	$Q(8)E^+$	429 250.17
$R(0)A_1^+$	465 713.34 ^{a)}	$Q(9)E^-$	429 357.75
		$R(0)E^+$	441 149.58 ^{a)}
		$R(1)E^-$	453 482.93 ^{a)}
		$R(2)E^+$	465 820.50 ^{a)}

^{a)} Assignments based on combination differences.

^{b)} The J -assignment of this line has not yet been unambiguously determined

is very similar to our far infrared laser sideband system [11, 12]. However no laser radiation has been put on the mixer and the monochromator has simply been replaced by a mirror. The powers up to the 5th harmonic of the klystron are comparable to those generated using the laser sideband method. The advantage, however, of harmonic generation, is an increase of approximately a factor of 3 in sensitivity. This is due to the much smaller amplitude noise of the klystrons relative to the molecular laser. In the frequency region between 300 and 550 GHz we are able to observe a fractional absorption of 10^{-5} . The different harmonics are separated from each other with the help of a Fabry-Perot interferometer. The resulting submillimeter beam is focussed with a 20 cm focal lens to an elongated 5 mm diameter focus located about 10 mm below the slit nozzle. A helium-cooled (1.5 K) Si bolometer is used to detect the radiation after passing through the molecular jet.

The observed linewidths are 600 kHz, which result from the residual Doppler broadening in the molecular beam. The fundamental radiation from the klystron is phase-lock stabilized to an external reference frequency. Hence, in contrast to the laser sideband system [12], frequency calibration is done implicitly and the uncertainty in the observed transition frequencies is completely determined by the linewidths and signal to noise ratios. In the present experiment the S/N at a RC time of 3 sec was 50 for the stronger transitions (*E*-level) and 10 for the weaker ones (*A*-level). One of the stronger transitions is shown in Fig. 1. The uncertainties in the frequencies quoted in Table 1 are 0.1 MHz.

The assignments of the observed transitions from Table 1 are based on the predictions of [8] and on the combination differences using the ($\Delta J=0, \pm 1$, $\Delta K_a=0$) rotational microwave transitions in the ($K_a=0$) and ($K_a=1$) states. This allows for an unambiguous identification of the observed submillimeter frequencies.

In conclusion we have observed a new subband of the water dimer. It will be possible to extract valuable complementary information for the theoretical understanding of the various tunneling motions in the (H_2O)₂ complex. A complete discussion will be given in a separate paper.

Acknowledgment

We like to acknowledge the help of Dr. L.H. Coudert for predictions of the ($K_a=0 \rightarrow 1$) subband and for making preliminary fits in the course of the experiment incorporating the new data. The authors wish to thank Messrs. E. van Leeuwen and F. van Rijn for their skillful technical assistance. This work was financially supported by the Dutch Organization for Scientific Research (FOM/NWO).

References

- [1] T.R. Dyke, K.M. Mack and J.S. Muentzer, J. Chem. Phys. 66, 498 (1977).
- [2] L.H. Coudert, F.J. Lovas, R.D. Suenram and J.T. Hougen, J. Chem. Phys. 87, 6290 (1987).
- [3] L. Martinache, S. Jans-Bürli, B. Vogelsanger, W. Kresa and A. Bauder, Chem. Phys. Lett. 149, 424 (1988).

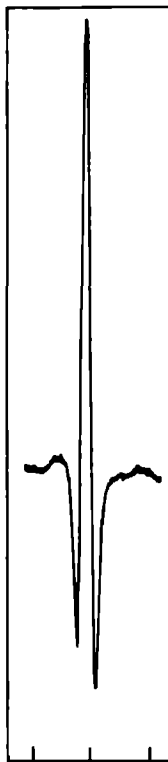


Figure 1. Recording of the $Q(3), E^-$ transition in $(\text{H}_2\text{O})_2$. The distance between the frequency markers is 5 MHz. The trace has been made at a RC time of 3 sec.

- [4] K.L. Busarow, R.C. Cohen, G.A. Blake, K.B. Laughlin, Y.T. Lee and R.J. Saykally, *J. Chem. Phys.* 90, 3937 (1989).
- [5] G.T. Fraser, R.D. Suenram and L.H. Coudert, *J. Chem. Phys.* 90, 6077 (1989).
- [6] G.T. Fraser, R.D. Suenram, L.H. Coudert and R.S. Frye, *J. Mol. Spectrosc.* 137, 244 (1989).
- [7] T.R. Dyke, *J. Chem. Phys.* 66, 492 (1977).
- [8] L.H. Coudert and J.T. Hougen, *J. Mol. Spectrosc.* 139, 259 (1990).
- [9] K. Veeken and J. Reuss, *Appl. Phys.* B38, 117 (1985).
- [10] K.L. Busarow, G.A. Blake, K.B. Laughlin, R.C. Cohen, Y.T. Lee and R.J. Saykally, *Chem. Phys. Lett.* 141, 289 (1987).
- [11] P. Verhoeve, M. Versluis, J.J. ter Meulen, W.L. Meerts and A. Dymanus, *Chem. Phys. Lett.* 161, 195 (1989).
- [12] P. Verhoeve, E. Zwart, M. Versluis, M. Drabbels, J.J. ter Meulen, W.L. Meerts, A. Dymanus and D. McLay, *Rev. Sci. Instrum.* 61, 1612 (1990).

Chapter 5

The submillimeter rotation-tunneling spectrum of the water dimer

E. Zwart, J.J. ter Meulen and W. Leo Meerts

Fysisch Laboratorium, University of Nijmegen,
Toernooiveld, 6525 ED Nijmegen, The Netherlands.

L.H. Coudert

Laboratoire de Physique Moléculaire et Atmosphérique,
Université Pierre et Marie Curie et C.N.R.S.,
Tour 13-4 Place Jussieu, 75252 Paris Cedex 05, France.

5.1 Abstract

Rotational tunneling transitions have been measured for the $(K_a=0, \text{lower}) \rightarrow (K_a=1, \text{upper})$ and the $(K_a=1, \text{lower}) \rightarrow (K_a=2, \text{upper})$ bands of $(\text{H}_2\text{O})_2$. Although some of these transitions were reported in an earlier publication, a more detailed discussion of the experiment and of the results is presented here. Transitions have been measured by direct absorption spectroscopy in a continuous slit nozzle expansion with the use of either harmonics from klystrons or sidebands. These data along with previous measurements have been analyzed with the use of an IAM-like treatment. A better determination of the A rotational constant and of the value of the largest tunneling splitting has been achieved.

5.2 Introduction

The water dimer has been the subject of much spectroscopic work during the past years. The initial goal of this research was to gain a better understanding of the interaction between the two monomers. If this interaction were fully understood, the interaction between three or more monomers could be investigated, leading to a better understanding of the condensation process. However, the structure and dynamics of the dimer have turned out to be difficult and, most of all, interesting enough to direct most of the work done until now at the dimer form.

The first MBER measurements of Dyke et al. [1] established the structure of the water dimer to be like the one drawn in Fig. 1. There is a single hydrogen bond between the two

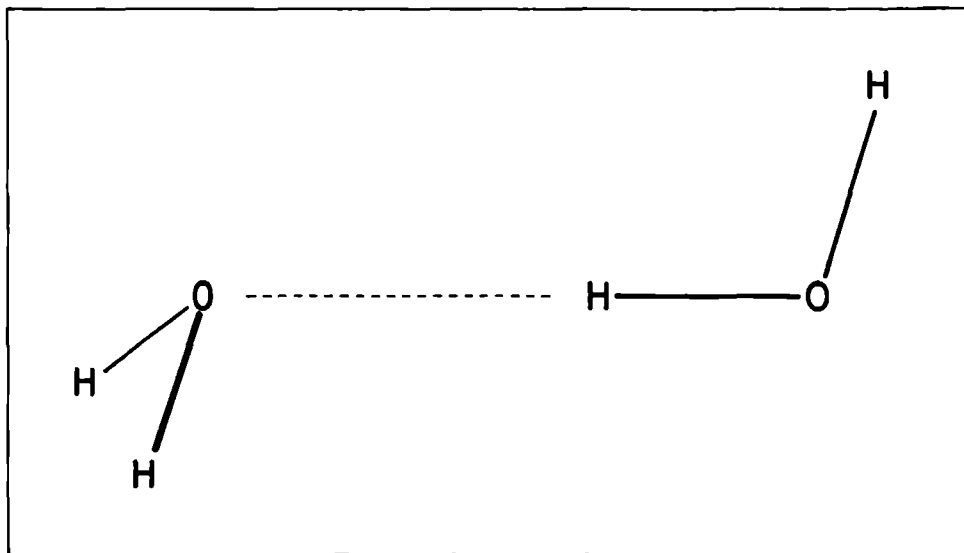


Figure 1. The equilibrium structure of $(\text{H}_2\text{O})_2$.

monomers. Later microwave [2, 3, 4, 5, 6, 7], far infrared [8] and infrared [9, 10] measurements and theoretical works [11, 12, 13] elucidated many details of the ground vibrational state in which several tunneling splittings arise because of large amplitude motions. All measurements were included in a fit, recently published by Coudert et al. [14].

In spite of the vast amount of spectroscopic effort, there is still uncertainty about the exact magnitude of the A rotational constant and about the value of the largest tunneling splitting, caused by the motion in which the hydrogen acceptor monomer rotates over 180° , interchanging its two hydrogen atoms. In the analysis of Coudert et al. [14] an accurate determination of these two parameters could not be carried out because they were correlated. Information on the nondegenerate tunneling states in $(K_a=1, \text{upper})$ was also missing and the magnitude of the tunneling splitting caused by the two interconversion large amplitude motions was not known for these states.

In a recent letter [15] we reported the observation of several submillimeter $\Delta K_a=1$ transitions. In the present paper the experiment and the results are discussed in more detail. Furthermore, a new band and supplementary measurements are presented. All data are analyzed with the use of the same formalism as that utilized by Coudert et al. [14], resulting in a better determination of the A rotational constant and of the magnitude of the largest tunneling splitting. More insight is also gained into the rotational dependence of the tunneling splittings.

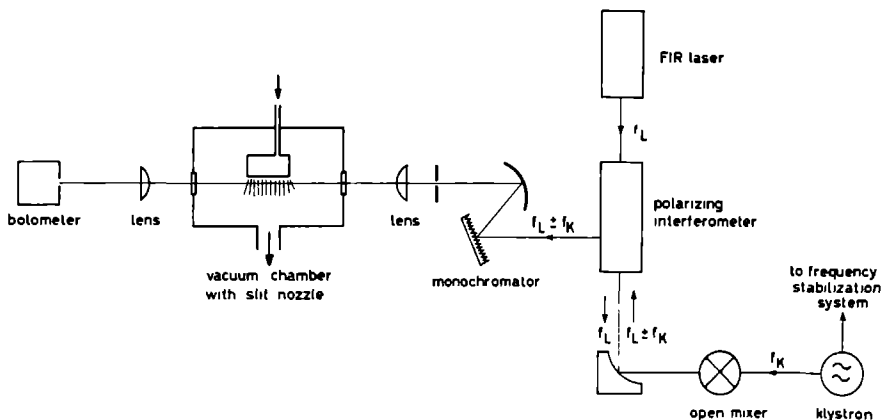


Figure 2. The FIR spectrometer.

5.3 Experimental

The spectrometer used in this work has been described in detail elsewhere [16]. Here its basic operation will be briefly explained. Its use for harmonic generation is discussed in some more detail, since this is essential for this paper and is not included in Ref. [16].

The radiation is generated with a tunable sideband spectrometer (see Fig. 2). The FIR laser is a molecular laser pumped by a 150 W CO₂ laser. By using different gases (e.g. CH₃OH, HCOOC) in the molecular laser and different pump lines from the CO₂ laser, approximately 30 strong (50 mW) FIR laser frequencies can be reached. By mixing the fixed frequency FIR laser radiation with tunable microwave radiation, tunable sum and difference frequencies (sidebands) are generated. The tunable microwave radiation is generated by klystrons (100 mW) in the 55-114 GHz range.

The generation of the sidebands takes place in an open structure with a GaAs Schottky barrier diode. The microwave radiation is coupled onto the diode by a pin in the waveguide and the FIR radiation is coupled by an antenna. The sidebands are radiated by the antenna into free space. The antenna pattern is improved by a corner reflector.

The tunable sidebands are separated from the much stronger laser radiation by a polarizing interferometer and a monochromator. The monochromator transmits either the sum or the difference frequency and this radiation is passed through the vacuum chamber where the absorption takes place. A Si bolometer at 1.5 K is used for the detection of the absorption signals.

This spectrometer can also be used for harmonic generation in the region 300-450 GHz by removing the FIR laser radiation. The harmonics are radiated into free space by the antenna of the mixer and are directed, like the sidebands, through the optical elements to the detector by mirrors and lenses. The antenna length used in both cases (sidebands and harmonics) is approximately 2 mm.

Previously we had to replace the grating (30° blaze angle, 3 grooves/mm) of the monochro-

mator by a mirror, because this grating did not operate below 550 GHz. The different harmonics were then separated by a Fabry Perot (10 lines/mm mesh). More recently a new grating (30° blaze angle, 1.33 grooves/mm) allows us to use the monochromator down to 300 GHz, which simplifies the operation of the spectrometer.

With the calibrated monochromator it is easy to select the harmonic needed for the experiment. The harmonic is optimized in the same way as the sidebands are. Coupling of the microwave power onto the diode is optimized with a movable plunger at the end of the waveguide. The corner reflector, which determines the antenna pattern, is set for highest power. Changing the bias voltage on the diode, the radiated power varies from zero to a maximum, with usually more than one maximum for the range of bias voltages used. The optimum bias voltage is different for every harmonic and depends on the incident microwave power.

The power of the generated harmonics is more than linearly dependent on the microwave power. With the available klystrons (approximately 100 mW), we cannot saturate the diode. Because of this only the most powerful klystrons are used. In our case this means using the 5th and 6th harmonic of klystrons around 60 GHz or the 4th and 5th harmonic of klystrons around 100 GHz.

The powers which can be generated for harmonics and sidebands are of the same order of magnitude. The frequency of the harmonics is precisely known, because the klystrons are phase-locked to a frequency standard. The frequency uncertainty of the sidebands is determined by the FIR laser. The uncertainty in the frequency of transitions measured with harmonics we estimate to be 0.1 MHz and of those with sidebands 1.0 MHz. The minimum fractional absorption obtainable with this spectrometer is approximately 10^{-5} .

The absorption takes place in a vacuum chamber with a continuously operating slit nozzle, pumped by a 4000 m³/h roots pump. The 4000 m³/h roots pump is backed by a 1200 m³/h roots pump and a 80 m³/h rotary pump. The slit is 4 cm long and 25-50 μ m wide. Its design is similar to the one described by Busarow et al. [17]. We used a backing pressure of 500 Torr Ar with a few per cent H₂O. The pressure in the vacuum chamber was 0.1 mbar. The beam of radiation is focused to a diameter of 5 mm as it passes 10 mm from the nozzle.

Due to the slit nozzle expansion, the linewidths are approximately three times smaller than linewidths obtained in an absorption cell or a pinhole expansion. Typical linewidths are 500 kHz full width at half maximum. We use frequency modulation with $2f$ ($2f=1\text{kHz}$) lock-in detection. Because of the limited speed of the bolometer we cannot use a higher modulation frequency.

In the expansion of H₂O and Ar, several complexes $(\text{Ar})_n(\text{H}_2\text{O})_m$ are formed. To check whether the transitions are not due to a complex with Ar, we substituted Ar with Kr. For (H₂O)₂ transitions the intensity dropped to approximately one third of the value obtained with Ar.

5.4 Results

Many details of the energy level diagram of the water dimer were determined by previous microwave, far infrared and infrared measurements (see Fig. 3 and Introduction for references). The water dimer is a near-symmetric rotor in which four large amplitude motions

lead to a splitting of the rotational levels into six sublevels. As stated by Dyke [11], the molecular symmetry group to be used is G_{16} and the six sublevels belong to one of the following symmetry species of this group : A_1^\pm , E^\pm , B_1^\pm , A_2^\mp , E^\mp , B_2^\mp ; where the upper (lower) sign is convenient when the symmetry species of the rotational level in the point group C_s of the dimer equilibrium configuration is A' (A''). For the understanding of the measured bands, the four large amplitude motions as well as their effects will be briefly described below.

The most feasible tunneling motion corresponds to a 180° rotation of the acceptor monomer, resulting in an exchange of the two hydrogen atoms of this monomer. As can be seen in Fig. 3, this motion separates the six tunneling sublevels into two sets : the first set corresponds to the three levels belonging to the symmetry species A_1^\pm , E^\pm and B_1^\pm ; the second set to the three levels belonging to the symmetry species A_2^\mp , E^\mp and B_2^\mp . From here on, for a given K_a value and depending on the relative energy of the two sets, one of them will be referred to as (K_a ,upper) and the other one as (K_a ,lower). The tunneling splitting associated with this large amplitude motion varies with K_a ; for $K_a=0$ it is about 280 GHz. One of the results of the present work is a good determination of this number (see Table 2).

The water dimer displays two different interconversion motions. The more feasible one involves geared rotations of the two monomer units while the other and less feasible one involves antigeared rotations of the same units. As emphasized by Fig. 3, these two tunneling motions shift the A_1^- , A_2^+ , B_1^+ and B_2^- levels up and the A_1^+ , A_2^- , B_1^- and B_2^+ levels down; the positions of the doubly degenerate levels are unaffected. The magnitude of the splitting is exaggerated in the figure. Depending on the set of levels being considered, the effects of the two interconversion motions are constructive or destructive. For $K_a=0$, the interconversion tunneling splitting is about 22.5 GHz for the lower set and 19.5 GHz for the upper set.

The fourth tunneling motion displayed by the water dimer is, from the point of view of feasibility, somewhere in between the two interconversion motions just described. This motion leads to an exchange of the donor monomer hydrogen atoms but does not further split the tunneling sublevels. It merely shifts the levels up or down depending on whether they are nondegenerate or doubly degenerate. The effects of this last tunneling motion are not taken into account in Fig. 3.

As in Ref. [14], the four tunneling motions are conveniently labeled with the number of the framework reached when starting the motion from framework number 1 [13]. Thus, with the use of the framework numbering of Ref. [12], the four previous tunneling motions in order of decreasing feasibility are the 1 \rightarrow 4, 1 \rightarrow 5, 1 \rightarrow 2 and 1 \rightarrow 7, the second and last labels being for the geared and antigeared interconversion motion, respectively. This labelling is also useful to characterize the parameters of each tunneling motion.

To understand the spectrum we observed, we must keep in mind that the selection rules are : $\Delta J=0,\pm 1$; $\Delta K_a=0,1$; $A_1^+ \leftrightarrow A_1^-$, $B_1^+ \leftrightarrow B_1^-$, $A_2^+ \leftrightarrow A_2^-$, $B_2^+ \leftrightarrow B_2^-$, $E^+ \leftrightarrow E^-$. The possible transitions for ($K_a=0$,lower) \rightarrow ($K_a=1$,upper) are drawn in Fig. 3. Since the rotational energy for a near prolate asymmetric rotor (with a given K_a) has to be superimposed on the drawn levels, the transitions will form 3 bands, similar to vibrational bands, with a P , Q and R branch. As is clear from Fig. 3, the bands can be denoted by the symmetries of the initial levels. (E.g. band (A_1^+ , B_1^-) with transition $P(4)A_1^+$). In the same way, for $K_a=1 \rightarrow K_a=2$ there will be 6 bands, 3 originating from ($K_a=1$,lower) and 3 from ($K_a=1$,upper). The band originating in ($K_a=1$,lower), which is presented in this paper, has also been drawn in Fig.

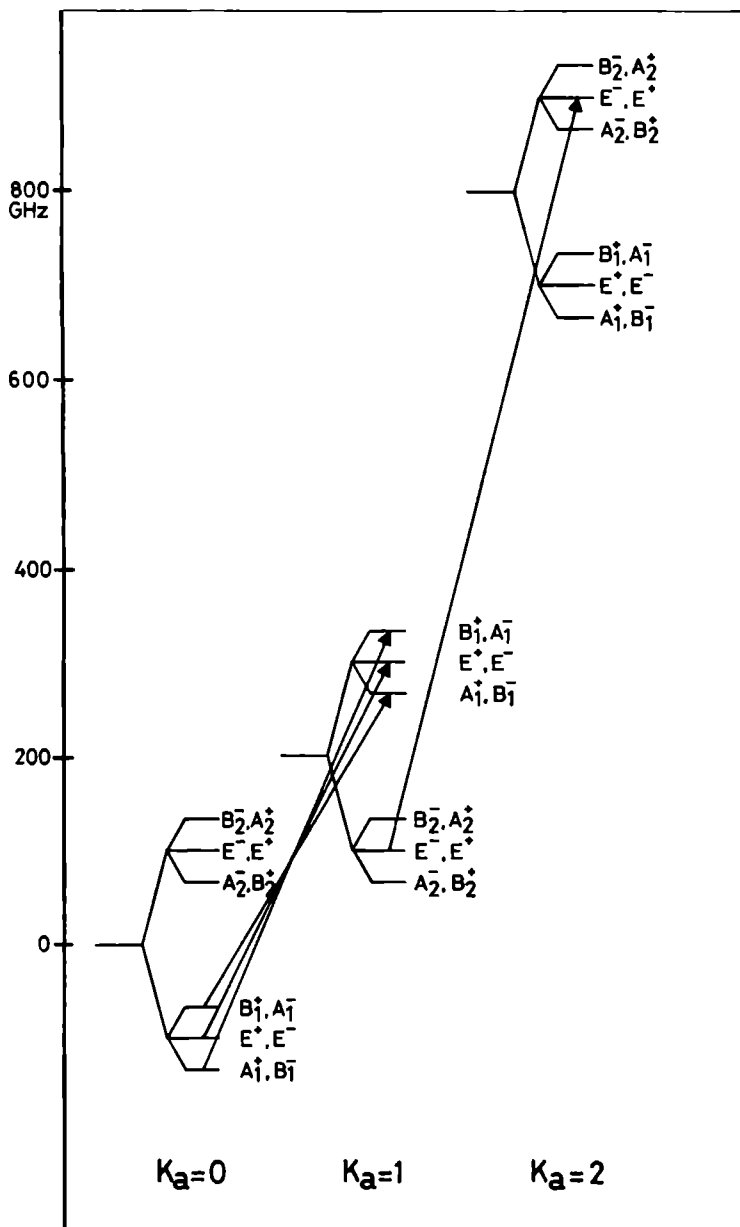


Figure 3. The energy level scheme of the ground vibrational state of $(\text{H}_2\text{O})_2$.

5.4.1 ($K_a=0$,lower) \rightarrow ($K_a=1$,upper)

From the above it is clear that the band origin of ($K_a=0$,lower) \rightarrow ($K_a=1$,upper) could not be determined very accurately from previous measurements. This origin lies at $A + \Delta\nu$, where A is the rotational constant and $\Delta\nu$ contains the effects of the largest tunneling splitting (the effects of the other tunneling motions are ignored for the sake of simplicity). At the time of the measurements only $A - \Delta\nu$ was known precisely [6, 7] and, although A and $\Delta\nu$ could have been calculated separately from [14], the values obtained would not have been very reliable due to the fact that these two parameters were correlated in the analysis presented there.

However, the relative positions of several transitions in the band were known, because of combination differences with microwave transitions in $K_a=0$ and $K_a=1$. Furthermore, the band extends over a large frequency region. Therefore, once one transition had been found, the rest of the band followed by guessing the assignment of the obtained transition.

In [15] the frequencies of the transitions we measured with harmonic generation can be found. These consist of 3 bands, with initial levels respectively (A_1^+ , B_1^-), (B_1^+ , A_1^-) and (E^+ , E^-). Since B_1^+ levels have 0 statistical weight, one transition out of two is missing in the first and second band. With the sideband system we have measured some additional transitions at higher frequencies. The R branch measurements were extended to higher J to get some more data for the fit, which did not work very well for the limited set of A_1^+ transitions reported in [15]. In the original measurements with harmonic generation there were some problems with the assignment of the Q branch involving levels of (A_1^+ , B_1^-) symmetry. With the sideband system, more power could be generated at the corresponding wavelength and a definite assignment could be made (see Fig. 4). The transition originally assigned as $Q(2)$, split up into two, now assigned as $Q(2)$ and $Q(4)$. This means that the transition originally called $Q(4)$ is actually $Q(6)$; also $Q(8)$ was found. The relative intensities of the $Q(2)$ - $Q(8)$ transitions are consistent with those found for other (H_2O)₂ Q branches. A_1^\pm levels have a statistical weight which is 3 times smaller than that of E^\pm levels. In our spectra, the transitions between E^+ levels had a signal to noise ratio of 50 and the transitions between A_1^+ levels 10 (with an RC time of 3 s). An effect which was also seen by Busarow et al. [8] is that P branch transitions are approximately 3 times weaker than Q and R branch transitions. The complete list of measured transitions can be found in Table 1. The notation used in this table is the same as in Ref. [14].

For the E^\pm symmetry levels, microwave measurements were available for both $K_a=0$ and $K_a=1$ and the assignment of many transitions from the P , Q and R branches could be checked with combination differences. However, it turned out that the transitions within ($K_a=1$,upper) were misassigned in Refs. [4, 6]; the levels were not assigned the proper component of the K -type doubling. A relabeling was carried out changing the K -type doubling component and making the change $E^\pm \rightarrow E^\mp$ in the symmetry species labels. Unexpectedly, the K -type doubling ‘changes’ for the doubly degenerate levels in ($K_a=1$,upper); more precisely, the levels for which the contribution from the asymmetry is $+\frac{1}{4}(B-C)J(J+1)$ are below those for which this contribution is $-\frac{1}{4}(B-C)J(J+1)$. For the A_1^+ levels, microwave measurements were only available for $K_a=0$. Therefore only P and R transitions with a

common final level could be checked.

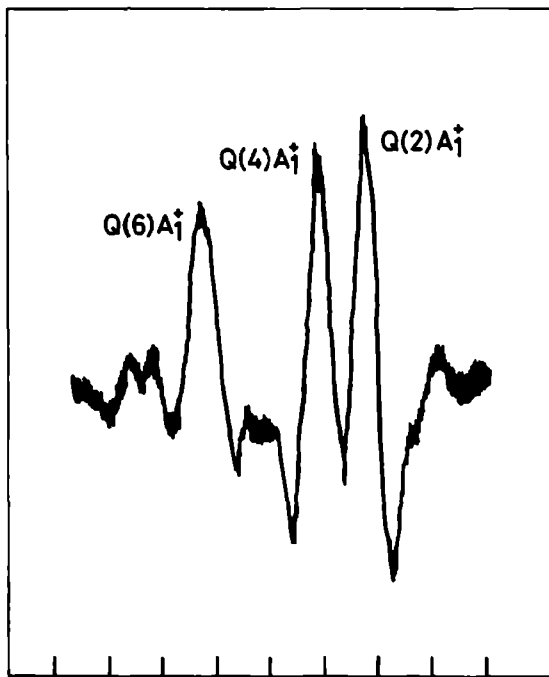


Figure 4. Three Q branch transitions. The distance between frequency markers is 1 MHz.

5.4.2 ($K_a=1, \text{lower}$) \rightarrow ($K_a=2, \text{upper}$)

The (A_2^-, B_2^+) and (B_2^-, A_2^+) bands of ($K_a=1, \text{lower}$) \rightarrow ($K_a=2, \text{upper}$) were published by Busarow et al. [8]. The assignment in terms of upper or lower is not yet certain for $K_a=2$. These bands were relatively strong, as strong as those described in the previous section, since they originate from levels which cannot relax to lower levels and which are, therefore, well populated [3]. However, the E^\pm ($K_a=1, \text{lower}$) levels can relax to the E^\pm ($K_a=0, \text{lower}$) levels and we expect the former levels to be much less populated than the latter ones. The energy difference between the two sets of levels being about 200 GHz, the E^\pm ($K_a=1, \text{lower}$) levels are seven times less populated than the E^\pm ($K_a=0, \text{lower}$) levels in a 5 K jet. It is worthwhile pointing out that this ratio depends very strongly on the temperature in the jet.

For the E^\pm levels, microwave measurements were available for both $K_a=1$ and $K_a=2$. This gave us the relative positions of the low J transitions of the band. An estimate of the band origin could have been carried out with the use of the results of [8] and assuming that it lies between the two bands measured in this reference. However, this estimation was not

deemed accurate enough since it involves neglecting the effects of the 1→2 large amplitude motion. Instead, we chose to carry out predictions starting from the results in [14].

For the high J transitions, the signals in an expansion with Ar and in one with N_2 were equally strong. For the low J transitions the expansion with Ar gave much better results. This indicates that probably even higher levels than ($K_a=1$,lower) can be accessed with N_2 as a carrier gas.

The transitions were all measured with the sideband spectrometer. Predictions turned out to be correct within 400 MHz. The transitions were very weak, as expected. Signal-to-noise ratios were not better than 10 at an RC time of 3 s. The P branch could not be observed, which is consistent with [8] and with our measurements of the ($K_a=0$,lower) → ($K_a=1$,upper) bands. The measured frequencies are listed in Table 1. The combination differences with microwave transitions fitted within the experimental accuracy (1.0 MHz).

To determine the sign of the K -type doubling (which behaved unexpectedly in $K_a=1$), we measured the four $Q(8)E^\pm$ and $R(8)E^\pm$ transitions. The K -type doubling in $K_a=2$ is very small, but increases with $(J-1)J(J+1)(J+2)$ from 11.20 MHz for $J=8$ to 17.52 MHz for $J=9$ [1]. Considering the value of the uncertainty of the measured frequencies (1.0 MHz), reliable information can be extracted from these transitions. The combination difference that can be made is

$$R(8)E^- - R(8)E^+ + Q(8)E^+ - Q(8)E^- = \pm\{(\text{doubling } J=8) + (\text{doubling } J=9)\}. \quad (5.1)$$

If the sign of the K -type doublings is different in ($K_a=1$,lower) and ($K_a=2$,upper) the sign to be used is the lower one and otherwise it is the upper one. Substitution gives in the left and right side of the equation +29.2 MHz and +28.72 MHz, respectively. Therefore the two levels have the same K -type doubling sign.

5.5 Analysis

For this analysis the theoretical formalism developed by Hougen [12] and Hougen and Coudert [13] was used and the same computer program as the one with which the analysis was performed in Ref. [14] was utilized. Details concerning the calculation of the Hamiltonian matrix elements, the size of the submatrices involved and the way they were truncated in this computer program can be found in this reference. We were led to introduce second order distortion terms in the asymmetric rotor Hamiltonian given in Eq. (20) of Ref. [14]. The Hamiltonian considered for the present analysis is as follows :

$$\begin{aligned} H_{1,1} = & AJ_z^2 + BJ_y^2 + CJ_x^2 - D_J\mathbf{J}^4 - D_{JK}\mathbf{J}^2J_z^2 - D_KJ_z^4 + d_1\mathbf{J}^2(J_+^2 + J_-^2) + \\ & d_2(J_+^4 + J_-^4) + H_J\mathbf{J}^6 + H_{JK}\mathbf{J}^4J_z^2 + H_{KJ}\mathbf{J}^2J_z^4 + H_KJ_z^6 + f_1\mathbf{J}^4(J_+^2 + J_-^2) + \\ & f_2\mathbf{J}^2(J_+^4 + J_-^4) + f_3(J_+^6 + J_-^6), \end{aligned} \quad (5.2)$$

where \mathbf{J} , J_x , J_y and J_z are the total angular momentum and its components and $J_\pm = J_x \pm iJ_y$. The Hamiltonian of Eq. (2) is written with Watson's S set of centrifugal parameters.

Two sets of data were included in the analysis. The first set consists of the measurements carried out in Refs. [1] - [8]; the second set corresponds to the measurements reported in [15] along with the new frequencies presented in this paper. It is important to point out that in the first global analysis carried out by Coudert et al. [14], only the first set of data was

Table 1 Assignment, measured frequencies, and observed minus calculated differences in the spectrum of the water dimer

J'	$\pm K^{(a)}$	$\Gamma^{(b)}$	J''	$\pm K^{(a)}$	$\Gamma^{(b)}$	FREQ ^(c)	REF ^(c)	O-C ^(d)	J'	$\pm K^{(a)}$	$\Gamma^{(b)}$	J''	$\pm K^{(a)}$	$\Gamma^{(b)}$	FREQ ^(c)	REF ^(c)	O-C ^(d)
1	0	E^-	0	0	E^+	12320 987	{1,3}	0 10	2	-1	B_2^-	2	1	B_2^+	16918 527	3	-0 05
2	0	E^+	1	0	E^-	24640 807	{1,3}	0 17	2	1	A_1^+	2	-1	A_2^-	15544 205	[3]	-0 01
3	0	E^-	2	0	E^+	38958 13	[6]	0 08	3	-1	B_2^+	2	-1	B_2^-	21189 816	[3]	0 03
4	0	E^+	3	0	E^-	49271 94	[6]	-0 03	3	1	A_2^-	2	1	A_2^+	20620 650	[3]	0 10
5	0	E^-	4	0	E^+	61580 86	[6]	-0 37	3	-1	A_2^+	2	-1	A_2^-	53753 29	[6]	-0 08
6	0	E^+	5	0	E^-	73884 03	[6]	-0 64	3	1	B_2^-	2	1	B_2^+	53015 86	[6]	-0 03
7	0	E^-	6	0	E^+	86179 50	[6]	-1 81	3	1	B_2^+	3	-1	B_2^-	14907 528	[3]	0 00
1	0	E^+	0	0	E^-	12132 810	{2,4,5}	-0 08	3	-1	A_2^+	3	1	A_2^-	17588 410	[3]	0 00
2	0	E^-	1	0	E^+	24284 320	{4,5}	-0 25	4	1	A_2^-	3	1	A_2^+	85275 95	[6]	-0 01
3	0	E^-	2	0	E^+	36464 94	[6]	-0 52	4	-1	B_2^-	3	-1	B_2^+	68233 20	[6]	0 10
4	0	E^-	3	0	E^+	48675 12	[6]	-0 98	4	1	B_2^-	3	1	B_2^+	32895 28	[6]	-0 16
1	0	A_2^+	0	0	A_2^-	31673 40	[7]	0 25	4	-1	A_2^+	3	-1	A_2^-	33594 83	[6]	0 08
1	0	B_2^+	0	0	B_2^-	-7354 864	{2,3}	0 00	4	-1	B_2^-	4	1	B_2^+	18430 396	[4]	0 06
2	0	A_2^-	1	0	A_2^+	4663 160	[2]	0 05	4	1	A_2^+	4	-1	A_2^-	14092 803	[4]	0 00
2	0	B_2^-	1	0	B_2^+	43797 03	[6]	0 54	5	1	A_2^-	4	1	A_2^+	46167 86	[6]	0 27
3	0	B_2^+	2	0	B_2^-	17122 618	{2,3}	0 03	5	-1	B_2^+	4	-1	B_2^-	45978 63	[6]	0 05
3	0	A_2^+	2	0	A_2^-	55916 67	[6]	0 57	5	1	A_2^+	4	1	A_2^-	78678 88	[6]	0 39
4	0	B_2^-	3	0	B_2^+	68043 50	[6]	0 57	5	1	B_2^-	5	-1	B_2^+	13120 210	[4]	-0 03
4	0	A_2^-	3	0	A_2^+	29416 387	[2]	-0 01	5	-1	A_2^-	5	1	A_2^+	19418 12	[6]	0 02
5	0	B_2^+	4	0	B_2^-	41734 73	[6]	-0 08	6	1	A_2^-	5	1	A_2^+	89775 12	[6]	0 19
5	0	A_2^+	4	0	A_2^-	80182 08	[6]	0 47	6	-1	B_2^+	5	-1	B_2^-	91086 90	[6]	0 66
6	0	A_2^-	5	0	A_2^+	54008 53	[6]	-0 13	6	1	B_2^-	5	1	B_2^+	57436 73	[6]	0 74
6	0	B_2^-	5	0	B_2^+	92334 56	[6]	-0 17	6	1	A_2^+	6	-1	A_2^-	12008 176	4]	-0 04
7	0	B_2^+	6	0	B_2^-	86410 42	[6]	0 21	7	1	B_2^+	7	-1	B_2^-	10772 506	4]	0 02
8	0	A_2^-	7	0	A_2^+	78755 59	[6]	0 22	5	-1	A_2^+	6	0	A_2^-	-36804 25	7]	-0 18
9	0	B_2^+	8	0	B_2^-	91099 28	[6]	0 25	4	-1	B_2^-	5	0	B_2^+	25899 06	[6]	0 38
1	0	A_1^-	0	0	A_1^+	34871 38	[7]	0 13	3	-1	A_2^+	4	0	A_2^-	-14826 98	[6]	0 54
2	0	A_1^+	1	0	A_1^-	2110 358	[4]	0 02	1	1	B_2^+	1	0	B_2^-	32112 47	[7]	0 66
3	0	A_1^-	2	0	A_1^+	59465 85	[6]	0 04	2	1	A_2^+	2	0	A_2^-	32297 22	[6]	0 33
4	0	A_1^+	3	0	A_1^-	28810 57	[6]	0 05	3	1	B_2^-	3	0	B_2^+	32553 28	[6]	0 00
5	0	A_1^-	4	0	A_1^+	84001 67	[6]	-0 04	4	1	A_2^-	4	0	A_2^+	32860 80	[6]	-0 31
6	0	A_1^+	5	0	A_1^-	51535 65	[6]	0 50	5	1	B_2^+	5	0	B_2^-	33199 97	7]	0 37
7	0	A_1^-	6	0	A_1^+	108469 87	[6]	-0 10	6	1	A_2^+	6	0	A_2^-	33552 54	[7]	0 23
1	-1	E^+	1	1	E^-	259 915	4	0 00	7	1	B_2^-	7	0	B_2^+	33903 33	[7]	0 45
2	-1	E^-	2	1	E^+	759 741	4	-0 05	2	-1	A_2^-	1	0	A_2^+	21616 23	[6]	0 45
3	-1	E^+	3	1	E^-	1468 081	4]	0 05	3	1	B_2^-	2	0	B_2^+	34768 42	[6]	0 08
4	-1	E^-	4	1	E^+	2351 680	[4]	0 05	1	0	E^+	2	-1	E^-	36609 62	7	0 85
5	1	E^+	5	1	E^-	3381 641	4]	0 05	3	0	E^+	2	1	E^-	24139 64	7]	0 07
1	1	E^+	1	1	E^-	5 096	4]	0 03	4	0	E^-	3	1	E^+	35286 60	7	0 94
2	1	E^-	2	-1	E^+	15 301	4]	0 08	3	1	A_1^-	4	0	A_1^+	404054 90	15]	-1 52
3	1	E^+	3	-1	E^-	30 543	[4]	0 05	2	-1	A_1^+	3	0	A_1^-	372784 99	[15]	0 45
4	1	E^-	4	-1	E^+	50 810	[4]	0 13	1	1	A_1^-	2	0	A_1^+	428731 67	[15]	0 30
2	1	E^+	1	1	E^-	24546 297	4]	-0 20	1	1	A_1^+	1	0	A_1^-	409708 10	[15]	-0 17
2	-1	E^-	1	-1	E^+	25046 436	4]	0 06	2	1	A_1^-	2	0	A_1^+	453392 0	WRK	0 66
2	1	E^+	1	1	E^-	24288 537	[4]	-0 04	3	1	A_1^+	3	0	A_1^-	409815 62	[15]	0 56
3	-1	E^+	2	-1	E^-	37528 24	[6]	0 11	4	1	A_1^-	4	0	A_1^+	453392 8	WRK	1 11
3	1	E^-	2	1	E^+	36819 84	[6]	0 05	5	1	A_1^-	5	0	A_1^+	410008 91	[15]	1 14
4	1	E^+	3	1	E^-	49087 86	6	0 10	6	1	A_1^-	6	0	A_1^+	453395 29	'15	0 98
4	1	E^-	3	-1	E^+	49971 36	6	0 22	7	1	A_1^+	7	0	A_1^-	410287 20	15	0 01
2	-1	E^-	1	1	E^+	24654 344	4]	0 01	8	1	A_1^-	8	0	A_1^+	453400 3	WRK	-1 62
2	1	E^+	1	1	E^-	24664 549	[4]	0 05	1	-1	A_1^-	0	0	A_1^+	465713 34	[15]	0 38
2	1	E^-	1	-1	E^+	24669 651	[4]	0 08	2	-1	A_1^+	1	0	A_1^-	434361 24	[15]	-0 35
3	1	E^+	2	1	E^-	36993 72	[6]	0 12	3	1	A_1^-	2	0	A_1^+	490332 0	WRK	0 86
3	-1	E^-	2	-1	E^+	36978 50	[6]	-0 06	4	-1	A_1^+	3	0	A_1^-	459083 49	[15]	0 71
4	-1	E^+	3	-1	E^-	49299 16	[6]	0 05	5	1	A_1^-	4	0	A_1^+	514910 9	WRK	-3 93
4	1	E^-	3	1	E^+	49319 49	[6]	0 18	6	-1	A_1^+	5	0	A_1^-	483844 2	WRK	1 16
1	1	B_2^-	1	-1	B_2^+	15982 874	[3]	0 03	7	-1	A_1^-	6	0	A_1^+	539441 2	WRK	-9 48
1	-1	A_2^+	1	1	A_2^-	16449 424	3	0 05	8	-1	A_1^+	7	0	A_1^-	508633 2	WRK	-2 47
2	1	B_2^+	1	1	B_2^-	8344 588	[3]	0 07	4	1	E^+	5	0	E^-	367308 53	[15]	0 06
2	-1	A_2^-	1	-1	A_2^+	8756 579	[3]	-0 01	3	-1	E^-	4	0	E^+	379590 38	15	0 11

 a) These columns give the K assignment of the levels. The $-K$ and $+K$ notation is explained in Ref [14]

 b) Γ is the symmetry species of the level in the group G_{16}

c) FREQ is the measured frequency in MHz, as taken from the reference(s) in the REF column or from this work when WRK is written

d) O-C is the observed minus calculated difference calculated with the constants in Table 2

Table 1 (continued) Assignment, measured frequencies, and observed minus calculated differences in the spectrum of the water dimer

J'	$\pm K^{(a)}$	$\Gamma^{(b)}$	J''	$\pm K^{(a)}$	$\Gamma^{(b)}$	FREQ ^c	REF ^c	O-C ^d	J'	$\pm K^{(a)}$	$\Gamma^{(b)}$	J''	$\pm K^{(a)}$	$\Gamma^{(b)}$	FREQ ^c	REF ^c	O-C ^d
2	-1	E^+	3	0	E	391883.86	[15]	-0.04	4	2	B_2^-	3	-1	B_2^+	719463.0	[8]	1.25
1	1	E	2	0	E	404187.79	[15]	0.20	5	-2	A_2^-	4	1	A_2^+	705953.9	[8]	-0.21
1	1	E^+	1	0	E	428833.58	[15]	0.28	5	2	A_2^+	4	1	A_2^-	731095.0	[8]	1.18
2	1	E^-	2	0	E^+	428857.38	[15]	0.22	5	-2	B_2^-	4	1	B_2^+	733185.6	[8]	0.33
3	1	E^+	3	0	E^-	428892.98	[15]	0.03	5	2	B_2^-	4	-1	B_2^+	703712.5	[8]	0.74
4	1	E	4	0	E^+	428940.45	[15]	0.20	6	-2	A_2^-	5	1	A_2^+	745652.1	[8]	1.26
5	1	E^+	5	0	E^-	428999.90	[15]	0.35	6	2	A_2^-	5	-1	A_2^+	715212.8	[8]	4.63
6	1	E^-	6	0	E^+	429071.26	[15]	-0.49	6	-2	B_2^-	5	1	B_2^+	718448.9	[8]	2.10
7	1	E^-	7	0	E^-	429154.64	[15]	-0.50	6	2	B_2^-	5	-1	B_2^+	742598.5	[8]	-0.55
8	1	E^-	8	0	E^-	429250.17	[15]	-0.23	7	-2	A_2^-	6	1	A_2^+	730972.8	[8]	1.89
9	1	E^+	9	0	E	429357.75	[15]	0.21	7	-2	B_2^-	6	1	B_2^+	758144.0	[8]	1.00
1	-1	E^-	0	0	E^+	441149.58	[15]	0.44	7	2	B_2^-	6	-1	B_2^+	728612.7	[8]	1.73
2	1	E^+	1	0	E^-	453482.93	[15]	0.34	8	2	A_2^-	7	-1	A_2^+	737936.0	[8]	0.10
3	-1	E^-	2	0	E^+	465820.50	[15]	-0.01	8	-2	B_2^-	7	1	B_2^+	743526.1	[8]	1.31
4	-1	E^+	3	0	E^-	471812.3	WRK	0.63	8	2	B_2^-	7	-1	B_2^+	765293.9	[8]	-0.83
5	-1	E^-	4	0	E^+	490505.2	WRK	0.39	9	-2	B_2^-	8	1	B_2^+	783204.9	[8]	4.38
6	1	E^+	5	0	E	502849.7	WRK	1.03	2	-2	E^+	2	-1	E^-	859778.9	WRK	2.89
7	-1	E^-	6	0	E^+	515193.4	WRK	1.45	2	2	E^-	2	1	E^+	660538.0	WRK	2.14
8	1	E^-	7	0	E^-	527536.9	WRK	3.54	3	-2	E^-	3	1	E^+	859178.7	WRK	2.43
9	-1	E^-	8	0	E^+	539877.5	WRK	5.93	3	2	E^+	3	1	E^-	860648.3	WRK	3.64
2	2	A_2^-	3	1	A_2	634590.0	8	-2.50	4	-2	E^+	4	-1	E^-	858440.1	WRK	2.76
2	-2	B_2^+	3	1	B_2	607318.0	[8]	1.59	4	2	E	4	1	E^+	860793.4	WRK	3.54
2	2	B_2^+	3	-1	B_2^+	633305.1	[8]	-0.55	5	-2	E^-	5	-1	E^+	857598.8	WRK	2.78
3	-2	B_2^-	4	1	B_2^-	622426.4	[8]	-2.41	5	2	E^+	5	1	E^-	860973.7	WRK	2.14
3	2	B_2^+	4	-1	B_2^-	592927.3	[8]	-1.31	6	-2	E^+	6	1	E^-	856652.2	WRK	1.23
4	-2	A_2^-	5	1	A_2^-	610301.8	[8]	2.52	6	2	E^-	6	1	E^+	861190.4	WRK	0.52
4	2	B_2^-	5	-1	B_2^-	807247.3	[8]	-2.36	7	-2	E^-	7	1	E^+	855640.8	WRK	-2.33
2	-2	A_2^-	2	-1	A_2^-	670757.1	[8]	0.37	7	2	E^+	7	1	E^-	861442.3	WRK	-2.70
2	2	A_2^-	2	1	A_2^-	844133.3	[8]	-1.52	8	-2	E^+	8	-1	E^-	854570.9	WRK	-6.06
2	-2	B_2^+	2	-1	B_2^+	643415.6	[8]	1.10	8	2	E^-	8	1	E^+	8661729.7	WRK	7.38
2	2	B_2^-	2	1	B_2^-	671414.8	[8]	0.79	2	2	E	1	-1	E^+	864827.0	WRK	2.56
3	2	A_2^-	3	-1	A_2^-	642859.2	[8]	0.94	2	-2	E^+	1	1	E^-	865087.1	WRK	2.80
3	2	A_2^-	3	1	A_2^-	671519.8	8	0.85	3	2	E^+	2	-1	E^-	866708.0	WRK	3.34
3	2	B_2^-	3	-1	B_2^-	670232.4	8	0.82	3	-2	E^-	2	1	E^+	897486.8	WRK	2.61
3	2	B_2^+	3	1	B_2^-	644253.0	8	1.39	9	2	E^-	8	-1	E^+	765241.9	WRK	-7.44
4	-2	A_2^-	4	-1	A_2^-	669585.3	8	0.59	9	2	E^-	8	1	E^+	772371.5	WRK	-9.51
4	2	A_2^-	4	1	A_2^-	644412.4	8	-1.32	3	2	E^-	2	2	E^+	36863.510	[1]	-0.22
4	-2	B_2^+	4	-1	B_2^-	642167.6	8	1.06	3	2	E^+	2	-2	E^-	36863.510	[1]	-0.04
4	2	B_2^-	4	1	B_2^+	671659.4	8	0.62	4	2	E^+	3	2	E^-	49146.130	[1]	0.12
5	2	A_2^-	5	1	A_2^-	641367.0	8	1.43	4	-2	E^-	3	-2	E^+	49146.130	[1]	0.32
5	2	A_2^-	5	1	A_2^-	671832.6	8	-0.83	3	2	E^+	2	2	E^-	36928.570	[1]	0.03
5	2	B_2^-	5	1	B_2^-	668777.2	8	1.05	3	-2	E^-	2	-2	E^+	36928.570	[1]	0.18
5	2	B_2^+	5	1	B_2^-	844611.4	8	-1.33	4	2	E^-	3	2	E^+	49232.470	[1]	-0.28
6	2	A_2^-	6	1	A_2^-	667883.5	8	0.62	4	-2	E^+	3	-2	E^-	49232.470	[1]	0.24
6	-2	B_2^+	6	-1	B_2^-	640478.9	8	-1.90	3	2	E^-	3	2	E^+	0.51	[1]	0.29
6	2	B_2^-	6	1	B_2^+	672042.4	8	0.42	4	2	E^+	4	-2	E^-	0.98	[1]	0.32
7	-2	A_2^-	7	-1	A_2^-	639522.6	8	0.25	5	2	E^-	5	-2	E^+	1.76	[1]	0.21
7	2	B_2^-	7	1	B_2^-	666904.4	[8]	0.49	8	2	E^+	6	-2	E^-	2.88	[1]	-0.21
8	-2	B_2^+	8	1	B_2^-	638504.6	[8]	0.97	7	2	E^-	7	2	E^+	4.50	[1]	-1.07
2	2	A_2^-	1	1	A_2^-	695963.1	[8]	-0.43	8	2	E^+	8	2	E^-	9.64	[1]	0.36
2	2	A_2^-	1	-1	A_2^+	668437.5	[8]	1.88	3	2	E^+	3	-2	E^-	0.26	[1]	0.00
2	2	B_2^+	1	1	B_2^-	668981.7	[8]	1.56	4	2	E^-	4	-2	E^+	0.80	[1]	0.01
2	2	B_2^-	1	-1	B_2^+	695741.2	[8]	0.37	5	2	E^+	5	-2	E^-	1.88	[1]	0.04
3	2	A_2^-	2	1	A_2^-	681070.0	[8]	0.70	6	2	E^-	6	-2	E^+	3.76	[1]	0.07
3	2	A_2^-	2	1	A_2^-	707684.0	[8]	0.09	7	2	E^+	7	-2	E^-	6.72	[1]	0.08
3	2	B_2^-	2	1	B_2^+	708339.2	[8]	0.95	8	2	E^-	8	2	E^+	11.20	[1]	0.14
3	2	B_2^+	2	1	B_2^-	680351.9	8	0.20	9	2	E^+	9	-2	E^-	17.52	[1]	0.14
4	-2	A_2^+	3	1	A_2^-	720749.1	8	1.23	10	2	E^-	10	-2	E^+	26.20	[1]	0.13
4	2	A_2^-	3	1	A_2^-	892100.3	8	-0.97	11	2	E^+	10	-2	E^-	37.71	[1]	0.07
4	2	B_2^+	3	1	B_2^-	693494.4	8	-0.04									

a) These columns give the K assignment of the levels. The $-K$ and $+K$ notation is explained in Ref [14]b) Γ is the symmetry species of the level in the group G_{16}

c) FREQ is the measured frequency in MHz as taken from the reference(s) in the REF column or from this work when WRK is written

d) O-C is the observed minus calculated difference calculated with the constants in Table 2

considered. In agreement with the aforementioned authors we chose the following weights in the least squares procedure : 2500 for the microwave data of Refs. [1, 2, 3, 4, 5]; 100 for the radiofrequency data of Ref. [1], for the microwave data of Fraser and coworkers [6, 7] and for the submillimeter data reported in [15]; and 1 for the far infrared data of Busarow et al. [8] and for the new frequencies presented in this work. The two $K=3$ transitions of Ref. [1] were excluded from the fit because they gave too large an observed-minus-calculated difference. Table 1 lists the assignment, the observed frequency and the observed-minus-calculated difference for each transition. The notation used for the rotational levels is defined in Ref. [14]. Transitions appearing both in Table 1 of this work and in Table 2 of Ref. [14] are assigned in the same way. However, as pointed out in this last reference, for some of these transitions the assignment is not the same as that given originally. This is true for the J assignment of one set of $\Delta J=0, K=2$ radiofrequency transitions of Dyke et al. [1], for the $K=1$ transitions involving nondegenerate levels of Coudert et al. [3] and for the $K=1$ transitions involving doubly degenerate levels of Refs. [4, 6] (see previous section).

Table 2 gives the values for the constants determined from the analysis. All the parameters mentioned in Section 2B and 2C of Ref. [14] as well as those from the rigid rotator of Eq. (2) were considered in preliminary fits of the data. However, only the parameters appearing in Table 2 were chosen in the last fitting iteration and were given nonzero value. In this table, parameters written under the ' $n=1$ ' label are non-tunneling usual asymmetric constants. In addition to the usual constants A , B and C there are four first order and two second order distortion constants. These latter constants, H_{KJ} and H_{JK} , were not used in the analysis of Ref. [14]. In Table 2, tunneling parameters are grouped according to the tunneling motion they correspond to. These motions as well as the parameters are labeled using the numbers 2, 4, 5 or 7, the meaning of which is given in the beginning of Section 3. There are two types of tunneling parameters in Table 2. The first type involves those written with Greek letters: θ_2 , φ_4 , φ_{4J} , θ_4 , θ_{4J} , φ_7 , φ_{7J} and θ_7 , which are angle-like constants necessary to account for the rotational dependence of the corresponding tunneling splitting (φ_{7J} is defined just like φ_{4J} [14]). A more detailed discussion of these parameters can be found in Refs. [13, 14]. The second type of parameters involves those written with roman letters : h_{nv} is the magnitude of the tunneling splitting; h_{nk} , h_{nJ} and f_n are first order distortion constants corresponding to the operators J_+^2 , \mathbf{J}^2 and $(J_+^2 + J^2)$, respectively, in the tunneling matrix elements; and h_{nkk} , h_{njk} and h_{nJJ} are second order distortion terms corresponding to the operators J_+^4 , $\mathbf{J}^2 J_+^2$ and \mathbf{J}^4 , respectively.

Comparing Table 2 of the present paper and Table 3 of Ref. [14] shows that parameters giving rise to a contribution in $J(J+1)$ to Hamiltonian matrix elements, \bar{B} , h_{2J} , h_{4J} and h_{5J} , are equally well defined in both analyses. However, larger changes can be seen for the uncertainty of parameters involved in the value of the subband centers. For instance the A rotational constant and the magnitude of the $1 \rightarrow 4$ tunneling splitting, h_{41} , have an uncertainty of 0.50 and 0.10 MHz respectively in this work and 450 and 250 MHz in Ref. [14]. This decrease is a consequence of the fact that three additional $\Delta K_a=1$ subbands were considered in the present analysis. The root mean square deviation of the fit for the 47 transitions weighed 2500, for the 102 transitions weighed 100 and for the 90 transitions weighed 1 is 0.080, 0.439 and 2.666 MHz respectively.

Table 2. Molecular parameters^{a)} for the water dimer

	$n = 1^b$		$n = 2^b$
A	227580.432(500)	h_{2v}	-697.583(126)
\bar{B}	6163.846(477)	θ_2	2.5079°(574)
$B - C$	26.665(958)	h_{2k}	-30.280(201)
D_{JK}	5.954(917)	h_{2j}	-0.1778(184)
D_J	0.048329(185)	f_2	0.04424(934)
$d_1 \times 10^3$	0.345(112)	h_{2jk}	0.03907(442)
$d_2 \times 10^3$	0.9572(112)	$h_{2jj} \times 10^3$	-0.5206(714)
H_{KJ}	0.699(200)		
$H_{JK} \times 10^3$	-0.346(109)		
			$n = 5^b$
	$n = 4^b$	h_{5v}	-5260.7101(177)
h_{4v}	-70128.436(104)	h_{5k}	32.135(664)
φ_4	210.397293°(64)	h_{5j}	1.26833(800)
θ_4	0.71967°(365)	f_5	-0.03308(578)
h_{4j}	-2.934(254)	h_{5kk}	558.978(668)
f_4	-6.851(259)	h_{5jk}	-0.4620(134)
h_{4jk}	-0.7725(386)	$h_{5jj} \times 10^3$	-0.1637(308)
$\varphi_{4j} \times 10^3$	-0.9848°(100)		
$\theta_{4j} \times 10^3$	-0.04607°(233)		
			$n = 7^b$
		h_{7v}	-378.0004(168)
		φ_7	126.94972°(680)
		θ_7	1.1805°(202)
		h_{7k}	-1849.64(180)
		h_{7j}	0.14357(775)
		h_{7jk}	0.2736(217)
		$\varphi_{7j} \times 10^3$	2.8232°(549)

^{a)} Obtained from analysis of the transitions reported in Table 1. All parameters are in MHz, except the θ and φ terms, which are in degrees. Numbers in parentheses are one standard deviation in the same unit as the last digit.

^{b)} n indicates the tunneling motion $1 \rightarrow n$ to which the parameters correspond.

5.6 Discussion

The far infrared region is a rather new frequency region for high resolution spectroscopy of van der Waals molecules. With the use of harmonic generation and submillimeter BWO's (both below 1000 GHz), FIR laser sidebands (below 2500 GHz) [16] or CO₂ laser difference frequency generation (below 6000 GHz) [18], very sensitive measurements can be made. However, most high resolution spectroscopic investigations of dimers were conducted at frequencies of 1000 GHz or lower

Van der Waals vibrations of (H₂O)₂ are expected in the as yet unexplored regions higher than 1000 GHz. Detection of these would provide valuable information for the determination of the intermolecular potential energy surface. Further information on $K_a \geq 3$ levels in the ground vibrational state would be interesting, since the position of these cannot be predicted with high precision by existing theory, as stated above. However, the detection of transitions originating in $K_a = 2$ or higher will be difficult with the production method of dimers used in this work, since the temperature in a jet is so low that these levels are barely populated. Perhaps low temperature cells are better suited in this case.

The formalism used to analyze the data allowed us to reproduce the frequency of the observed transitions in a fairly satisfactory manner. It was possible to determine fairly accurately and with a much smaller uncertainty than in [14] two important spectroscopic parameters, the A rotational constant and the magnitude of the 1→4 tunneling splitting. Also, a good understanding of the rotational dependence of the 1→4 tunneling splitting was achieved. According to Table 2 of Ref. [13], the predicted value for φ_4 is 221.907° which is in fairly good agreement with the one obtained in this analysis: 210.397°. However, several problems still remain. The first one lies in the too large number of parameters, 38, necessary to account for the frequency of the 239 transitions. The second one lies in the value of some of the distortion parameters involved in the tunneling matrix elements (h_{nk} , h_{nj} , etc.). For instance, Table 2 shows that the first order distortion parameter h_{7k} , corresponding approximately to a $(K_a)^2$ contribution in the tunneling matrix element, has a value which cannot be considered as small when compared with the magnitude of the corresponding tunneling splitting, h_{7i} . These two drawbacks of the present analysis seem to indicate that, in addition to complicated tunneling-rotation Coriolis couplings for which the theoretical formalism [13, 14] accounts, some unusual centrifugal effects take place in the water dimer.

Acknowledgment

The authors are grateful to Dr. J. Hougen who had an important part in this manuscript. Furthermore the authors wish to thank Prof. J. Reuss for his encouraging interest and E. v. Leeuwen for his technical assistance.

References

- [1] T.R. Dyke, K.M. Mack and J.S. Muentner, J. Chem. Phys. 66, 498 (1977).
- [2] J.A. Odutola, T.A. Hu, D. Prinslow, S.E. O'Dell and T.R. Dyke, J. Chem. Phys. 88, 5352 (1988).

- [3] L.H. Coudert, F.J. Lovas, R.D. Suenram and J.T. Hougen, *J. Chem. Phys.* 87, 6290 (1987).
- [4] T.A. Hu and T.R. Dyke, *J. Chem. Phys.* 91, 7348 (1989).
- [5] L. Martinache, S. Jans-Bürli, B. Vogelsanger, W. Kresa and A. Bauder, *Chem. Phys. Lett.* 149, 424 (1988).
- [6] G.T. Fraser, R.D. Suenram and L.H. Coudert, *J. Chem. Phys.* 90, 6077 (1989).
- [7] G.T. Fraser, R.D. Suenram, L.H. Coudert and R.S. Frye, *J. Mol. Spectrosc.* 137, 244 (1989).
- [8] K.L. Busarow, R.C. Cohen, G.A. Blake, K.B. Laughlin, Y.T. Lee and R.J. Saykally, *J. Chem. Phys.* 90, 3937 (1989).
- [9] Z.S. Huang and R.E. Miller, *J. Chem. Phys.* 88, 8008 (1988).
- [10] Z.S. Huang and R.E. Miller, *J. Chem. Phys.* 91, 6613 (1989).
- [11] T.R. Dyke, *J. Chem. Phys.* 66, 492 (1977).
- [12] J.T. Hougen, *J. Mol. Spectrosc.* 114, 395 (1985).
- [13] L.H. Coudert and J.T. Hougen, *J. Mol. Spectrosc.* 130, 86 (1988).
- [14] L.H. Coudert and J.T. Hougen, *J. Mol. Spectrosc.* 139, 259 (1990).
- [15] E. Zwart, J.J. ter Meulen and W.L. Meerts, *Chem. Phys. Lett.* 166, 500 (1990).
- [16] P. Verhoeve, E. Zwart, M. Versluis, M. Drabbels, J.J. ter Meulen, W.L. Meerts, A. Dymanus and D.B. McLay, *Rev. Scient. Instr.* 61, 1612 (1990).
- [17] K.L. Busarow, G.A. Blake, K.B. Laughlin, R.C. Cohen, Y.T. Lee and R.J. Saykally, *J. Chem. Phys.* 89, 1268 (1988).
- [18] K.M. Evenson, D.A. Jennings and F.R. Peterson, *Appl. Phys. Lett.* 44, 576 (1984).

Chapter 6

The submillimeter rotation-tunneling spectrum of $(\text{D}_2\text{O})_2$

E. Zwart, J.J. ter Meulen and W. Leo Meerts

Fysisch laboratorium, University of Nijmegen,
Toernooiveld, 6525 ED Nijmegen, The Netherlands.

6.1 Abstract

By direct absorption of submillimeter radiation in a planar supersonic jet, we have measured $K_a=1 \rightarrow K_a=2$ transitions of the fully deuterated water dimer $(\text{D}_2\text{O})_2$ in the region between 350 and 430 GHz. Several previously unknown constants could be derived. The A -rotational constant is determined as 120327.492(32) MHz. The sum or the difference of the largest tunneling splittings for $K_a=1$ and $K_a=2$ is approximately 21 GHz. The tunneling matrix element h_{2v} has been found to be a factor of 100 smaller than in $(\text{H}_2\text{O})_2$.

6.2 Introduction

The water dimer, $(\text{H}_2\text{O})_2$, has been the subject of extensive studies over the past years (see [1, 2] and references therein). It has been found that the vibrational ground state splits into 6 states as a result of tunneling. In Fig. 1 this splitting is drawn schematically. Each of the 6 vibrational tunneling levels has its own rotational structure, which is that of a near prolate symmetric top. The rotational structure is only indicated by drawing the first two K_a levels. The various J levels for one K_a are rather close together and are not drawn.

In a first approximation this splitting can be described by two tunneling motions. The tunneling motion with the lowest barrier corresponds to a 180° rotation of the hydrogen accepting H_2O monomer as a result of which the two hydrogen atoms are interchanged. This splits the vibrational ground state into two states, separated by approximately 200 GHz. These states are split again into three states by the interconversion tunneling motion in which the hydrogen donor/acceptor roles of the two H_2O monomers are interchanged. The result is a state shifted upward, a state shifted downward and a (doubly degenerate) state which is not shifted from the position without interconversion tunneling. The energy difference between the two nondegenerate states is usually called the interconversion tunneling splitting and amounts approximately to 20 GHz.

The fully deuterated species, $(\text{D}_2\text{O})_2$, probably has a similar energy level scheme. However, the tunneling splittings will be smaller. The expected energy level diagram is also

drawn in Fig. 1. In the theoretical model developed by Coudert and Hougen [3], which was used to fit all available experimental data of $(\text{H}_2\text{O})_2$, a high tunneling barrier was assumed. In particular for the internal rotation of the hydrogen accepting H_2O monomer, there may be some doubt about this assumption. The fully deuterated water dimer, $(\text{D}_2\text{O})_2$, will be a good candidate to test the high barrier assumption.

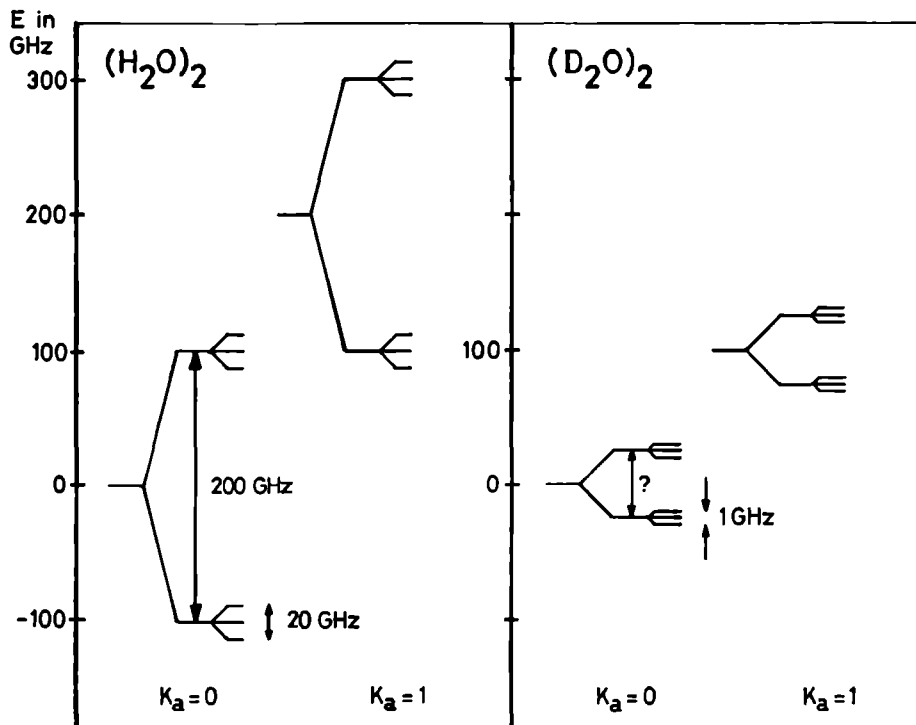


Figure 1. Energy level diagram of the lowest levels of $(\text{H}_2\text{O})_2$ and $(\text{D}_2\text{O})_2$.

Until now, only microwave measurements have been reported for $(\text{D}_2\text{O})_2$ [4, 5, 6, 7]. Dyke et al. [4] have measured $\Delta J=1$ rotational transitions for $K_a=2$ and $K_a=3$ and $\Delta J=0$ RF transitions for $K_a=2$. Coudert et al. [5] and Odutola et al. [6] have measured $\Delta J=1$ rotational and rotational tunneling transitions for $K_a=0$. Suenram et al. [7] have extended the previous work. They have measured many transitions for $K_a=0$ and $K_a=1$. Transitions in all symmetry states were found. As a result of these microwave measurements, for many rotational constants accurate values are known for the various tunneling levels for $K_a=0$ and $K_a=1$; in addition the interconversion tunneling splittings have been determined. The latter turned out to be approximately 1 GHz, i.e. a factor of 20 smaller than in $(\text{H}_2\text{O})_2$. Since no $\Delta K_a=1$ transitions were measured, the A -rotational constant and the largest tunneling splitting are not known precisely from the rotational data.

In this letter we present measurements of submillimeter transitions from $K_a=1$ to $K_a=2$. We have found 4 of the 6 possible bands. With these new results, the A -rotational constant is obtained and several tunneling splittings are derived or estimated.

6.3 Experimental

The spectrometer used in this work has been described in detail in [8] and [2, 9]. The radiation used in this work is produced by generating harmonics of microwave radiation from klystrons. Most lines have been measured with the 6th harmonic of a 60 GHz klystron. The tuning range of the fundamental is 10 GHz and its power 100 mW. The harmonics are generated in an open structure multiplier with a Schottky barrier diode and radiated in free space by an antenna. The harmonic needed for the experiment is filtered out with a monochromator. The radiation is detected by a 1.5 K Si bolometer in a direct absorption experiment.

The dimers are formed in a continuous expansion of Ar and D₂O, produced with a slit nozzle. The slit is 4 cm long and 15 μ m wide. The backing pressure is 500 Torr and the pressure in the vacuum chamber 0.05 Torr. The vacuum chamber is pumped by a 4000 m³/h roots pump. By passing Ar over D₂O, we produce a gas mixture with a few per cent. D₂O in Ar.

The S/N ratio of the measured lines was at most 10 with an RC time of 3 s.

6.4 Results

In order to facilitate the understanding of the observed bands, the $K_a=1$ and $K_a=2$ levels are drawn with enlarged tunneling splittings in Fig. 2. The symmetries in the figure are the symmetries of the rotational vibrational tunneling wavefunctions in G_{16} [10]. For $K_a>0$ each state is split due to asymmetry splitting and the following rules hold for the symmetries of the two components of a K -type doublet. For the upper component the symmetry on the left (right) must be taken for J even (odd). For the lower component the symmetry on the left (right) must be taken for J odd (even). E^\pm levels between A_1^1 , B_1^1 levels are called E_1^\pm and E^\pm levels between A_2^\pm , B_2^\mp levels are called E_2^\pm . E_1^\pm and E_2^\pm are no symmetries from G_{16} , but are convenient to distinguish the various E^\pm levels [7, 11]. Also given in the figure are the statistical weights. Selection rules for electric dipole transitions are $E_1^\pm \leftrightarrow E_1^\mp$, $E_2^\pm \leftrightarrow E_2^\mp$, $A_1^\pm \leftrightarrow A_1^\mp$, $A_2^\pm \leftrightarrow A_2^\mp$, $B_1^\pm \leftrightarrow B_1^\mp$, $B_2^\pm \leftrightarrow B_2^\mp$. Transitions $E_1^\pm \leftrightarrow E_2^\mp$ are not forbidden, but are assumed to be very weak in the high barrier limit [11]. The various transitions between $K_a=1$ and $K_a=2$ are drawn. Each arrow indicates a set of transitions following the above symmetry selection rules and the additional selection rules $\Delta J=0, \pm 1$. It is clear that the spectrum will consist of 6 bands, similar to vibrational bands, with P , Q and R branches. We will denote the bands by the symmetries of the initial states (e.g. (A_1^+, B_1^-)) and a line from a band by the J transition and the symmetry of the initial state (e.g. $R(4)A_1^+$). We have found 4 of the 6 possible bands. The other bands are probably too weak.

It has to be noted that the sign of the largest tunneling splitting cannot unambiguously be determined by theory and furthermore that this sign can be different for different K_a . This will be discussed in the next section.

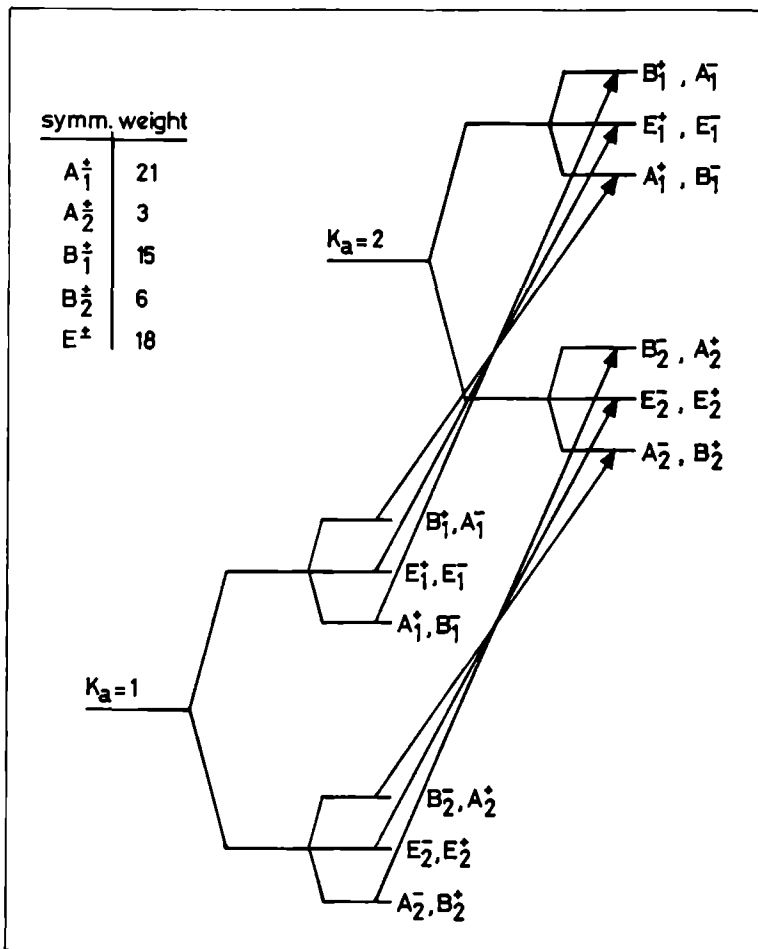


Figure 2. Energy level diagram for the $K_a=1$ and $K_a=2$ levels of $(D_2O)_2$. The allowed transitions between vibrational tunneling states and the symmetries of the rotational vibrational tunneling wavefunctions and their statistical weights are also given. For the symmetries of the two components of a K -type doublet the following rules hold. For the upper component the symmetry on the left (right) must be taken for J even (odd). For the lower component the symmetry on the left (right) must be taken for J odd (even).

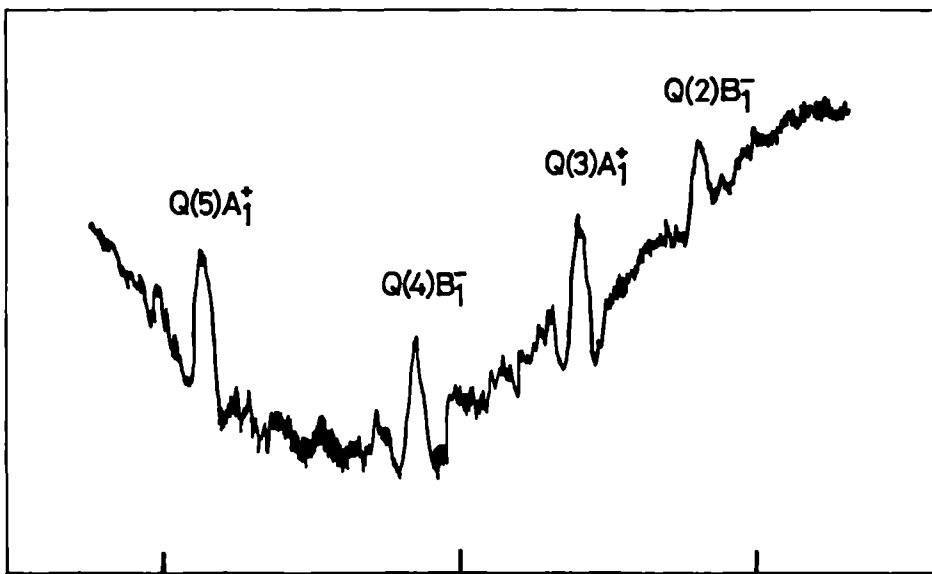


Figure 3. Part of the Q branch of the (A_1^+, B_1^-) band. The RC time is 3 s. The distance between the frequency markers is 10 MHz.

Fig. 3 is a part of the Q branch of the (A_1^+, B_1^-) band. This represents only one half of the Q branch. (In this part the lines are rather close together). Due to asymmetry doubling every line from a band appears twice. Because of the low intensity of the lines, the bands were not found in initial, fast scans. In that case only Ar-D₂O bands were observed [12]. Next, in slow scans, a few lines of (D₂O)₂ were detected. To distinguish from lines of complexes with Ar, we replaced Ar by Kr. With the help of the known microwave transitions and their spectroscopic constants, the other lines could be predicted and were then found. Especially the asymmetry constants for $K_a=1$ from [7] were very helpful in assigning the observed spectra. (The asymmetry splittings in $K_a=2$ are small).

We were only able to detect Q and R branch transitions. No P branch lines were detected, though their positions are very accurately known from combination differences with microwave results. For (H₂O)₂ it was found [9, 13] that the P lines are a few times weaker than Q or R lines. From Fig. 3 it is clear that we cannot afford to lose more than a factor of 3 in intensity. We therefore assume that the sensitivity is too low to detect P branch lines.

For the two bands of the E^1 levels, microwave measurements have been made in both initial and final states, so for these bands combination differences can be used to check our assignments. The combination differences agreed to within 0.1 MHz, which is approximately the accuracy of our frequency measurements. For the other two bands only microwave measurements in the initial states are available, so only combination differences can be

calculated between two submillimeter transitions with a common upper state. Unfortunately this was not possible for the present results because of the lack of P lines.

Additionally the relative intensities of the observed transitions confirm the assignments. Lines in the bands of E^\pm symmetry show no intensity alternation, whereas the other two bands do have an intensity alternation. The latter was to be expected from the ratio of statistical weights of A_1^+ and B_1^+ symmetry 21/15. Due to the low intensity of the lines, the exact intensity ratio is difficult to measure. However, a comparison of the strengths of two lines from a K -type doublet clearly shows intensity alternations. Furthermore bands which could not be detected are, due to their statistical weights, appreciably weaker than the observed ones. (See Fig. 2.)

The four bands were fitted separately to a near-prolate symmetric top formula. The same procedure was used by Suenram et al. [7]. The transitions were assumed to be c -type. The constants, given in Table 5, have their usual meanings. The parameter d is the distortion in the asymmetry constant for $K_a=1$. The constant c describes the asymmetry splitting in $K_a=2$ and is the same as used by Dyke et al. [4], i.e. the asymmetry splitting in $K_a=2$ is given by $c(J-1)J(J+1)(J+2)$. In all cases we obtained acceptable fits as can be seen from Tables 1-4. The resulting parameters are listed in Table 5.

6.5 Discussion

The standard deviations of the fits are somewhat smaller than the estimated uncertainty of the measured frequencies. The constants from the fit agree very well with those obtained from Refs. [4] and [7]. This proves that the assignment of the two bands which could not be checked with combination differences must be correct. From the results of the fit several constants which were previously unknown can be derived. This will be discussed below and the results are summarized in Table 6.

The interconversion tunneling splitting between (A_1^+, B_1^-) and (B_1^+, A_1^-) levels for $K_a=2$ can easily be calculated and the result is 808.72(16) MHz. Comparing this splitting with those for $K_a=0$ (1172 MHz) and $K_a=1$ (1077 MHz), we find that it strongly decreases with increasing K_a . A similar result was found for $(\text{H}_2\text{O})_2$.

There exists another tunneling motion in the water dimer in which the hydrogens of the hydrogen donating water monomer are interchanged. This tunneling motion causes shifts of the energy levels. Coudert and Hougen [14] proposed that for $(\text{H}_2\text{O})_2$ and $(\text{D}_2\text{O})_2$ levels of E symmetry are moved upward for K_a even and downward for K_a odd, respectively. For levels of A and B symmetry the levels shift downward and upward for K_a even and odd, respectively. If we neglect the dependence on the rotational tunneling state this shift is given by $|h_{2v}|$. Here h_{2v} is a matrix element from Ref. [14], whose value is proposed to be negative. It will be clear that as a result of this tunneling motion the $K_a=1 \rightarrow 2$ bands will be shifted upward (E levels) or downward (A, B levels) by $2|h_{2v}|$. The band origins yield $|h_{2v}|$. From the results of Table 5 we calculate $h_{2v} = -6.420(34)$ MHz. This value is approximately a factor of 100 smaller than in $(\text{H}_2\text{O})_2$ [15].

Again neglecting the dependence of the tunneling shift, described by h_{2v} , on the rotational tunneling state, the mean of the band origins of the two bands of E symmetry, $\bar{\nu}$, obeys

$$\bar{\nu} = 3A + |2h_{2v}|,$$

Table 1. Observed and calculated frequencies for the (E_2^- , E_2^+) band (in MHz).

Transition	Observed	Obs-calc
$Q(2)E_2^-$	350543.41	-0.01
$Q(2)E_2^+$	350722.40	-0.02
$Q(3)E_2^+$	350439.37	0.00
$Q(3)E_2^-$	350797.43	0.00
$Q(4)E_2^-$	350300.63	0.04
$Q(4)E_2^+$	350897.51	0.02
$Q(5)E_2^+$	350127.00	-0.02
$Q(5)E_2^-$	351022.61	-0.03
$Q(6)E_2^-$	349918.63	0.00
$Q(6)E_2^+$	351172.94	0.01
$R(1)E_2^+$	372324.02	0.02
$R(1)E_2^-$	372383.62	0.00
$R(2)E_2^-$	383108.23	0.00
$R(2)E_2^+$	383286.97	-0.01
$R(3)E_2^+$	393855.36	-0.03
$R(3)E_2^-$	394212.61	-0.01
$R(4)E_2^-$	404564.74	0.00
$R(4)E_2^+$	405159.59	0.02
$R(5)E_2^+$	415235.58	0.00
$R(5)E_2^-$	416126.84	-0.01

Table 2. Observed and calculated frequencies for the (E_1^- , E_1^+) band (in MHz).

Transition	Observed	Obs-calc
$Q(2)E_1^+$	371248.93	0.02
$Q(2)E_1^-$	371348.24	-0.02
$Q(3)E_1^-$	371154.70	0.00
$Q(3)E_1^+$	371353.46	0.03
$Q(4)E_1^+$	371029.15	-0.04
$Q(4)E_1^-$	371360.50	0.02
$Q(5)E_1^-$	370872.50	0.02
$Q(5)E_1^+$	371369.52	-0.02
$R(1)E_1^-$	393012.64	0.01
$R(1)E_1^+$	393045.73	-0.01
$R(2)E_1^+$	403798.16	-0.03
$R(2)E_1^-$	403897.49	0.01
$R(3)E_1^-$	414549.95	0.00
$R(3)E_1^+$	414748.48	0.01
$R(4)E_1^+$	425267.19	0.01
$R(4)E_1^-$	425597.94	-0.01

Table 3. Observed and calculated frequencies for the (B_1^+ , A_1^-) band (in MHz).

Transition	Observed	Obs-calc
$Q(2)B_1^+$	370282.21	0.00
$Q(2)A_1^-$	370381.32	0.03
$Q(3)A_1^-$	370189.67	0.02
$Q(3)B_1^+$	370387.86	-0.02
$Q(4)B_1^+$	370066.38	0.00
$Q(4)A_1^-$	370396.80	-0.03
$Q(5)A_1^-$	369912.50	-0.01
$Q(5)B_1^+$	370408.33	0.02
$R(1)A_1^-$	392045.05	-0.02
$R(1)B_1^+$	392078.06	-0.03
$R(2)B_1^+$	402831.91	0.06
$R(2)A_1^-$	402930.86	-0.02
$R(3)A_1^-$	413585.42	-0.01
$R(3)B_1^+$	413783.45	0.02
$R(4)B_1^+$	424305.09	-0.01
$R(4)A_1^-$	424635.00	0.00

Table 4. Observed and calculated frequencies for the (A_1^+ , B_1^-) band in MHz.

Transition	Observed	Obs.-calc
$Q(2)A_1^+$	372164.77	-0.01
$Q(2)B_1^-$	372264.07	-0.04
$Q(3)B_1^-$	372069.49	0.04
$Q(3)A_1^+$	372268.17	0.02
$Q(4)A_1^+$	371942.44	-0.01
$Q(4)B_1^-$	372273.67	-0.02
$Q(5)B_1^-$	371783.88	0.00
$Q(5)A_1^+$	372280.87	0.01
$R(1)B_1^-$	393929.15	0.00
$R(1)A_1^+$	393962.28	0.03
$R(2)A_1^+$	404713.88	-0.02
$R(2)B_1^-$	404813.17	0.00
$R(3)B_1^-$	415464.45	-0.01
$R(3)A_1^+$	415662.96	0.00
$R(4)A_1^+$	426180.13	0.01
$R(4)B_1^-$	426510.84	0.00

Table 5. Molecular constants of (D_2O)₂ and their errors obtained from the least squares fit of the various bands. The errors in the constants are the errors which result from the estimated uncertainty in the observed frequencies (0.1 MHz). The standard deviations are approximately a factor of 4 smaller. ν_0 (band origin), \bar{B}'' , \bar{B}' , $B''-C'''$ and σ (stand. dev.) are in MHz; D'' , D' , d'' and c' in kHz.

	(E_2^-, E_2^+)	(E_1^+, E_1^-)	(B_1^+, A_1^-)	(A_1^+, B_1^-)
ν_0	350647.442(84)	371343.19(11)	370374.85(11)	372260.18(11)
\bar{B}''	5430.505(14)	5432.934(18)	5432.740(18)	5433.100(18)
D''	35.45(25)	35.55(47)	35.51(47)	35.79(47)
$B''-C'''$	59.661(16)	33.1133(64)	33.0282(64)	33.1079(64)
d''	0.42(12)			
\bar{B}'	5428.085(15)	5425.493(22)	5425.549(22)	5425.471(22)
D'	35.46(26)	34.40(53)	34.10(53)	34.59(53)
c'	1.722(62)	0.43(11)	0.45(11)	0.43(11)
σ	0.017	0.019	0.022	0.019

Table 6. Constants and their errors obtained from the observed bands. $\Delta\nu_{int}$ is the interconversion tunneling splitting between (A_1^+, B_1^-) and (B_1^-, A_1^-) levels for $K_a=2$. All quantities are in MHz.

Constant	Value
$\Delta\nu_{int}$	808.72(16)
h_{2v}	-6.420(34)
A	120327.492(32)

where A is the rotational constant along the a -axis. Substituting $\bar{\nu}$ and h_{2v} in this equation we find $A = 120327.492(32)$ MHz.

Probably the most interesting quantity which cannot be determined from microwave spectroscopy concerns the largest tunneling motion for $(D_2O)_2$. From the submillimeter results we can obtain information about this quantity. However, there is some ambiguity which depends on the ordering of the levels. There are three possibilities, depicted in Fig. 4. In Fig. 4a the ordering for $K_a=1$ is the same as in $(H_2O)_2$. This assumption is supported by the observation that transitions in the (E_2^+, E_2^-) band are approximately 1.5 times stronger than those in the (E_1^+, E_1^-) band. Fig. 4a implies that the tunneling splitting in $K_a=2$ is 21 GHz larger than the tunneling splitting in $K_a=1$. If the levels are ordered as in Fig. 4b the splitting in $K_a=2$ is 21 GHz smaller than the splitting in $K_a=1$, i.e. a decrease of the tunneling splitting is found similar to that for the interconversion tunneling splitting. The ordering in Fig. 4c implies that the sum of the splittings in $K_a=1$ and $K_a=2$ is 21 GHz. In that case the tunneling splitting would be a factor of 20 smaller than for $(H_2O)_2$, which is the same factor as for the interconversion tunneling splitting. Though we have a weak preference for the assumption of Fig. 4a, we cannot unambiguously prove either of the assumptions.

Acknowledgement

The authors are grateful to Prof. J. Reuss and Dr. J. Hougen for having encouraged them to work on this problem. The authors wish to thank Mr. E. van Leeuwen, Mr. J. Holtkamp and Mr. F. van Rijn for their technical assistance. This work was financially supported by the Dutch Organization for Scientific Research (FOM/NWO).

References

- [1] G.T. Fraser, to be published in International Reviews in Physical Chemistry.

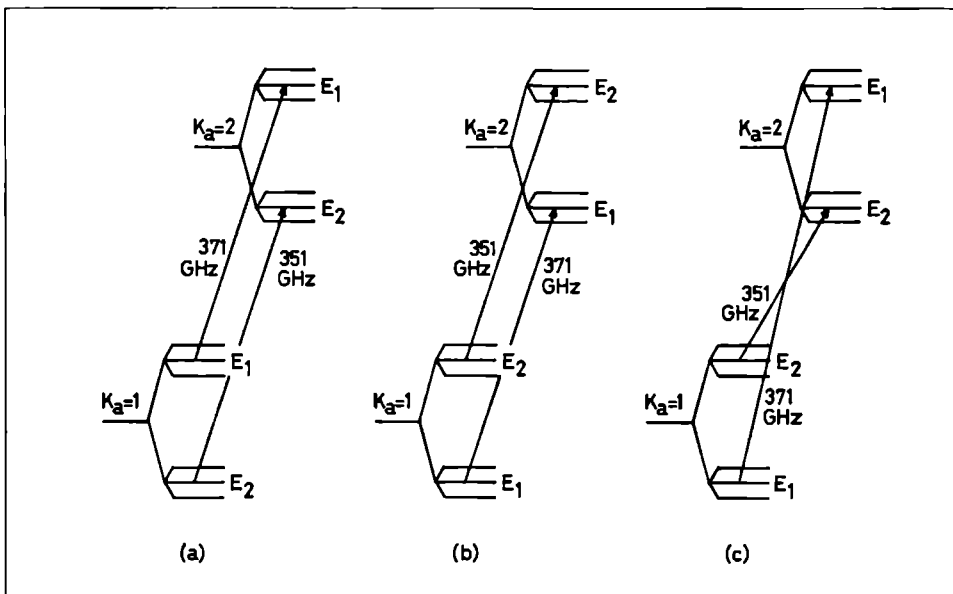


Figure 4. The various possible assignments of the observed bands. E_1 and E_2 denote the levels for which the possible rotational vibrational tunneling symmetries are E_1^- and E_2^- respectively.

- [2] E. Zwart, J.J. ter Meulen and W.L. Meerts, *Chem. Phys. Lett.* 166 (1990) 500.
- [3] L.H. Coudert and J.T. Hougen, *J. Mol. Spectrosc.* 139 (1990) 259.
- [4] T.R. Dyke, K.M. Mack and J.S. Muentner, *J. Chem. Phys.* 66 (1977) 498.
- [5] L.H. Coudert, F.J. Lovas, R.D. Suenram and J.T. Hougen, *J. Chem. Phys.* 87 (1987) 6290.
- [6] J.A. Odutola, T.A. Hu, D. Prinslow, S.E. O'Dell and T.R. Dyke, *J. Chem. Phys.* 88 (1988) 5352.
- [7] R.D. Suenram, G.T. Fraser and F.J. Lovas, *J. Mol. Spectrosc.* 138 (1989) 440.
- [8] P. Verhoeve, E. Zwart, M. Drabbels, M. Versluis, J.J. ter Meulen, A. Dymanus and D. McLay, to be published in *Rev. Scient. Instr.*
- [9] E. Zwart, J.J. ter Meulen, W.L. Meerts and L.H. Coudert, in preparation.
- [10] T.R. Dyke, *J. Chem. Phys.* 66 (1977) 492.
- [11] G.T. Fraser, R.D. Suenram and L.H. Coudert, *J. Chem. Phys.* 90 (1989) 6077.
- [12] E. Zwart, J.J. ter Meulen and W.L. Meerts, in preparation.
- [13] K.L. Busarow, R.C. Cohen, G.A. Blake, K.B. Laughlin, Y.T. Lee and R.J. Saykally, *J. Chem. Phys.* 90 (1989) 3937.
- [14] L.H. Coudert and J.T. Hougen, *J. Mol. Spectrosc.* 130 (1988) 86.
- [15] G.T. Fraser, R.D. Suenram, L.H. Coudert and R.S. Fryc, *J. Mol. Spectrosc.* 137 (1989) 244.

Chapter 7

Unassigned bands of $(\text{NH}_3)_2$

7.1 Introduction

Gas phase spectroscopy of $(\text{NH}_3)_2$ was started a few years ago in the infrared and in the microwave frequency regions. The infrared results were obtained by several groups [1, 2, 3, 4, 5] and it was found that the spectrum is broadened by predissociation. The predissociation spectrum around $10 \mu\text{m}$ consists of two broad and partially structured peaks. No results for the internal motions in the complex could be obtained.

The microwave spectrum, measured in the group of Klemperer, by Fraser et al. [2] and by Nelson et al. [6, 7] consists of four rotational transitions, belonging to two tunneling levels. From the values of electric-dipole moments and electric-quadrupole coupling constants, determined for several isotopomers of $(\text{NH}_3)_2$, the conclusion was drawn that the equilibrium structure is not the expected hydrogen bonded structure. A group theoretical analysis was also made [8]. To determine the nature of the energy levels it was assumed that $(\text{NH}_3)_2$ can be described with a model allowing tunneling through high barriers, similar to what has been found for $(\text{H}_2\text{O})_2$ (see [9, 10] and references therein) and $(\text{HF})_2$. Recently, a far infrared study between 630 and 840 GHz was conducted in Saykally's group by Havenith et al. [11]. Six bands could be rotationally assigned. They were discussed within the above-mentioned high barrier tunneling model. Evidence was obtained that this model is correct.

During scans through a supersonic expansion with a gas mixture of NH_3 (3%) in Ar between 200 and 500 GHz (approximately 30% of this region was actually scanned), we found three strong $(\text{NH}_3)_2$ bands. Since only one band has levels in common with the bands studied by Havenith et al., assignment to tunneling levels is rather difficult and here we will only present the observed bands and some remarks which might help future assignment. It has to be noted that there are still some unassigned lines in the investigated region. In the higher frequency region (above 350 GHz), the density of $(\text{NH}_3)_n$ lines is rather high. Below 350 GHz most detected transitions could be assigned to Ar- NH_3 . The Ar- NH_3 results have been reported separately [12, 13] Experimental details can be found there.

7.2 Results

The rotational assignment of the bands follows from the transitions involving the lowest J 's. One band is $K=0 \rightarrow 0$, and consists of a P and an R branch. The other two bands are $|K|=1 \rightarrow 1$ and consist of a P , Q and R branch. The intensities of the transitions of the Q branches behave like those of a parallel transition, as expected. Only one of the $|K|=1 \rightarrow 1$ bands shows well resolved K -type doublets. The two lines from a doublet have the same

intensity. The other $|K|=1\rightarrow 1$ band only shows a splitting for high J values. Probably this splitting is due to K -type doubling.

The observed transitions are listed in Table 1. The estimated uncertainties in the observed frequencies are 0.10 MHz. In Tables 1a and 1b only the J value is given to denote the energy levels. In Table 1c the asymmetric rotor notation is used, since for every J there are two possible energy levels. Several transitions of the two $|K|=1\rightarrow 1$ bands could be checked for consistency with combination differences. The transition frequencies of the $K=0\rightarrow 0$ band have been fitted with the usual expression for the energy levels

$$E = E_0 + BJ(J+1) - DJ^2(J+1)^2 + HJ^3(J+1)^3. \quad (7.1)$$

Eq. 1 is also used for the $|K|=1\rightarrow 1$ band with band origin at 453 GHz, since this band shows no K -type doubling. For the $|K|=1\rightarrow 1$ band with band origin at 486 GHz we used

$$E = E_0 + BJ(J+1) - DJ^2(J+1)^2 + HJ^3(J+1)^3 \pm [(1/4)(B-C)J(J+1) - dJ^2(J+1)^2 + hJ^3(J+1)^3]. \quad (7.2)$$

The constants, obtained from the fit, are listed in Table 2. The residuals of the fit are listed in Table 1.

With the use of the same method as described in [13], relative integrated absorption intensities for $R(3)$ transitions of the bands presented here and for the strongest bands of [11] have been determined. The results are given in Table 3. The estimated uncertainties in the tabulated intensities are 30%.

7.3 Discussion

Since we are not able to assign our bands, we will not go into the details of the methods used by Nelson and Havenith to interpret their spectra. The results of these studies will be used below. In short, it was assumed that $(\text{NH}_3)_2$ possesses a well defined equilibrium structure. Due to tunneling, the energy levels split up. To describe the nature of these tunneling levels the molecular symmetry (MS) group G_{36} was used. Apart from tunneling effects, the spectrum is similar to that of a near prolate asymmetric rotor and thus quantum numbers J and K or J , K_a and K_c can be used. The same model was successfully used for $(\text{H}_2\text{O})_2$ and $(\text{HF})_2$. Havenith concluded that all bands described in [11] involve a vibrational transition with an approximate vibrational transition frequency of approximately 600 GHz.

The intensities of Table 3 show that the observed bands are strong. In particular the $K=0\rightarrow 0$ band is as strong as or somewhat stronger than the strong $K=0\rightarrow 0$ bands of [11]. It should be noted that the intensities of Table 3 have to be corrected with a frequency dependent factor to find the relative magnitudes of the squares of the transition dipole moments. The most interesting features of the observed bands are :

- 1). $K=0\rightarrow 0$, band origin at 483 GHz. This band has the same lower level as the $K=0\rightarrow 1$ transition at 734 GHz, found by Havenith. This was checked by calculating combination differences. The latter transition was assigned as $A_1\rightarrow A_3$. Here A_1 and A_3 are the symmetries of the vibrational tunneling levels (i.e. without overall rotation) under the group G_{16} . With the use of the model of Ref. [11], our transition involves a vibrational transition. The band origin is rather low, however, compared with the expected value. The strength

Table 1a. $K=0\rightarrow 0$ band with band origin at 483 GHz; observed frequencies and residuals of the fit (in MHz).

J'	J''	Frequency	Obs-Cal
8	9	383425.35	0.00
7	8	395324.85	-0.01
6	7	407030.22	0.03
5	6	418538.25	0.00
4	5	429846.17	-0.02
3	4	440951.39	-0.01
2	3	451851.51	0.01
1	2	462544.37	0.01
0	1	473028.10	0.00
1	0	493361.85	-0.01
2	1	503209.32	0.00
3	2	512842.51	0.00
4	3	522260.77	0.00

Table 1b. $|K|=1\rightarrow 1$ band with band origin at 453 GHz; observed frequencies and residuals of the fit (in MHz).

J'	J''	Frequency	Obs-Cal
5	6	394443.63	-0.01
4	5	404262.96	0.03
3	4	414075.83	-0.04
2	3	423900.65	-0.03
1	2	433754.32	0.03
1	1	453656.39	-0.01
2	2	453764.64	0.03
3	3	453913.37	0.03
2	1	473666.66	-0.05
3	2	483777.31	0.04
4	3	493924.97	-0.03
5	4	504093.69	0.00
6	5	514264.15	0.00

Table 1c. $|K|=1\rightarrow 1$ band with band origin at 486 GHz; observed frequencies and residuals of the fit (in MHz).

$J'_{K'_a, K'_c}$	$J''_{K''_a, K''_c}$	Frequency	Obs-Cal
6 ₁₆	7 ₁₇	408864.25	0.20
6 ₁₅	7 ₁₆	409242.96	0.00
5 ₁₅	6 ₁₆	420725.76	-0.87
5 ₁₄	6 ₁₅	421031.29	-0.04
4 ₁₄	5 ₁₅	432388.56	0.84
4 ₁₃	5 ₁₄	432616.78	0.35
3 ₁₃	4 ₁₄	443825.84	0.26
3 ₁₂	4 ₁₃	443976.91	-0.12
2 ₁₂	3 ₁₃	455007.43	-0.65
2 ₁₁	3 ₁₂	455088.46	-0.31
1 ₁₁	2 ₁₂	465902.24	-0.04
1 ₁₀	2 ₁₁	465929.26	0.37
1 ₁₀	1 ₁₁	486433.19	0.61
1 ₁₁	1 ₁₀	486398.24	0.13
2 ₁₁	2 ₁₂	485843.64	-0.08
2 ₁₂	2 ₁₁	485744.75	-0.59
3 ₁₂	3 ₁₃	484980.92	-0.06
3 ₁₃	3 ₁₂	484798.12	0.03
2 ₁₂	1 ₁₁	506248.68	-0.35
2 ₁₁	1 ₁₀	506339.61	0.07
3 ₁₃	2 ₁₂	515553.29	0.25
3 ₁₂	2 ₁₁	515718.21	-0.03
4 ₁₄	3 ₁₃	524592.01	0.20
4 ₁₃	3 ₁₂	524838.03	0.17

Table 2. Constants obtained from the fit^{a)}.

	$K=0 \rightarrow 0$	$ K =1 \rightarrow 1$	$ K =1 \rightarrow 1$
ν_{BO}	483301.067(54)	453599.485(96)	486731.35(35)
B''	5136.601(13)	4974.023(24)	5125.409(53)
D''	58.53(34)	-191.7(1.3)	58.8(1.5)
H''		-605(20)	
$B'' - C''$			1.965(46)
B'	5030.494(13)	5002.952(12)	4966.441(95)
D'	48.47(50)	46.71(24)	-428.2(5.2)
H'			-2498(73)
$B' - C'$			33.38(14)
d'			111.7(3.1)
h'			857(53)
σ	0.01	0.03	0.38

^{a)} ν_{BO} is the band origin; σ is the standard deviation of the fit; see Eqs. 1 and 2 for the other constants; all constants are in MHz, except D and d in kHz and H and h in Hz. Between parentheses we list either the errors, calculated from the estimated 0.10 MHz frequency uncertainties (first two columns) or the standard deviations (last column), whichever are larger.

Table 3. Relative integrated absorption intensities of the $R(3)$ transitions of several bands of $(\text{NH}_3)_2$.

	Frequency ^{a)}	Intensity ^{b)}
$ K =1 \rightarrow 1^c)$	493924.97	59
$K=0 \rightarrow 0^c)$	522260.77	100
$ K =1 \rightarrow 1^c)$	524838.03	30
$K=0 \rightarrow 0^d)$	654916.66	83
$K=0 \rightarrow 0^d)$	656097.23	88

^{a)} The estimated uncertainties in the measured line positions are 0.10 MHz.

^{b)} The estimated uncertainties in the measured intensities are 30 %.

^{c)} This work.

^{d)} Ref. [11].

of the band, compared with that of the $K=0\rightarrow 0$ bands observed by Havenith (see Table 3), is unexpected in view of nuclear spin statistics. The nuclear spin statistical weight of A symmetry states (our band) is approximately two times less than that of G symmetry states (Havenith's band) [11].

2). $|K|=1\rightarrow 1$, band origin at 453 GHz. This band has no level in common with the bands of [11]. A remarkable effect of this band is that the K -type doubling is not resolved in this band. For high J value we do see a splitting however, which is probably due to K -type doubling.

3). $|K|=1\rightarrow 1$, band origin at 486 GHz. This band also has no level in common with the bands of [11]. The equal intensity of the two components of a K -type doublet indicates that the symmetry of the vibration tunneling functions must be G , E_1 or E_2 [11]. The sign of the K -type doubling is equal for upper and lower state. This is contrary to what has been found for the bands of [11].

Acknowledgement

We would like to thank Dr. M. Havenith for several stimulating discussions.

References

- [1] M.J. Howard, S. Burdensky, C.F. Giese and W.R. Gentry, *J. Phys. Chem.* 79, 192 (1983).
- [2] G.T. Fraser, D.D. Nelson, Jr., A. Charo and W. Klemperer, *J. Chem. Phys.* 82, 2535 (1985).
- [3] M. Snels, R. Fantoni, R. Sanders and W.L. Meerts, *Chem. Phys.* 115, 79 (1987).
- [4] B. Heijmen, A. Bizzarri, S. Stolte and J. Reuss, *Chem. Phys.* 126, 201 (1988).
- [5] F. Huisken and T. Pertsch, *Chem. Phys.* 126, 213 (1988).
- [6] D.D. Nelson, Jr., G.T. Fraser and W. Klemperer, *J. Chem. Phys.* 83, 6201 (1985).
- [7] D.D. Nelson, Jr., W. Klemperer, G.T. Fraser, F.J. Lovas and R.D. Sucram, *J. Chem. Phys.* 87, 6364 (1987).
- [8] D.D. Nelson, Jr. and W. Klemperer, *J. Chem. Phys.* 87, 139 (1987).
- [9] L.H. Coudert and J.T. Hougen, *J. Mol. Spectrosc.* 139, 259 (1990).
- [10] E. Zwart, J.J. ter Meulen and W.L. Meerts, *Chem. Phys. Lett.* 166, 500 (1990).
- [11] M. Havenith, Thesis, University of Bonn, 1990.
- [12] E. Zwart and W.L. Meerts, submitted to *Chem. Phys.*
- [13] E. Zwart, H. Linnartz, W.L. Meerts, G.T. Fraser, D.D. Nelson, Jr. and W. Klemperer, in preparation.

Chapter 8

The submillimeter rotation-tunneling spectrum of Ar-D₂O and Ar-NH₃

E. Zwart and W. Leo Meerts

Fysisch Laboratorium, University of Nijmegen,
Toernooiveld, 6525 ED, Nijmegen.

8.1 Abstract

Two bands for Ar-D₂O and one band for Ar-NH₃ have been observed for the first time in the frequency region 300-500 GHz. For both complexes the bands are explained in terms of a nearly free internal rotor model, following earlier investigations of this type of complexes. We found evidence that this model is correct for Ar-D₂O. Two of the internal rotor states studied for the Ar-D₂O complex show a Coriolis interaction and the interaction constant is determined. The hyperfine constants for the studied excited state of the Ar-NH₃ complex turn out to be large.

8.2 Introduction

The energy levels of weakly bound complexes are in many ways different from the energy levels of rigid molecules. Due to the fact that the barriers to internal motion are often rather low, effects like the inversion motion in NH₃ or the internal rotation of a CH₃ group can be important. The two limiting cases for such a complex are in general terms the rigid case and the case in which one of the subunits can freely rotate within the complex.

If the complex behaves more like a rigid rotor as e.g. (H₂O)₂ [1, 2] the internal motions can be described by the high tunneling barrier model which was also used for the inversion motion in NH₃. The tunneling through the barriers splits the vibrational ground state of (H₂O)₂ into 6 vibration tunneling levels. The rotational energy level structure of the (H₂O)₂ in its equilibrium configuration, which is that of a near prolate asymmetric rotor, is superimposed on this.

If, on the other hand, the complex is more like a molecule with a freely rotating subunit the high barrier model can no longer be used. The situation is usually not completely analogous to the well known case of internal rotation in which e.g. a CH₃ group can almost freely rotate around a fixed axis. In a nonrigid complex the internal rotation can be around any axis.

Many complexes with Ar have been studied in the past 15 years. Though the binding with an Ar atom is generally expected to be rather weak, some complexes, like Ar-CO₂ [3] could be described with the rigid rotor model. In Ar-H₂ [4] on the other hand, the H₂ molecule was found to be almost freely rotating within the complex. Ar-HCl [5] and Ar-HF [6] are also in the low barrier limit. From extensive experimental results, accurate potential surfaces could be derived. For the complexes of Ar with the polyatomic molecules H₂O and NH₃ there are strong indications but still no real experimental evidence that they behave like Ar-HCl and Ar-HF. Work on Ar-H₂O and Ar-NH₃ is still in progress and the details of the internal motions and the potential energy surface will probably be unraveled in the next few years.

Far infrared transitions of Ar-H₂O have been reported by Cohen et al. [7, 8]. Four bands were published. These could be explained both with a high tunneling barrier model and with a nearly free internal rotor model. The latter was regarded as the most probable. No far infrared results have been published yet for the complex with the fully deuterated water molecule, Ar-D₂O [9]. Very recently microwave measurements of Ar-H₂O for several H₂O isotopic species were made by Fraser et al. [10].

Microwave results were published by Fraser et al. [11] and by Nelson et al. [12] for Ar-NH₃. Three $\Delta K=0$, $\Delta J=1$ rotational transitions in $K=0$ have been assigned. Many other transitions were observed but these could not be assigned. Evidence was obtained that the NH₃ subunit in the complex is inverting (like free NH₃) and nearly freely rotating. Also infrared transitions found by Bizarri et al. [13] provided a strong indication that the NH₃ is inverting within the Ar-NH₃. No transitions in the far infrared region have been published [14]. Recently, ab initio calculations have been made by van Bladel et al. [15]. These calculations predict that the complex can be described in the limit of a free internal rotor.

In the present paper one band for Ar-NH₃ and two bands for Ar-D₂O are reported for the first time. The rotational assignment for all observed transitions in a band was unambiguous. For each of the bands a tentative assignment of the van der Waals motion in the complex is given. For Ar-D₂O the bands strongly suggest that this complex is in the nearly free internal rotor limit, which is a strong indication that Ar-H₂O is also in this limit.

8.3 Experiment

The spectra were recorded by a direct absorption experiment of submillimeter radiation in a supersonic expansion [2]. The radiation is produced by generating harmonics of a 60 GHz klystron in an open structure multiplier. The harmonic which is used for the experiment is selected with a grating. The power of the fundamental radiation is approximately 100 mW with a tuning range of 10 GHz. The radiation is detected by a Si or InSb bolometer. The estimated uncertainty of measured linepositions is 0.1 MHz.

The complexes are formed in a supersonic expansion from a continuous slit nozzle of 4 cm long and 15-25 μm wide. The construction is similar to the one described by Busarow et al. [16]. The backing pressure is 500 mbar and the pressure in the vacuum chamber is $5 \cdot 10^{-2}$ mbar. The vacuum chamber is pumped by a 4000 m³/h roots pump. A mixture of a few percent D₂O or NH₃ in Ar is expanded through the slit. The mixture with D₂O is produced by blowing the Ar through a vessel containing D₂O. The mixture with NH₃ is produced by

adding NH_3 by means of a needle valve to the Ar gas tube leading to the nozzle. To check if the transitions are due to complexes with Ar we exchanged Ar for Kr or Ne. One of the Ar- D_2O transitions was measured with a mixture of 50% HDO, 25% D_2O and 25% H_2O . The line strength decreased approximately a factor of 4 compared with the strength with pure D_2O , thus proving that the transition is not from Ar-HDO.

In the search for Ar- D_2O transitions several 10 GHz frequency intervals between 320 and 420 GHz were scanned. Since the P and R branches extend over a wide frequency range with a line spacing of approximately 6 GHz, it was not necessary to scan the complete frequency region. The same procedure was used for Ar- NH_3 . Here several intervals of 10 GHz between 380 and 500 GHz were investigated. The maximum signal to noise ratios of both Ar- D_2O and Ar- NH_3 transitions were 50 at an RC time of 1 s.

8.4 Theoretical

As discussed in the Introduction it is expected that the Ar- D_2O and Ar- NH_3 complexes can be described with a nearly free internal rotor model. In a recent paper [17] Hutson discussed this model for Ar-(asymmetric rotor) or Ar-(symmetric rotor) complexes. It was used to explain the far infrared spectrum of Ar- H_2O observed by Cohen et al. We will use the Ar- H_2O results to explain our Ar- D_2O spectra, assuming that the spectra are similar. The symmetries of the first order wavefunctions described by Hutson and the Coriolis interactions will be evaluated. Furthermore we will discuss the results of new ab initio calculations for the Ar- NH_3 complex which were recently obtained by van Bladel et al.

In the following the term molecule stands for the molecule (i.e. H_2O , D_2O or NH_3) part of the complex. If the D_2O is freely rotating within the complex, i.e. if the potential surface is isotropic for the D_2O monomer, the lowest energy levels can be described by the rotational energy levels of D_2O , the end over end rotation of the (diatomic like) complex frame and the van der Waals stretch. The total energy is the sum of the three contributions. This case is drawn on the left hand side of Figs. 1a and 1b. The stretching frequency is assumed to be approximately equal to that of Ar- H_2O . The end over end rotational energy levels are too closely spaced for the scale of the figure and are not drawn. Figs. 1a and 1b correspond to states with different spin states as will be explained below.

According to Hutson the end over end rotational quantum number ℓ is no longer a good quantum number for most Ar-(molecule) complexes (with Ar- H_2 as the most prominent exception). This is due to the fact that the anisotropic part of the potential couples states with different ℓ . In case of sufficiently high anisotropy the projection of the total angular momentum J on the complex axis, denoted by K , is nearly a good quantum number. This is the case for most molecules in low J states. The Hamiltonian equation for the angular motions can be solved in a basis of

$$|j, k, K, J, M\rangle = \left[\frac{(2J+1)(2j+1)}{32\pi^3} \right]^{1/2} D_{MK}^{j*}(\alpha, \beta, 0) D_{Kk}^{j*}(\phi, \theta, \chi) \quad (8.1)$$

Here the D 's are rotation matrices and the D^* 's symmetric top wavefunctions in the convention of Ref. [18]. Small letters refer to the molecule rotational quantum numbers and capital letters to the rotational quantum numbers of the complex as a whole. The rotation of the molecule is viewed in a frame with the complex axis as z -axis. For this reason the quantum

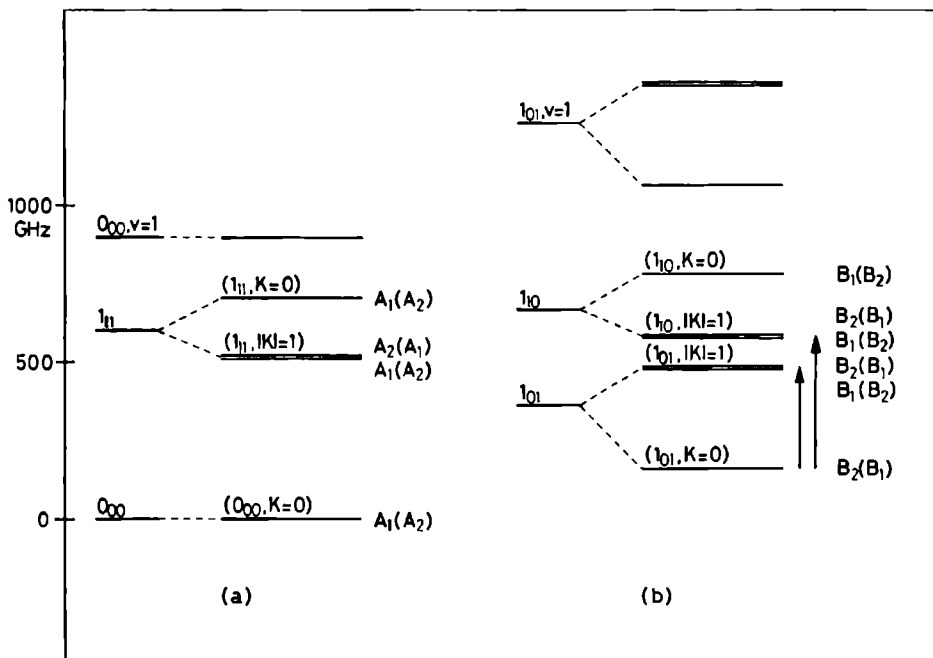


Figure 1. Energy level scheme of Ar-D₂O.

Table 1. Effect of the $C_{2v}(M)$ group operations on the basisfunctions from Eq. 1.

E	$ j, k, K, J, M\rangle =$	$ j, k, K, J, M\rangle$
(12)	$ j, k, K, J, M\rangle = (-1)^k$	$ j, k, K, J, M\rangle$
E^*	$ j, k, K, J, M\rangle = (-1)^{J+k}$	$ j, -k, -K, J, M\rangle$
(12)*	$ j, k, K, J, M\rangle = (-1)^J$	$ j, -k, -K, J, M\rangle$

number K appears twice and the third angle in D_{MK}^{J*} is set to 0. The Euler angles α and β define the direction in the space fixed frame of reference of the vector pointing from the center of mass of the molecule to the Ar and thus describe the rotation of the complex as a whole. The complex fixed axes system is obtained by first rotating the space fixed frame over an angle α around the z -axis and then over β around the new y -axis. The third axes system which is used is the molecule fixed axes system. The z -axis of this axes system is defined to be along the C_2 axis of the molecule. The x -axis is in the plane of the molecule. The Euler angles ϕ , θ and γ define the orientation of the molecule fixed axes system in the complex fixed axes system and thus describe the rotation of the molecule relative to the complex frame.

The advantage of using the quantum number K rather than ℓ is that the intermolecular potential only has matrix elements diagonal in K . States with different K are only coupled by Coriolis interaction. However, this is only a minor effect and therefore K is nearly a good quantum number. By the analogy with a linear molecule with vibrational angular momentum states with $|K|=0,1,\dots$ are often called Σ, Π, \dots , respectively. It should furthermore be noted that the matrix elements of the potential energy operator are independent of J and M and that this operator couples states with different j and k . Consequently J and M are good quantum numbers, while j and k are not.

According to Hutson the first approximation solutions of the Hamiltonian for Ar-D₂O can be obtained from a linear combination of the functions from Eq. 1. The part describing the molecule rotation is the usual asymmetric rotor function. Next, symmetric and anti-symmetric combinations of states with $+K$ and $-K$ must be taken similar to the usual procedure for symmetric rotor functions. Those first order solutions are constructed to form a basis for irreducible representations of the molecular symmetry group $C_{2v}(M)$ [19]. After calculating the transformation properties of the Euler angles in Eq. 1, the transformation properties of the basis functions from Eq. 1 can be derived. In Table 1 the resulting transformations are given and from these the symmetries of the first order solutions directly follow. In Table 2 these solutions and their symmetries are given. They are denoted by the monomer rotational state and the absolute value of K , e.g. $(1_{01}; |K|=1)$. The symmetry is given first for even J and between parentheses for odd J .

Hutson also gives the non diagonal matrix elements for the Coriolis interaction.

$$\langle j, k, K, J, M | H_{Cor} | j, k, K \pm 1, J, M \rangle = B_{Cor} [J(J+1) - K(K \pm 1)]^{1/2} [J(J+1) - K(K \pm 1)]^{1/2} \quad (8.2)$$

where B_{Cor} is equal to the B rotational constant for the end over end rotation of the complex.

Table 2. First order wavefunctions of the Ar-D₂O states and their symmetries.

wavefunction	state,symmetry
$ 0, 0, 0, J, M\rangle$	$(0_{00};K=0), A_1(A_2)$
$ 1, 0, 0, J, M\rangle$	$(1_{11};K=0), A_1(A_2)$
$\{ 1, 0, 1, J, M\rangle + 1, 0, -1, J, M\rangle\}/\sqrt{2}$	$(1_{11}; K =1), A_1(A_2)$
$\{ 1, 0, 1, J, M\rangle - 1, 0, -1, J, M\rangle\}/\sqrt{2}$	$(1_{11}; K =1), A_2(A_1)$
$\{ 1, 1, 0, J, M\rangle + 1, -1, 0, J, M\rangle\}/\sqrt{2}$	$(1_{10};K=0), B_1(B_2)$
$\{ 1, 1, 0, J, M\rangle - 1, -1, 0, J, M\rangle\}/\sqrt{2}$	$(1_{01};K=0), B_2(B_1)$
$\{ 1, 1, 1, J, M\rangle + 1, -1, 1, J, M\rangle +$ $ 1, -1, -1, J, M\rangle + 1, 1, -1, J, M\rangle\}/2$	$(1_{10}; K =1), B_1(B_2)$
$\{ 1, 1, 1, J, M\rangle + 1, -1, 1, J, M\rangle -$ $ 1, -1, -1, J, M\rangle - 1, 1, -1, J, M\rangle\}/2$	$(1_{10}; K =1), B_2(B_1)$
$\{ 1, 1, 1, J, M\rangle - 1, -1, 1, J, M\rangle +$ $ 1, -1, -1, J, M\rangle - 1, 1, -1, J, M\rangle\}/2$	$(1_{01}; K =1), B_1(B_2)$
$\{ 1, 1, 1, J, M\rangle - 1, -1, 1, J, M\rangle -$ $ 1, -1, -1, J, M\rangle + 1, 1, -1, J, M\rangle\}/2$	$(1_{01}; K =1), B_2(B_1)$

This equation allows the calculation of the off diagonal Coriolis matrix elements between the states from Table 2. The result is that there is only Coriolis interaction between two states which correlate with the same molecule rotational state. Furthermore the interaction only occurs between states which have both the same symmetry and the same J . In case the off diagonal matrix element between two states of Table 2 is nonvanishing this is equal to $2B_{Cor}\sqrt{J(J+1)}$.

The vibration rotation energy level diagrams of Ar-H₂O and Ar-D₂O are very similar. The difference is that the rotational constants of the D₂O molecule are approximately a factor of 2 smaller than those of H₂O, as a result of which internal rotor transitions of Ar-D₂O will be lower in frequency than those of Ar-H₂O. In addition the statistical weights are different for the two complexes. For Ar-D₂O, A_1 and A_2 states have a statistical weight of 6 and B_1 and B_2 states have a weight of 3. The corresponding states of Ar-H₂O have a statistical weight of 1 and 3 respectively. The same is true for the isolated D₂O and H₂O molecules.

We are now in a position to construct the energy level diagram of Ar-D₂O in the case of nearly free internal rotation. This is depicted on the right hand side of Figs. 1a and 1b. As a result of the anisotropy of the potential each free rotor state splits into two (degenerate) states with $|K|=1$ and one state with $K=0$. The two $|K|=1$ states are split by Coriolis interaction. The ordering of $K=0$ and $|K|=1$ states is assumed to be the same as for Ar-H₂O. The ordering of the levels in Fig 1b also follows from the tentative assignment of the bands we have observed. (See the next section.) The symmetries in the molecular symmetry group $C_{2v}(M)$ are given for even J and between parentheses for odd J . Since

states of different nuclear spin symmetry are assumed to relax separately in a molecular beam, they are drawn separately in Fig. 1.

Which states interact as a result of the anisotropy of the potential (and will be mixed) follows from symmetry considerations. Since J and the $C_{2v}(M)$ symmetries are good symmetry labels for the solutions of the vibration rotation Hamiltonian and since the potential must be symmetric for the operations of $C_{2v}(M)$ there are only couplings between states that have both the same J and the same symmetry species from $C_{2v}(M)$. Furthermore, the potential is diagonal in K , so only $K=0 \leftrightarrow K=0$ and $|K|=1 \leftrightarrow |K|=1$ interactions can occur. Eg. in Fig. 1b all $|K|=1$ states with symmetry species $B_1(B_2)$ can interact and similarly all $|K|=1$ states with $B_2(B_1)$. Consequently, 'pure' $(1_{01}; |K|=1)$ and $(1_{10}; |K|=1)$ wavefunctions will be mixed. The selection rules for Coriolis interaction are given above. The rule that only states of the same J and the same symmetry species interact also follows from the fact that Coriolis interaction is a vibration rotation interaction as are the interactions caused by the anisotropy of the potential. In this case the extra rule is that there is only Coriolis interaction between states which correlate with the same molecule rotational state. It is clear from Fig. 1 that Coriolis interaction causes a splitting of two degenerate $|K|=1$ states because one is affected while the other is not.

The symmetry of the electric dipole moment is A_2 (symmetric for all permutations and antisymmetric for all permutation inversions). The selection rules for electric dipole transitions are therefore : $A_1 \leftrightarrow A_2$ and $B_1 \leftrightarrow B_2$. Further $\Delta J=0, \pm 1$.

For Ar-NH₃ the situation is analogous. The molecular symmetry group is $D_{3h}(M)$ or, if inversion tunneling is neglected, $C_{3v}(M)$. If inversion is neglected the basis functions from Eq. 1 can be used to solve the Hamiltonian. The first order solutions, which are basis functions for the irreducible representations of the group $C_{3v}(M)$ can be obtained in the same way as for Ar-D₂O and Ar-H₂O. Only now the molecule part of the complex is a symmetric top. This has been worked out by van Bladel et al. who have recently performed new ab initio calculations for Ar-NH₃ in which they neglected the NH₃ inversion motion. These results will be briefly reviewed here and the results will be compared with those of Ar-H₂O.

The left hand side of Figs. 2a and 2b gives the energy levels in the limit of free rotation of the NH₃ molecule. As for Ar-H₂O the energy is a sum of the energies of the NH₃ rotation, the end over end rotation of the complex and the van der Waals stretch of the complex. The right hand side of Figs. 2a and 2b is taken from the ab initio calculations. Because the inversion motion in NH₃ has been neglected the symmetries of the vibration rotation wavefunctions are characterized by $C_{3v}(M)$. The A_1 and A_2 states which combine with A_1 nuclear spin state symmetry (weight 12) and E states which have E nuclear spin state symmetry (weight 12) are drawn separately. The energy levels are labeled by the first order solutions which sets the symmetric rotor wavefunction of the free NH₃ molecule with which the solution correlates and the absolute value of K . The symmetries are given for even J and between parentheses for odd J . The interactions which occur between the first order solutions follow the same rules as for Ar-D₂O. An interesting result of the ab initio calculations is that the states which we have called internal rotor state ($j=1, k=0; K=0$) and stretch state ($j=0, k=0; K=0; v_s=1$), respectively, in our crude first approximation are in fact heavily mixed. The selection rules for electric dipole transitions are $A_1 \leftrightarrow A_2$ and $E \leftrightarrow E$.

The A_1 and A_2 states of the Ar-NH₃ complex are very similar to the corresponding states

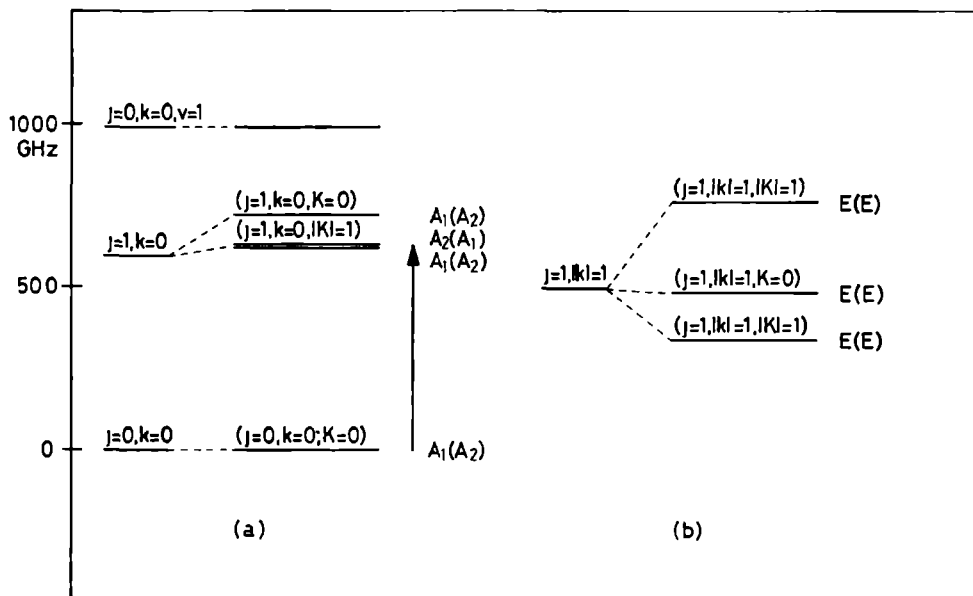


Figure 2. Energy level scheme of Ar-NH₃, neglecting the NH₃ inversion.

of Ar-H₂O and Ar-D₂O. The $j=1, k=0$ state of NH₃ splits into a $K=0$ and two $|K|=1$ states as a result of the anisotropic part of the potential. The Coriolis interaction splits the two $|K|=1$ states. The E states behave completely differently from what is known from Ar-H₂O. The two $|K|=1$ states have the same symmetry for a given J and obtain a large splitting due to the anisotropic potential.

Fraser et al. and Bizarri et al. have obtained an indication in their spectra that the NH₃ can invert in Ar-NH₃. In that case the appropriate molecular symmetry group is $D_{3h}(M)$. Van Bladel et al. have worked out the group theoretical consequences of this. Each of the E states splits into two and transitions will become doublets. However, this is not the case for transitions that correlate with $A_1 \leftrightarrow A_2$ transitions in $C_{3v}(M)$. In that case one component does not exist because of a statistical weight of 0. Consequently, the spectrum will be similar to the spectrum in which the NH₃ inversion in the complex is neglected.

8.5 Results

8.5.1 Ar-D₂O

For the Ar-D₂O complex we have studied two bands of the type $K=0 \rightarrow |K|=1$. Both bands consist of a P , Q and R branch. Each of the $|K|=1$ states is split into two states with a separation which is approximately proportional to $J(J+1)$. This is characteristic of Coriolis interaction or asymmetry doubling. From combination differences, using P and R branch transitions, it was found that both bands we observed have a common initial state. The observed bands are tentatively assigned as $(1_{01}; K=0) \rightarrow (1_{01}; |K|=1)$ and $(1_{01}; K=0) \rightarrow (1_{10}; |K|=1)$. The transition frequency of the $1_{01} \rightarrow 1_{10}$ rotational transition of the free D₂O molecule is 317 GHz which is in the frequency range in which the Ar-D₂O transitions were found. The sign of the doubling of $|K|=1$ states is as expected from Fig. 1. Fraser et al. reported microwave transitions within $(1_{01}; K=0)$. Ground state combination differences prove that their assignment agrees with the assignment proposed for the submillimeter results.

Cohen et al. also detected the $(1_{01}; K=0) \rightarrow (1_{10}; |K|=1)$ band for Ar-H₂O. The $(1_{01}; K=0) \rightarrow (1_{01}; |K|=1)$ band was not seen for Ar-H₂O. This may be caused by the fact that the latter band is probably around 300 GHz or lower where Cohen et al. have not searched. Furthermore, as was shown by Hutson, the band is expected to be very weak. The $(1_{01}; K=0) \rightarrow (1_{01}; |K|=1)$ transition of this complex correlates with the $1_{01} \rightarrow 1_{01}$ transition of H₂O. This transition is not allowed for free H₂O. However, if our assignment is correct, the $(1_{01}; |K|=1)$ and $(1_{10}; |K|=1)$ states of Ar-D₂O are only separated by 90 GHz. Consequently, these states will be strongly mixed by the anisotropic potential. Therefore, the eigenfunctions of the total Hamiltonian for these states are linear combinations of 'pure' $(1_{01}; |K|=1)$ and $(1_{10}; |K|=1)$ states. Since the $1_{01} \rightarrow 1_{10}$ transition is allowed for free D₂O both bands initially called $(1_{01}; K=0) \rightarrow (1_{01}; |K|=1)$ and $(1_{01}; K=0) \rightarrow (1_{10}; |K|=1)$ respectively become allowed for the Ar-D₂O complex. The intensity of the former band is expected to be somewhat weaker than that of the latter. A factor of 3 was found experimentally.

We will now consider other possible assignments of the observed bands. There are 4 possibilities: excitation of a van der Waals stretching vibration, a different D₂O rotational state assignment, hot bands and the possibility that the complex is nearly rigid.

The complex stretching vibration is expected to lie at approximately the same frequency as in Ar-H₂O. Since in Ar-H₂O the stretch was observed around 900 GHz [8] it is not expected that it will occur around 400 GHz in Ar-D₂O. Furthermore the effective rotational constants in the excited stretching states are expected to be significantly smaller than in the ground states (5-10 percent for Ar-H₂O). The results of the fits which are discussed below show that this is not the case.

The lowest transition connecting A_1 and A_2 states is expected around 600 GHz, since in the free rotor limit this transition correlates with the $0_{00} \rightarrow 1_{11}$ transition of free D₂O at 607 GHz. However in that case only one $K=0 \rightarrow |K|=1$ band is expected, which is in contrast with the observation of two of those bands. A possibility which should be taken into consideration is that the assignments of the two observed bands could be switched. As discussed above, the observed intensities do not favor this possibility.

Thirdly it is possible that hot bands were detected. The rotational temperature in the beam is estimated to be 5 K. At this temperature the population of levels 240 GHz above the ground state is a factor of 10 lower than that of ground state levels. Considering the strength of our spectrum observation of transitions originating in excited levels 240 GHz above the ground state can be regarded as an upper limit. In this case one of the $|K|=1$ states should be an excited complex stretch. As has already been discussed the B rotational constants indicate that this is not the case.

The last and perhaps most interesting consideration that should be made is whether we are right in assuming that the complex is in the nearly free internal rotor limit. If the complex is in the high barrier limit the bands have to be explained in terms of bending vibrational states, rotational states of a near prolate asymmetric rotor and tunneling through high barriers (as e.g. in (H₂O)₂). In this limit the two $K=0 \rightarrow |K|=1$ bands correspond to rotational transitions of a near prolate symmetric rotor. However, there can only exist a single $|K|=0 \rightarrow 1$ transition at such low frequencies. If we then assume, in this limit, that each state is split into two by the tunneling motion in which the two D atoms of D₂O change places we are again not able to explain the observation of two bands. If tunneling splitting is present two $|K|=0 \rightarrow 1$ bands should exist, but these do not have a common ground state. In short, it is concluded that the two observed bands can only be explained with the nearly free internal rotor model. This is a strong indication that Ar-H₂O is also in this limit.

Contributions from Coriolis interaction are hard to take correctly into account in a fit of the observed frequencies. The non zero off diagonal matrix elements between the first order solutions are given in the previous section. However, the two $|K|=1$ states are expected to be strongly mixed as is discussed above. Stretch wavefunctions or higher j rotational wavefunctions will also have a contribution to the exact wavefunctions. (See also the Ar-NH₃ paper by van Bladel et al.) Furthermore, we did not measure transitions involving ($1_{10}; K=0$) states. The latter will show Coriolis interaction with the ($1_{10}; |K|=1$) states.

In order to get a feeling for the effects of the Coriolis interaction it is instructive to calculate the contribution using the first order wavefunctions from Table 2. For every J one of the two $|K|=1$ states will not be affected by the interaction, while the other $|K|=1$ state interacts with the $K=0$ state which correlates with the same molecule rotational state and which has the same J . The unperturbed energies can be written as

$$E_0 = \nu_0 + B_0 J(J+1) - D_0 J^2(J+1)^2 + H_0 J^3(J+1)^3 + \dots$$

$$E_1 = \nu_1 + B_1 J(J+1) - D_1 J^2(J+1)^2 + H_1 J^3(J+1)^3 + \dots \quad (8.3)$$

while the Coriolis interaction takes the form

$$H_{Cor} = 2B_{Cor} \sqrt{J(J+1)}. \quad (8.4)$$

The coefficients 0 and 1 denote the absolute value of K . Because the interaction is between states of the same J , a 2×2 matrix has to be diagonalized for each J . The perturbed energies can therefore be easily calculated. The results are

$$\begin{aligned} E'_0 &= \nu_0 + B'_0 J(J+1) - D'_0 J^2(J+1)^2 + H'_0 J^3(J+1)^3 + \dots \\ E'_1 &= \nu_1 + B'_1 J(J+1) - D'_1 J^2(J+1)^2 + H'_1 J^3(J+1)^3 + \dots \end{aligned} \quad (8.5)$$

with

$$\begin{aligned} B'_0 &= B_0 \mp 4B_{Cor}^2/\Delta\nu \\ B'_1 &= B_1 \pm 4B_{Cor}^2/\Delta\nu. \end{aligned} \quad (8.6)$$

Here

$$\Delta\nu = |\nu_1 - \nu_0|, \quad (8.7)$$

is the band origin of the $K=0 \leftrightarrow |K|=1$ transition. The upper signs have to be used if $|K|=1$ is the upper state, and the lower signs otherwise. These expressions are only useful if the perturbing states are not too close together (i.e. if $B_{Cor}/\Delta\nu \ll 1$). Otherwise terms with a high power of $J(J+1)$ are important.

From these equations it can be concluded that we can fit the bands with a power series in $J(J+1)$. The unperturbed B values and $B_{Cor}^2/\Delta\nu$ can be deduced from the effective constants from the fit. The measured frequencies and the deviations from the fitted ones are given in Tables 3 and 4. The effective constants are given in Table 5. For the $(1_{01}; K=0) \rightarrow (1_{01}; |K|=1)$ transition $B_{Cor}^2/\Delta\nu$ and $\Delta\nu$ are both known. This results in $B_{Cor} = 2593.31$ MHz, which is indeed approximately equal to B_0 and B_1 .

8.5.2 Ar-NH₃

For Ar-NH₃ we studied one $K=0 \rightarrow |K|=1$ band showing a P , Q and R branch. From combination differences it is clear that the ground state is the same as the state studied by Nelson et al. The transitions in our spectra show a partially resolved hyperfine structure. The $|K|=1$ state is split into two states with a separation which is approximately proportional to $J(J+1)$, as in Ar-H₂O and Ar-D₂O.

The band has been assigned as $(j=0, k=0; K=0) \rightarrow (j=1, k=0; |K|=1)$. This assignment is the only one that fits into the scheme of Fig. 2. The two $(j=1, k=1; |K|=1)$ states are split too much and in addition the splitting is not proportional to $J(J+1)$. Nelson's assignment of the ground state agrees with ours. The fact that the inversion doubling is not observed also confirms that the observed transitions are between A states.

The observed Ar-NH₃ transitions show a hyperfine structure caused by the electric quadrupole moment of the ¹⁴N nucleus. Because the nuclear spin of the ¹⁴N nucleus is 1, each level with $J \geq 1$ splits into three levels. Although this splits each transition in a P , Q or R branch into many hyperfine components, we observe a splitting into only two or three.

Table 3. Frequencies of the Ar-D₂O ($1_{01};K=0$) \rightarrow ($1_{01};|K|=1$) band (in MHz).

Transition	Observed	Obs-calc
<i>P</i> (9)	286151.60	0.01
<i>P</i> (8)	290294.16	-0.02
<i>P</i> (7)	294584.78	0.01
<i>P</i> (6)	299029.93	0.00
<i>P</i> (5)	303635.47	0.01
<i>P</i> (4)	308406.24	0.01
<i>P</i> (3)	313346.09	0.00
<i>P</i> (2)	318457.69	-0.02
<i>Q</i> (1)	329209.16	-0.01
<i>Q</i> (2)	329225.88	0.00
<i>Q</i> (3)	329249.43	0.00
<i>Q</i> (4)	329278.03	0.00
<i>Q</i> (5)	329309.36	0.00
<i>Q</i> (6)	329340.61	-0.01
<i>Q</i> (7)	329368.59	-0.01
<i>Q</i> (8)	329389.75	0.01
<i>Q</i> (9)	329400.26	0.00
<i>R</i> (0)	334830.48	0.00
<i>R</i> (1)	340629.81	0.01
<i>R</i> (2)	346594.45	0.00
<i>R</i> (3)	352719.13	0.00
<i>R</i> (4)	358997.30	-0.01
<i>R</i> (5)	365421.36	0.04
<i>R</i> (6)	371982.39	-0.05
<i>R</i> (7)	378671.09	-0.02
<i>R</i> (8)	385477.11	0.05
<i>R</i> (9)	392389.53	-0.02

Table 4. Frequencies of the Ar-D₂O ($1_{01};K=0$) \rightarrow ($1_{10};|K|=1$) band (in MHz).

Transition	Observed	Obs-calc
<i>P</i> (9)	380426.47	0.00
<i>P</i> (8)	383658.52	0.00
<i>P</i> (7)	387168.84	-0.01
<i>P</i> (6)	390958.16	0.00
<i>P</i> (5)	395026.72	0.01
<i>P</i> (4)	399374.40	-0.01
<i>P</i> (3)	404000.86	-0.01
<i>P</i> (2)	408905.45	0.00
<i>Q</i> (1)	419686.25	0.00
<i>Q</i> (2)	419967.95	0.02
<i>Q</i> (3)	420389.80	-0.03
<i>Q</i> (4)	420951.17	0.01
<i>Q</i> (5)	421650.90	0.00
<i>Q</i> (6)	422487.66	0.01
<i>Q</i> (7)	423459.73	0.00
<i>Q</i> (8)	424565.04	0.00
<i>Q</i> (9)	425801.07	0.00
<i>R</i> (0)	425278.22	0.01
<i>R</i> (1)	431284.54	-0.01
<i>R</i> (2)	437562.59	-0.01
<i>R</i> (3)	444110.37	0.02

Table 5. Constants of the Ar-D₂O bands and their errors (resulting from the estimated accuracy of line positions of 0.1 MHz). The constants involving ν_{BO} (band origin), B and σ (standard deviation of the fit) are in MHz. The D 's are in kHz and the H 's are in Hz. The constants after σ are calculated with the results from the fit.

	$(1_{01};K=0) \rightarrow (1_{01}; K =1)$	$(1_{01};K=0) \rightarrow (1_{10}; K =1)$
ν_{BO}	329200.500(54)	419545.289(59)
B'_0	2729.114(10)	2729.112(16)
D'_0	52.96(24)	52.96(63)
H'_0	-13.5(1.7)	-13.4(7.2)
B'_1	2815.2130(92)	2866.584(19)
	2733.497(12)	2799.615(18)
D'_1	110.24(18)	61.65(90)
	78.66(31)	63.21(68)
H'_1	23.2(1.1)	-32(13)
	5.0(2.3)	-22.2(7.4)
σ	0.02	0.01
B_0	2810.830(11)	
B_1	2733.497(12)	2866.584(19)
$B_{Cor}^2/\Delta\nu$	20.4290(18)	16.7423(21)

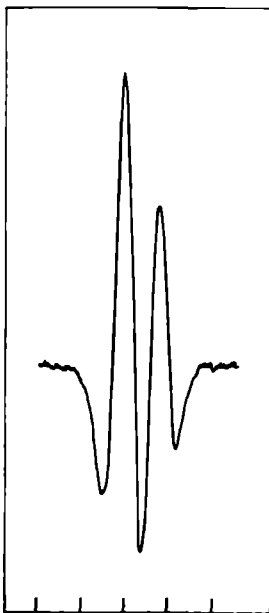


Figure 3. Hyperfine splitting of the Ar-NH₃ $R(3)$ transition. The distance between the frequency markers is 1 MHz.

All transitions in which only levels with $J \geq 3$ are involved split into two components, with an intensity ratio of approximately 1:2. (See Fig. 3.) For high J only transitions in which the change in the total angular momentum F equals the change in the quantum number J are important. This is a good approximation for the above-mentioned transitions with $J \geq 3$ at the level of accuracy of the present discussion. In this approximation each transition splits into three hyperfine components. Two of these are rather close together and cannot be resolved in our experiment, yielding a total absorption which is twice as strong as the individual absorptions. We have used the transitions between levels with $J \geq 3$ to obtain the rotational and hyperfine constants for the states studied for this complex. The observed frequencies were fitted to the Hamiltonian described below. In transitions involving levels with $J < 3$ more than three hyperfine components have an appreciable contribution to the observed lineshapes and consequently these transitions were not included in the fit. An exception is $R(0)$ in which the three possible transitions are well resolved.

The A states of Ar-NH₃ are similar to the Ar-D₂O states discussed above. Therefore the rotational transitions, neglecting hyperfine effects, can be fitted using effective rotational constants B , D and H . For the quadrupole hyperfine interactions the expressions from Townes and Schawlow [20] for a linear molecule with vibrational angular momentum or a near prolate symmetric rotor are used.

$$K = 0: H = -cQq_{aa}^{(0)} f(I, J, F)$$

$$|K|=1: H = \left(eQq_{aa}^{(1)} \frac{3 - J(J+1)}{J(J+1)} \pm \frac{1}{2} eQ(q_{bb} - q_{cc})^{(1)} \right) f(I, J, F) \quad (8.8)$$

The coefficients 0 and 1 denote again the absolute value of K . In the Discussion below it will be shown that it is indeed appropriate to use the formulas from Eq. 8. The expression $f(I, J, F)$ is Casimir's function [20]. The value of $eQq_{aa}^{(0)}$ has been determined by Nelson et al. [12]. Since our accuracy is considerably less, $eQq_{aa}^{(0)}$ is held fixed at the value determined from microwave results in the fit. The upper sign in the second equation must be used for the upper component of the doublet and the lower sign for the lower component.

The accuracy of the measured line positions is estimated to be 0.1 MHz. In this value the deviation due to the partial overlap of lines (see Fig. 3) has been taken into account. For the two completely overlapping lines the mean of the individual frequencies, given by Eq. 8 is used in the fit. The results from the fit are given in Table 6. The value of $\langle P_2(\cos \theta) \rangle^{(1)}$, where 1 stands for $|K|=1$ as above, has been determined using the expression [12]

$$eQq_{aa}^{(1)} = eQq^{(NH_3)} \langle P_2(\cos \theta) \rangle^{(1)}, \quad (8.9)$$

with $eQq^{(NH_3)} = -4.08983(2)$ MHz. Table 7 gives the frequencies of the transitions we studied. The hyperfine free transition frequencies have been calculated with the rotational constants from Table 6.

8.6 Discussion

We are now in a position to compare the experimental results for Ar-NH₃ with those found in the ab initio calculations of [15]. The ab initio value of the band origin of the ($j=0, k=0; K=0$) \rightarrow ($j=1, k=0; |K|=1$) transition is 635 GHz which is somewhat larger than the experimentally determined value of 492 GHz. The discrepancy indicates that the relative energies of internal rotor states are very much dependent on the details of the potential energy surface. This was to be expected, since in different internal rotor states the NH₃ molecule has a very different distribution of orientations. The values of $\langle P_2(\cos \theta) \rangle^{(1)}$ found by the ab initio calculations (-0.185) and experiment ($-0.223(27)$) are in reasonable agreement.

In a first approximation (see below) the quadrupole interaction can be calculated once the wavefunction is known exactly. It is therefore possible to get an impression about the correctness of our first order wavefunctions by calculating the quadrupole splittings for these states. The quadrupole energy can be determined by Casimir's expression [20]

$$\begin{aligned} E_Q &= eQq_J \frac{2J+3}{J} f(I, J, F), \text{ with} \\ q_J &= \left\langle J, M=J \left| \frac{\partial^2 V}{\partial Z^2} \right| J, M=J \right\rangle \end{aligned} \quad (8.10)$$

The term to be calculated is q_J ; V is the potential at the ¹⁴N nucleus and the derivative is relative to the space fixed Z -axis. The potential V is assumed to be the same as in free NH₃; i.e. the contributions which arise as a result of the vicinity of the Ar atom are neglected. In the molecule fixed axis system the irreducible tensor $q^{(2)}$ representing the second derivatives of the potential is very simple. We write

$$\frac{\partial^2 V}{\partial z^2} = q_0^{(2)} = q^{(NH_3)} \quad (8.11)$$

Table 6. Constants of the Ar-NH₃ bands and their errors (resulting from the estimated accuracy of line positions of 0.1 MHz). The constants involving ν_{BO} (band origin), B , eQq and σ (standard deviation of the fit) are in MHz. The D 's are in kHz. The constant $eQq_{aa}^{(0)}$ is taken from [12]. The constants after σ are calculated with the results from the fit.

($j=0, k=0; K=0$) \rightarrow ($j=1, k=0; K =1$)	
ν_{BO}	492114.434(80)
B'_0	2876.846(14)
D'_0	88.72(25)
B'_1	2890.708(13)
	2801.946(16)
D'_1	87.06(24)
	90.50(36)
$eQq_{aa}^{(0)}$	0.350
$eQq_{aa}^{(1)}$	0.91(11)
$eQ(q_{bb} - q_{cc})^{(1)}$	-5.01(19)
σ	0.05
B_1	2890.708(13)
$B_{Cor}^2/\Delta\nu$	22.19050(86)
$\langle P_2(\cos \theta) \rangle^{(1)}$	-0.221(26)

Table 7. Frequencies of the Ar-NH₃ ($j=0, k=0; K=0$) \rightarrow ($j=1, k=0; |K|=1$) band. The first column of frequencies gives the calculated hyperfine free transition frequencies. The next columns give the deviations from these of the observed hyperfine components. From left to right the intensity of the hyperfine components decreases. As discussed in the text, only transitions between levels with $J \geq 3$ have been used in the fit. All frequencies are in MHz. The uncertainty is approximately 0.1 MHz.

Transition	Calculated hyperfine free transitions	Observed hyperfine components		
<i>P</i> (9)	435187.85	+0.35	-0.42	
<i>P</i> (8)	442066.59	+0.18	-0.56	
<i>P</i> (7)	448811.36	+0.26	-0.53	
<i>P</i> (6)	455420.33	+0.33	-0.47	
<i>P</i> (5)	461891.62	+0.32	-0.46	
<i>P</i> (4)	468223.32	+0.31	-0.53	
<i>P</i> (3)	474413.48	+0.08	-0.71	
<i>P</i> (2)	480460.08	-0.02	-1.04	
<i>Q</i> (1)	492142.16	-0.39	+0.32	-1.42
<i>Q</i> (2)	492197.67	-0.39	+0.51	
<i>Q</i> (3)	492281.02	-0.43	+0.63	
<i>Q</i> (4)	492392.34	-0.42	+0.69	
<i>Q</i> (5)	492531.78	-0.37	+0.76	
<i>Q</i> (6)	492699.56	-0.37	+0.79	
<i>Q</i> (7)	492895.90	-0.38	+0.79	
<i>Q</i> (8)	493121.08	-0.35	+0.82	
<i>Q</i> (9)	493375.42	-0.39	+0.77	
<i>R</i> (0)	497717.96	-0.08	-1.02	+1.29
<i>R</i> (1)	503169.51	+0.12	-0.68	
<i>R</i> (3)	513607.78	+0.35	-0.45	
<i>R</i> (4)	518589.93	+0.25	-0.56	

Table 8. Quadrupole constants for Ar-NH₃, calculated from the first order wavefunctions. The wavefunctions are taken from Ref. [15]

Wavefunction	State	Constants
$ 0, 0, 0, J, M\rangle$	$(j=0, k=0; K=0)$	$eQq_{aa} = 0$
$ 1, 0, 0, J, M\rangle$	$(j=1, k=0; K=0)$	$eQq_{aa} = -1.64 \text{ MHz}$
$\{ 1, 0, 1, J, M\rangle \pm$ $ 1, 0, -1, J, M\rangle\}/\sqrt{2}$	$(j=1, k=0; K =1)$	$eQq_{aa} = 0.82 \text{ MHz}$ $(eQq_{bb} - eQq_{cc}) = -4.91 \text{ MHz}$

in this system. The irreducible tensor in the space fixed axes system can be calculated, because we can go from one system to the other by rotating over the Euler angles α , β , ϕ , θ and χ .

$$\frac{\partial^2 V}{\partial Z^2} = q^{(NH_3)} D_{0p}^{(2)*}(\alpha, \beta, 0) D_{p0}^{(2)*}(\phi, \theta, \chi) \quad (8.12)$$

The matrix elements of $\partial^2 V / \partial Z^2$ between the first order solutions of the Hamiltonian equation can be easily calculated now, since the resulting integrals contain products of three rotation matrices and can be expressed in 3j-symbols. We have done the calculation for some states, taken from Ref. [15]. It turns out that the expressions from Eq. 8 are obtained. The states and the corresponding constants are given in Table 8. The experimentally determined quadrupole constant for the $(j=0, k=0; K=0)$ state is not equal to 0, as in Table 8. It is however small, as expected. The constants for the $(j=1, k=0; |K|=1)$ state from Table 8 are however within the experimental accuracy equal to those experimentally obtained.

Analysis of the usually rather complex spectra of weakly bound complexes is an interesting task in itself for many cases. Furthermore, if enough data have been accumulated for a given complex these can be used to determine the potential energy surface for the internal motions [17]. Effective rotational constants, hyperfine constants and band origins all provide useful information. We have not attempted to determine the potential energy surface, since at present we do not have enough results for both Ar-D₂O and Ar-NH₃ and since the theory in which all the above-mentioned relevant constants can be used is not yet available.

Acknowledgments

The authors are grateful to Prof. J. Reuss, Dr. J.J. ter Meulen, J. van Bladel and Prof. A. van der Avoird for their stimulating interest and for many helpful discussions. The authors are grateful to Dr. G.T. Fraser for sending them a preprint of his Ar-H₂O paper. The authors thank E. v. Leeuwen for his technical assistance. This work was financially supported by the Dutch Organization for Scientific Research (FOM/NWO).

References

- [1] G.T. Fraser, to be published in *International Reviews in Physical Chemistry*, and references therein.
- [2] E. Zwart, J.J. ter Meulen and W.L. Meerts, *Chem. Phys. Lett.* 166, 500 (1990), and references therein.
- [3] J.M. Steed, T.A. Dixon and W.A. Klemperer, *J. Chem. Phys.* 70, 4095 (1979).
- [4] R.J. Le Roy and J.M. Hutson, *J. Chem. Phys.* 86, 837 (1987), and references therein.
- [5] J.M. Hutson, *J. Chem. Phys.* 89, 4550 (1988), and references therein.
- [6] D.J. Nesbitt, M.S. Child and D.C. Clary, *J. Chem. Phys.* 90, 4855 (1989), and references therein.
- [7] R.C. Cohen, K.L. Busarow, K.B. Laughlin, G.A. Blake, M.Havenith, Y.T. Lee and R.J. Saykally, *J. Chem. Phys.* 89, 4494 (1988).
- [8] R.C. Cohen, K.L. Busarow, Y.T. Lee and R.J. Saykally, *J. Chem. Phys.* 92, 169 (1990).
- [9] Preliminary results have been reported on bands correlating with the $0_{00} \rightarrow 1_{11}$ transition of free D_2O on the 45th Symposium on Molecular Spectroscopy, Columbus, Ohio, June 11–15. Abstract TA 5, by S.Suzuki, P.A. Stockman, P.G. Green, R.E. Bumgarner and G.A. Blake. These results are complementary to those presented here.
- [10] G.T. Fraser, F.J. Lovas, R.D. Suenram and K. Matsumura, to be published in *J. Mol. Spectr.*
- [11] G.T. Fraser, D.D. Nelson Jr., A. Charo and W. Klemperer, *J. Chem. Phys.* 82, 2535 (1985).
- [12] D.D. Nelson Jr., G.T. Fraser, K.I. Peterson, K. Zhao, W. Klemperer, F.J. Lovas and R.D. Suenram, *J. Chem. Phys.* 85, 5512 (1986).
- [13] A. Bizarri, B. Heijmen, S. Stolte and J. Reuss, *Z. Phys. D* 10, 291 (1988).
- [14] Parallel to this work, new transitions have been reported on the 45th Symposium on Molecular Spectroscopy. Columbus, Ohio, June 11 15, 1990. Abstract TA 6, by C.A. Schmuttenmaer, R.C. Cohen and R.J. Saykally. Three bands were reported. The lowest of these is the same as the band presented in this paper.
- [15] J.W.I. van Bladel, A. van der Avoird and P.E.S. Wormer, to be published.
- [16] K.L. Busarow, G.A. Blake, K.B. Laughlin, R.C. Cohen, Y.T. Lee and R.J. Saykally, *J. Chem. Phys.* 89, 1268 (1988).
- [17] J.M. Hutson, *J. Chem. Phys.* 92, 157 (1990).
- [18] D.M. Brink and G.R. Satchler, *Angular Momentum* (Clarendon Press, Oxford, 1962).

- [19] P.R. Bunker, *Molecular Symmetry and Spectroscopy* (Academic Press, New York, 1979).
- [20] C.H Townes and A.L Schawlow, *Microwave Spectroscopy* (Dover Publications Inc., New York, 1975).

Chapter 9

Microwave and submillimeter spectroscopy of Ar-NH₃ states correlating with Ar + NH₃($j=1, |k|=1$)

E. Zwart, H. Linnartz and W. Leo Meerts
Fysisch Laboratorium, University of Nijmegen,
Toernooiveld, 6525 ED Nijmegen, The Netherlands.

G.T. Fraser
Molecular Physics Division, National Institute of Standards and Technology,
Gaithersburg, Maryland 20899.

D.D. Nelson, Jr.¹ and W. Klemperer
Department of Chemistry, Harvard University,
Cambridge, Massachusetts 02138.

9.1 Abstract

Microwave and submillimeter transitions for Ar-NH₃ have been observed and assigned for the two Σ and Π states correlating asymptotically with Ar + NH₃($j=1, |k|=1$). The Σ states are found to lie below the two Π states and are split by approximately the inversion splitting of free NH₃. For the Π states the NH₃ inversion tunneling is nearly quenched, being only weakly allowed through Coriolis interactions with the nearby Σ states. The observed microwave and submillimeter spectra also allow the determination of ¹⁴N quadrupole coupling constants and relative submillimeter absorption intensities. All the above results are interpreted using a model internal-rotation inversion Hamiltonian, leading to detailed information about the anisotropy of the intermolecular potential.

¹Present address :
Aerodyne Research Corporation
45 Manning Road
Billerica, MA 01821
U.S.A.

9.2 Introduction

The investigation of weakly bound complexes involving NH_3 allows the systematic examination of the effects of the van der Waals interaction on the NH_3 inversion tunneling. In free NH_3 this tunneling motion has been well studied with microwave and infrared spectroscopy. The tunneling splitting for the ground vibrational state is found to be 0.8 cm^{-1} , increasing to 36 cm^{-1} for the first excited vibrational state (ν_2) associated with the umbrella coordinate [1].

Upon complexation NH_3 generally acts as a hydrogen acceptor and binds axially or near axially to its binding partner [2]. This leads to a large asymmetry in the NH_3 inversion potential which quenches the NH_3 tunneling. Ar-NH_3 has been regarded as an exception to this case. Using molecular-beam electric-resonance spectroscopy (MBER) Fraser et al. [3] reported, without assignment, a series of transitions for Ar-NH_3 between 19 and 20 GHz which they interpreted as direct inversion transitions. Fraser et al. [3] also observed an infrared transition from the ground vibrational state of the complex to the ν_2 excited state. Bizarri et al. [4] later found two more such transitions, located 32 and 36 cm^{-1} above the transition of Fraser et al. [3]. Since the inversion splitting of the ν_2 excited state of free NH_3 is 36 cm^{-1} , these infrared observations were taken as further evidence that the NH_3 inversion frequency is essentially unchanged upon complexation.

In a more recent microwave study, Nelson et al. [5] observed an additional set of transitions for Ar-NH_3 which they assigned to the ground state of the complex, correlating asymptotically with $\text{Ar} + \text{NH}_3(j=0, k=0)$. Here, j and k are the rotational quantum numbers for free NH_3 . The electric dipole moment and nuclear quadrupole coupling constant indicate that the NH_3 subunit is undergoing nearly free internal rotation within the complex. Further evidence for the free-rotor picture came from several far-infrared [6, 7, 8] and near-infrared [9, 10] investigations of other Ar-NH_3 states correlating with $\text{NH}_3(j, k=0)$. Two different ab initio calculations of the potential energy surface have recently been performed by Chalański et al. [11] and by Bulski et al. [12], respectively. The latter calculations were combined with dynamical calculations [13, 14] which provide additional insight into the internal-rotation dynamics of this complex.

The nearly free internal rotation of the NH_3 unit within the complex allows us to describe the internal rotor states of Ar-NH_3 by their correlation with $\text{Ar} + \text{NH}_3(j, k)$. There exist two distinct nuclear-spin modifications of Ar-NH_3 , which are denoted by ortho and para. Collision-induced or electric-multipole transitions between these two spin states are 'nuclear-spin' forbidden. The lowest energy ortho state correlates with $\text{Ar} + \text{NH}_3(j=0, k=0)$; the lowest energy para state with $\text{Ar} + \text{NH}_3(j=1, |k|=1)$. The effect of NH_3 inversion tunneling is similar to that in free NH_3 . Every j, k state of Ar-NH_3 is tunneling doubled. For the $k=0$ ortho state one of these components has a statistical weight of zero. This makes it difficult to get direct information on the NH_3 inversion splitting in these states. For para Ar-NH_3 both components of the inversion doublet have a non-zero statistical weight.

As discussed above, states of Ar-NH_3 which correlate with $\text{Ar} + \text{NH}_3(j=1, |k|=1)$ are also expected to be populated in the above molecular beam studies since these are the lowest states of para Ar-NH_3 . In the present paper we present microwave and submillimeter measurements of these states and interpret the results using a model internal-rotation inversion Hamiltonian. For $\text{Ar-NH}_3(j=1, |k|=1)$ two types of internal-rotor states result, denoted

$\Pi(j=1,|k|=1)$ and $\Sigma(j=1,|k|=1)$, corresponding to whether the internal angular momentum is directed along (Π) or perpendicular to (Σ) the radial coordinate. We find for the Σ states that the inversion tunneling splitting is nearly the same as in free NH_3 , whereas for the Π states the resulting asymmetry of the NH_3 inversion potential nearly quenches tunneling. Only by Coriolis mixing of the Π and Σ states via overall rotation is tunneling allowed for the Π state. This same Coriolis interaction is the source of the intensity for the pure-inversion Q branch initially observed by Fraser et al. [3].

9.3 Experiment

The molecular-beam measurements were done with microwave spectrometers at NIST and Harvard University and a submillimeter spectrometer at the University of Nijmegen. In each case, a molecular beam of Ar-NH_3 was produced by an adiabatic expansion of an NH_3/Ar or an $\text{NH}_3/\text{Ar}/\text{He}$ mixture. The cold rotational temperatures produced by the expansions (1-10 K), together with the large rotational constant of NH_3 ensures that most of the Ar-NH_3 molecules will be in the lowest levels correlating with $\text{Ar-NH}_3(j=0,k=0)$ (ortho) or $\text{Ar-NH}_3(j=1,|k|=1)$ (para).

The microwave results consist of previously unassigned molecular-beam electric-resonance transitions [3] and new pulsed-nozzle Fourier-transform microwave (FTMW) and electric-resonance optothermal (EROS) measurements. The FTMW [15, 16] and EROS [17, 18] apparatus have been described in detail elsewhere.

The submillimeter apparatus is based on the direct absorption of harmonics from a klystron by a planar supersonic jet [19]. The harmonics are generated in a Schottky barrier diode and are radiated into free space by a 2 mm long antenna backed by a movable corner reflector. Klystrons around 60 or 70 GHz were used in most cases. A parabolic mirror located approximately 10 cm from the antenna produces a parallel beam of radiation. The desired harmonic is selected with a monochromator with a grating of 0.8 or 1.3 grooves/mm. The radiation is guided by lenses and mirrors through the supersonic jet onto an InSb hot-electron bolometer. The radiation is frequency modulated at 5 kHz and the detector output is monitored at twice this frequency using a phase-sensitive detector. The planar jet is produced by expanding a mixture of a few per cent NH_3 in Ar through a 4 cm long x 15 μm wide slit nozzle [20] at a backing pressure of approximately 600 Torr.

Approximate relative integrated absorption intensities of the submillimeter transitions were determined by normalizing the observed signal by the total power, measured immediately after recording a transition. To obtain integrated absorption intensities, both the height and the width of a line have to be determined. The recorded lineshapes are determined by several factors, including Doppler and pressure broadening, unresolved quadrupole hyperfine structure and the frequency modulation (FM) amplitude. The product of the height and the width of a line can be estimated by determining the peak height as a function of the FM amplitude. This product of height and width is used to determine relative integrated absorption intensities. This procedure has proved useful here, since we are only interested in relative intensities. The estimated uncertainties in the measured relative intensities are 30 %. The accuracy is sufficient to determine several striking intensity effects, as will be discussed later.

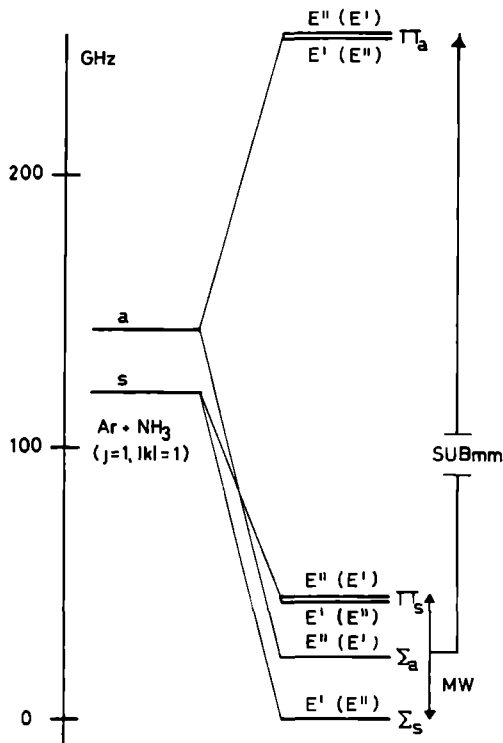


Figure 1. Energy level scheme of Ar-NH₃ states correlating with Ar + NH₃($j=1, |k|=1$).

9.4 Results

In the Discussion section below a dynamical model is presented to interpret the observed spectrum. Here, we will give a qualitative picture of the dynamics to clarify the spectral observations. The energy-level scheme can be understood by taking an approach similar to that used to discuss Ar-H₂O [21, 22, 23]. Here, we have the additional complication of the NH₃ inversion. The states of Ar-NH₃ are described by a model in which the inversion and free rotation of the NH₃ subunit are hindered by the anisotropy of the interaction with the Ar atom. The observed states correlate asymptotically with Ar + NH₃($j=1, |k|=1; v=0,1$), where $v=0$ and 1 denote the symmetric and antisymmetric tunneling states, respectively. In the left-hand side of Fig. 1 the energy level diagram for Ar-NH₃ is shown at infinite radial separation, where the potential interaction between the Ar and NH₃ vanishes.

In the right-hand side of Fig. 1, the energy-level scheme which results from the anisotropic interaction of the NH₃ with the Ar is given. Every level is split into a Σ (or $K=0$) state and two Π (or $|K|=1$) states. As has been discussed by Hutson [21] for Ar-H₂O, for sufficiently

high internal-rotation barriers the projection K (called Ω in [13, 14]) of the total angular momentum J onto the a -axis of the complex is nearly a good quantum number. This is approximately the case for Ar-NH₃. Here, we will use the similarity of Ar-NH₃ ($J=1, |k|=1$) to a linear molecule with vibrational angular momentum and take Σ and Π to denote states with $|K| = 0$ and 1 respectively. We will also use subscripts s and a to specify whether the level correlates with the symmetric or antisymmetric inversion state of NH₃.

It should be noted that the symmetric and antisymmetric components of the Π states are strongly mixed as a result of the anisotropy of the potential, nearly quenching tunneling in these states. The small splittings of the Π state levels shown in the figure are Coriolis induced through interactions with the nearby Σ states. This is all that remains of tunneling in these states. The two Σ states, on the other hand, are not strongly mixed by the intermolecular potential so that these states stay split at approximately the inversion splitting of free NH₃. The origin of these effects can be appreciated by examination of Fig. 2 where we show approximate ‘zero-point’ geometries of the Π and Σ states. The presence of the Ar makes the NH₃ inversion potential extremely asymmetric for the Π state, but not so for the Σ state. The present measurements do not allow us to determine which of the two Π states belong to the observed Π_s and Π_a states. The ab initio calculations from [12] show, however, that the potential energy is lower for the configuration in which the H atoms are directed away from the Ar.

End-over-end rotation gives rise to a series of Σ levels with $J = 0, 1, 2, \dots$ and Π levels with $J = 1, 2, 3, \dots$. The symmetries of the rotation internal-rotation tunneling states under the molecular symmetry group $D_{3h}(M)$ [24] are also given in Fig. 1. The symmetries are given for even J , with the odd J symmetries enclosed in parentheses. The Coriolis interaction between the Σ and Π states only mixes states of the same J and of the same symmetry under $D_{3h}(M)$. The observed microwave transitions are within and between the four lowest lying internal-rotor levels of Fig. 1. The submillimeter transitions are between the four lowest and the two highest lying levels. The electric-dipole selection rules are $E' \leftrightarrow E''$ with $\Delta J = 0, \pm 1$.

The observed microwave transition frequencies are listed in Table 1. We also tabulate the hyperfine corrected microwave frequencies when hyperfine splittings are observed. These corrected frequencies have been used in the fit described below. The observed submillimeter transitions are given in Table 2. The submillimeter transitions showed no hyperfine splittings at the FM amplitude which resulted in the largest signals. The frequencies measured with these optimum FM amplitudes have been used in the fit. Upon lowering of the FM amplitude half of the transitions showed resolved hyperfine structure, but still the resolution was insufficient to determine reliable quadrupole coupling constants.

Since the microwave spectrum is strongly perturbed by the $\Pi - \Sigma$ Coriolis interaction, the initial assignments of the microwave transitions were made by using the observed hyperfine patterns to identify the J states of the transitions and by using microwave-microwave double-resonance experiments. The latter experiments were carried out by exploiting the double-resonance capabilities of the MBER and EROS spectrometers. The assignment of the first submillimeter lines, which were $\Pi \leftarrow \Sigma$ transitions, was easier since the spectrum consists of two bands, similar in structure to vibrational bands, both with P , Q , and R branches. The assigned microwave and submillimeter transitions turned out to involve common levels. A collaborative effort resulted in many new assigned lines, e.g. the $\Sigma \leftarrow \Sigma$ microwave

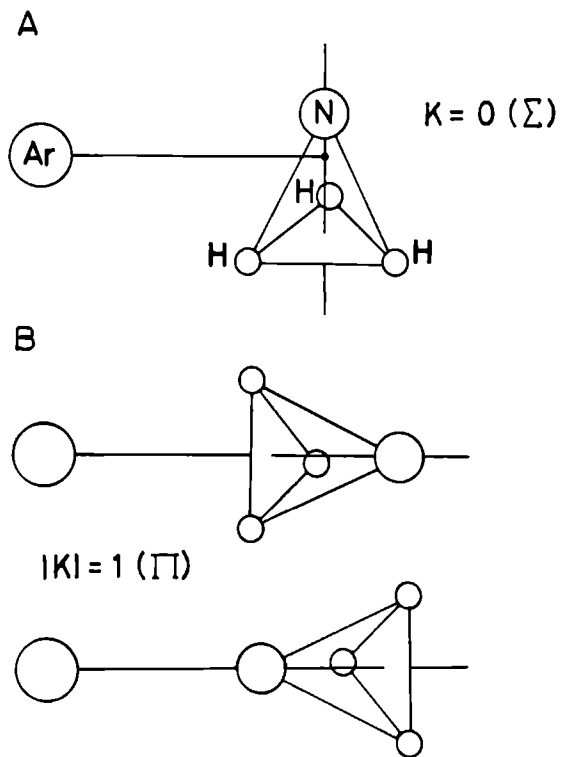


Figure 2. Approximate 'zero-point' geometries for the Σ and Π states from Fig. 1.

Table 1 Observed microwave transitions for the Ar-NH₃ states correlating with Ar + NH₃($j=1, |k|=1$)^a

	J'	J''	F'	F''	Sym'	Sym''	Frequency	Obs-Cal
Σ_a	Σ_a	1	1		E'	E''	22283 191	0 113
		2	2		E''	E'	21661 723	-0 055
		3	3		E'	E''	21025 297	-0 119
		4	4		E''	E'	20477 477	-0 058
		5	5		E'	E''	20048 820	0 086
		6	6		E''	E'	19734 921	0 098
			6	6			19734 881	
			5	5			19734 942	
			7	7			19734 942	
		7	7		E'	E''	19519 696	0 014
			7	7			19519 656	
			6	6			19519 717	
			8	8			19519 717	
		8	8		E''	E'	19385 152	-0 142
			7	7			19385 172	
			9	9			19385 172	
		9	9		E'	E''	19315 249	0 052
			8	8			19315 269	
			10	10			19315 269	
			10	10		E''	E'	19297(2)
$\Sigma_a - \Sigma_a$	3	2			E''	E'	15326 304	-0 042
			4	3			15326 303	
		3	2			15326 303		
		2	1			15326 371		
	4	3			E'	E''	20628 994	-0 015
$\Sigma_a - \Sigma_a$	3	2			E'	E''	14689 878	-0 107
			4	3			14689 877	
		3	2			14689 877		
		2	1			14689 943		
	4	3			E''	E'	20081 179	0 051
		5	4				20081 187	
	4	3				20081 187		
	3	2				20081 187		
$\Pi_a - \Sigma_a$	1	2			E''	E'	36601 36	-0 226
					E'	E''	34186 98	-0 234
					E''	E'	32783 53	-0 189
					E'	E''	32177 78	-0 049

Table 1 Continued

	J'	J''	F'	F''	Sym'	Sym''	Frequency	Obs-Cal		
	5	6			E''	E'	32186 82	0 031		
$\Pi_a - \Sigma_a$	1	2		1	2			15314 877		
				2	2		E'	E''	15315 010	-0 046
					2	3			15315 374	
					1	1			15315 451	
					0	1			15315 774	
				2	3		E''	E'	14091 851	0 125
					2	3			14091 505	
					3	3			14091 619	
					3	4			14091 966	
					1	2			14092 155	
		3	4		E'	E''	13771 678	0 090		
			3	4			13771 361			
			4	4			13771 442			
			4	5			13771 789			
			2	3			13771 917			
		4	5		E''	E'	14006 741	-0 080		
			4	5			14006 439			
			5	5			14006 510			
			5	6			14006 857			
			3	4			14006 944			
	5	6		E'	E''	14587 193	-0 176			
		5	6			14586 904				
		6	7			14587 304				
		4	5			14587 381				
	6	7		E''	E'	15387 754	-0 036			
		6	7			15387 471				
		7	8			15387 860				
		5	6			15387 938				
	7	8		E'	E''	16331 178	0 229			
		7	8			16330 896				
		8	9			16331 290				
		6	7			16331 354				
	8	9		E''	E'	17367 465	-0 094			
		8	9			17367 182				
		9	10			17367 576				
		7	8			17367 642				

Table 1 Continued

	J'	J''	F'	F''	Sym'	Sym''	Frequency	Obs-Cal
	1	1			E''	E'	24448 31	-0 463
	2	2			E'	E''	27851 59	-0 192
	3	3			E''	E'	32387 27	-0 042
	4	4			E'	E''	37724 83	-0 032
	1	0			E'	E''	29448 97	-0 447
	2	1			E''	E'	38290 45	-0 225
$\Pi_a - \Pi_a$	2	1			E''	E'	13466 453	0 064
			1	0			13466 323	
			2	2			13466 323	
			3	2			13466 461	
			2	1			13466 461	
			1	1			13466 662	
	2	1			E'	E''	12911 937	-0 037
	3	2			E'	E''	19761 006	0 016
			2	1			19760 955	
			4	3			19761 000	
			3	2			19761 034	
	3	2			E''	E'	19225 560	0 046

^{a)} Experimental uncertainties in the frequency measurements are approximately 5 in units of the last significant digit

Table 2 Observed submillimeter transitions for the Ar $\text{NH}_3(j=1, |k|=1)^a$

	J'	J''	Sym'	Sym''	Frequency	Obs-Cal
$\Pi_a - \Sigma_a$	1	2	E''	E'	241945 44	0 15
	2	3	E'	E''	238036 13	0 16
	3	4	E''	E'	234528 38	0 24
	4	5	E'	E''	231323 90	0 19
	5	6	E''	E'	228344 30	0 04
	6	7	E'	E''	225530 80	-0 13
	7	8	E''	E'	222840 88	-0 24
	8	9	E'	E''	220244 81	-0 01
	9	10	E''	E'	217722 20	0 80
	1	1	E'	E''	252110 37	-0 06
	2	2	E''	E'	253467 13	0 01
	3	3	E'	E''	255367 41	0 03
	4	4	E''	E'	257700 06	0 02
	5	5	E'	E''	260366 09	0 03
	6	6	E''	E'	263286 24	-0 08
	7	7	E'	E''	266401 34	-0 10
	8	8	E''	E'	269668 49	-0 07
	9	9	E'	E''	273057 77	0 23
	10	10	E''	E'	276548 97	1 08
	1	0	E''	E'	257109 49	-0 04
	2	1	E'	E''	263492 53	-0 05
	3	2	E''	E'	270483 62	0 12
	4	3	E'	E''	277977 45	0 16
	5	4	E''	E'	285860 64	0 22
	6	5	E'	E''	294031 38	0 07
	7	6	E''	E'	302408 03	-0 02
	8	7	E'	E''	310928 11	-0 21
	9	8	E''	E'	319545 79	-0 26
	10	9	E'	E''	328227 76	0 01
$\Pi_a - \Sigma_a$	1	2	E'	E''	220318 56	0 18
	2	3	E''	E'	217115 53	0 17
	3	4	E'	E''	214260 96	0 12
	4	5	E''	E'	211626 66	-0 08
	5	6	E'	E''	209139 42	-0 23
	6	7	E''	E'	206757 63	-0 22
	7	8	E'	E''	204457 94	-0 06
	8	9	E''	E'	202228 06	0 06

Table 2 Continued

	J'	J''	Sym'	Sym''	Frequency	Obs-Cal
	9	10	E'	E''	200062 61	-0 51
	1	1	E''	E'	229792 32	-0 16
	2	2	E'	E''	231700 80	0 26
	3	3	E''	E'	234132 05	0 31
	4	4	E'	E''	236871 02	0 27
	5	5	E''	E'	239787 22	0 10
	6	6	E'	E''	242804 76	-0 13
	7	7	E''	E'	245879 41	-0 17
	8	8	E'	E''	248984 73	-0 15
	9	9	E''	E'	252105 43	-0 07
	1	0	E'	E''	234452 11	-0 37
	2	1	E''	E'	241314 13	-0 18
	3	2	E'	E''	249032 01	0 06
	4	3	E''	E'	257303 79	0 16
	5	4	E'	E''	265913 23	0 14
	6	5	E''	E'	274729 17	0 00
	7	6	E'	E''	283675 30	-0 11
	8	7	E''	E'	292707 00	-0 02
	9	8	E'	E''	301797 80	0 19
	10	9	E''	E'	310932 13	0 15
	11	10	E'	E''	320101 51	-0 86
$\Pi_a - \Pi_c$	3	4	E''	E'	176325 88	0 13
	3	4	E'	E''	174658 25	0 00
	2	2	E''	E'	203953 84	0 28
	3	3	E'	E''	201954 86	0 20
	4	4	E''	E'	199497 66	0 02
	5	5	E'	E''	196687 45	-0 23
	6	6	E''	E'	193611 13	-0 43
	7	7	E'	E''	190337 55	-0 32
	8	8	E''	E'	186920 90	0 68
	1	1	E''	E'	204968 30	0 11
	2	2	E'	E''	202918 92	0 09
	3	3	E''	E'	200279 13	0 11
	4	4	E'	E''	197268 31	0 15
	5	5	E''	E'	194022 16	0 09
	6	6	E'	E''	190623 33	-0 13

Table 2 Continued

J'	J''	Sym'	Sym''	Frequency	Obs-Cal
7	7	E''	E'	187124 53	-0 34
8	8	E'	E''	183562 01	-0 05
2	1	E'	E''	216761 00	0 27
3	2	E''	E'	220970 27	0 33
4	3	E'	E''	224564 88	0 32
5	4	E''	E'	227658 20	0 17
6	5	E'	E''	230352 82	-0 11
7	6	E''	E'	232732 94	-0 36
8	7	E'	E''	234864 29	-0 45
9	8	E''	E'	236798 16	0 45
2	1	E''	E'	216490 23	0 21
3	2	E'	E''	220250 23	-0 01
4	3	E''	E'	223450 89	-0 03
5	4	E'	E''	226310 52	0 02
6	5	E''	E'	228964 13	0 01
7	6	E'	E''	231493 85	-0 12
8	7	E''	E'	233952 07	-0 24
9	8	E'	E''	236375 09	0 30

^{a)} Experimental uncertainties in the frequency measurements are approximately 0.10 MHz

direct-inversion transitions and the weak $\Pi \leftarrow \Pi$ submillimeter bands.

The observed microwave and submillimeter transitions are consistent with Fig. 1 and the relative energies in the figure are drawn to scale. The two data sets are also consistent with each other, as verified by using combination differences. An assignment to the ortho Ar-NH₃ $\Sigma(j=0, k=0)$ ground state can be excluded since this state is well characterized and shows no common combination differences or effective rotational constants with the states presented here.

All assigned frequencies have been fitted to effective rotational constants by using the following energy-level expression for each of the 6 levels drawn in Fig. 1,

$$E_{i,J} = E_i + B_i J(J+1) - D_i J^2(J+1)^2 \quad (9.1)$$

where E_i is the energy-level origin, and B_i and D_i are rotation and distortion constants of level i . To distinguish between the two Π_s levels, the one lower in energy is denoted by $\Pi_{s,lower}$ and the upper by $\Pi_{s,upper}$. The same notation is used for the two Π_a levels. Off-diagonal Coriolis matrix elements $\alpha_{\Sigma\Pi} \sqrt{J(J+1)/2}$ were used between the lowest Σ and Π states, i.e. between levels Σ_s and $\Pi_{s,lower}$ and between levels Σ_a and $\Pi_{s,upper}$. The E_i 's are taken relative to the lowest energy $\Sigma_s(j=1, |k|=1)$ level by setting $E(\Sigma_s) = 0$. The energy-level origins of the two Coriolis-split Π_s states were constrained to be equal. The same constraint was also used for the two Π_a levels. It was found that for the Coriolis-coupled states the best B and D constants to report are the sum and difference of the constants for the two coupled states. The difference is strongly correlated with the Coriolis constant, while the sum is not, and therefore the error in the sum is small relative to that of the difference. In Table 3 we list the constants obtained from the fit, with the residuals from the fit being given in Tables 1 and 2.

Using the procedure described in the experimental section, relative integrated absorption intensities have been determined for several submillimeter transitions. The results for the various transitions between levels of para Ar-NH₃ are discussed in a following section. There these results are compared with theoretical calculations. We have also compared the intensities of the submillimeter bands presented in the present paper, i.e. those of para Ar-NH₃ with two already known bands between levels of ortho Ar-NH₃. The intensities of four $R(3)$ transitions have been determined, one shortly after the other, using harmonics from a klystron operating around 70 GHz. Only the grating of the monochromator had to be changed between different measurements. This way equal conditions are obtained to ensure the reliability of the measurements. The results are listed in Table 4.

9.5 Dynamical model

The rotation internal-rotation tunneling states of Ar-NH₃ can be modeled using an extension of the rod-ball and asymmetric-top-ball descriptions applied previously to the rare-gas hydrogen halide and Ar-H₂O complexes [25]. Here, we will consider an inverting and rotating NH₃ unit coupled to an Ar atom through an interaction potential V . We will constrain all the coordinates of the NH₃ unit at their 'zero-point' values, except for the tunneling coordinate, α . Also, since we are mainly interested in characterizing the internal-rotation inversion states of the complex and since we do not study states with excitation of the radial coordinate, we will further reduce the dimensionality of the problem by fixing the radial

Table 3a. Band origins obtained from the fit (in MHz).

Σ_s	Σ_a	Π_s	Π_a
E 0 ^{a)}	22691.922(45)	45276.381(71)	251400.15(30)

^{a)} Constrained in the fit.

Table 3b. Effective constants of the Σ_s , Σ_a and Π_s states obtained from the fit (in MHz).

	$\Sigma_s; \Pi_{s,lower}$	$\Sigma_a; \Pi_{s,upper}$
$(B_\Sigma + B_\Pi)/2$	2881.0463(50)	2872.7229(42)
$(B_\Sigma - B_\Pi)/2$	-21.8(10)	-16.56(13)
$(D_\Sigma + D_\Pi)/2$	0.09581(14)	0.10047(11)
$(D_\Sigma - D_\Pi)/2$	-0.03406(82)	-0.118265(86)
$\alpha_{\Sigma\Pi}$	5613.4(81)	5080.20(62)

Table 3c. Effective constants of the Π_a states obtained from the fit (in MHz).

	$\Pi_{a,lower}$	$\Pi_{a,upper}$
B	2854.834(10)	2872.251(14)
D	0.07241(14)	0.06384(13)

Table 4. Measured relative integrated absorption intensities^{a)} of several submillimeter $R(3)$ transitions^{b)}.

Transition	Form	Frequency	Intensity
$\Pi \leftarrow \Pi, R(3)^c$	para	224564.88	2.0
$\Pi \leftarrow \Sigma, R(3)^c$	para	277977.45	31
$\Pi \leftarrow \Sigma, R(3)^d$	ortho	513607.96	1000
$\Sigma \leftarrow \Sigma, R(3)^e$	ortho	815476.28	397

^{a)} The estimated uncertainties in the measured intensities are 30 %.

^{b)} Experimental uncertainties in the frequency measurements are 0.10 MHz.

^{c)} This work.

^{d)} Refs. [7, 8]

^{e)} Ref. [6]

coordinate, R , at an effective center of mass separation, R_{cm} . With these considerations, the Hamiltonian for the Ar-NH₃ complex can be expressed as

$$H = H_{rot} + h_{inv}(\alpha) + V(\theta, \phi, \alpha) \quad (9.2)$$

where

$$H_{rot} = B_d \vec{\ell}^2 + b(\alpha) \vec{j}^2 + [c(\alpha) - b(\alpha)] j_c^2, \quad (9.3)$$

$B_d = \hbar^2 / (2\mu R_{cm}^2)$, μ is the pseudo-diatomic reduced mass, $\vec{\ell}$ is the orbital angular momentum associated with end-over-end rotation of the complex, \vec{j} is the angular momentum of the NH₃ unit with projection j_c along the NH₃ symmetry axis (i.e. c -axis), $b(\alpha)$ and $c(\alpha)$ are the rotational constants of NH₃ as a function of α , h_{inv} is the inversion Hamiltonian for free NH₃, and $V(\theta, \phi, \alpha)$ is the interaction potential between Ar and NH₃. The polar coordinates (R, θ, ϕ) specify the orientation of the Ar with respect to an (x, y, z) cartesian axis system fixed on the NH₃ with origin at the NH₃ center of mass and z -axis along the NH₃ symmetry axis, as shown in Fig. 3. Although for our purposes the definition of the tunneling coordinate is somewhat arbitrary, for convenience's sake we will take α to be the angle between the N-H bonds and the negative z -axis.

Matrix elements of H are evaluated in the coupled basis, $|JMjk\ell v\rangle$, where $\vec{J} = \vec{\ell} + \vec{j}$, constructed from products of spherical harmonics $Y_{l,m_l}(\theta_{sf}, \phi_{sf})$ symmetric-top functions $D_{m,k}^{j,*}(\alpha, \beta, \gamma)$ [26], and NH₃ tunneling wavefunctions $\Psi_v(\alpha)$ ($v = 0, 1, \dots$). Here, θ_{sf} and ϕ_{sf} are the polar coordinates necessary to specify the orientation of a unit vector along R with respect to some space-fixed (X, Y, Z) axis system, and (α, β, γ) are the Euler angles between the NH₃ body-fixed axis system and this same space-fixed axis system. To simplify the evaluation of matrix elements of $V(\theta, \phi, \alpha)$, we expand $V(\theta, \phi, \alpha)$ in renormalized spherical

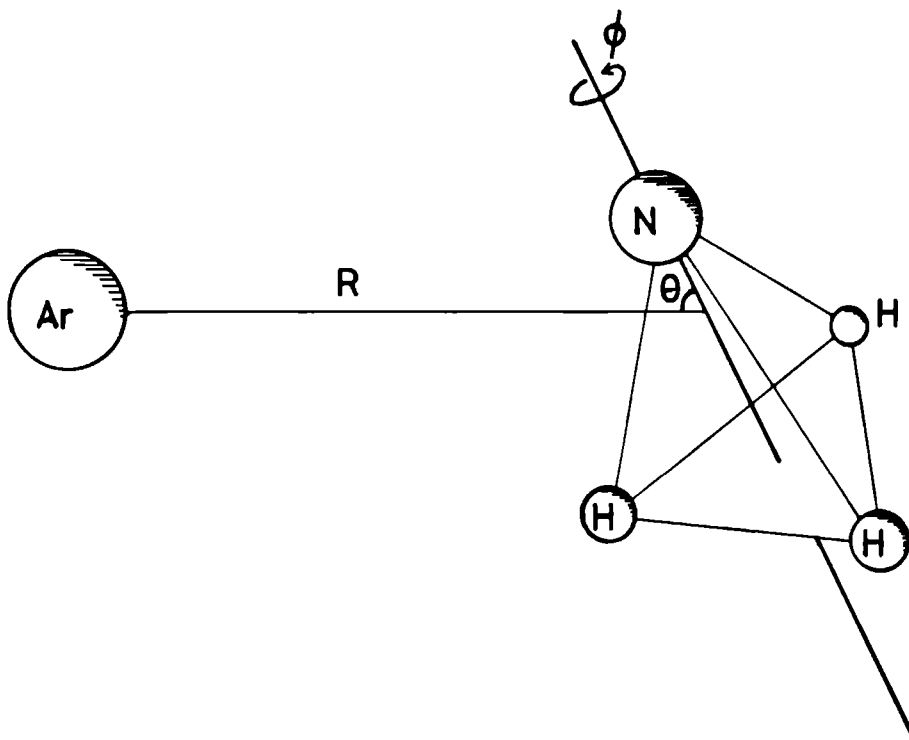


Figure 3. The polar coordinates (R, θ, ϕ) specifying the position of the Ar atom relative to the NH₃ frame.

harmonics [26], $C_{pq}(\theta, \phi)$ as

$$V(\theta, \phi, \alpha) = \sum_{-p \leq q \leq p \wedge p > 0} v_{pq}(\alpha) C_{pq}(\theta, \phi) \quad (9.4)$$

where the v_{pq} are independent of θ and ϕ . Consideration of the transformation properties of θ , ϕ and α in the molecular symmetry group of Ar-NH₃, which is identical to that used to characterize free NH₃ and is denoted $D_{3h}(M)$ [2], allows us to reexpress Eq. 4 as

$$V(\theta, \phi, \alpha) = \frac{1}{6} \sum_{-p \leq q \leq p \wedge p \geq 0} [1 + 2 \cos(\frac{2\pi q}{3})] V_{pq}(\alpha) [C_{pq}(\theta, \phi) + (-1)^q C_{p-q}(\theta, \phi)] \quad (9.5)$$

where

$$V_{pq}(\alpha) = \frac{1}{2} [(-1)^{p-q} v_{pq}(\pi - \alpha) + v_{pq}(\alpha)] \quad (9.6)$$

The matrix elements of $H_{rot} + h_{inv}$ are diagonal in the $|JM_j k l v\rangle$ basis,

$$\langle JM_j k l v | H | JM_j k l v \rangle = B_d \ell(\ell + 1) + b_v j(j + 1) + (c_v - b_v) k^2 + w_v \quad (9.7)$$

where the w_v 's are the term values of the NH₃ inversion potential, with $w_1 - w_0 = 0.7934083$ cm⁻¹ being the NH₃ ground-state tunneling splitting. Also in Eq. 7, $b_0 = 9.9466422$ cm⁻¹, $b_1 = 9.9415887$ cm⁻¹, $c_0 - b_0 = -3.7199204$ cm⁻¹, and $c_1 - b_1 = -3.7128676$ cm⁻¹, are the zero-point rotational constants for the symmetric and antisymmetric tunneling states of free NH₃, as determined by Urban et al. [1].

The potential matrix elements are both diagonal and off-diagonal in j , k , ℓ and v ,

$$\begin{aligned} & \langle JM_j' k' \ell' v' | V(\theta, \phi, \alpha) | JM_j k l v \rangle = \\ & \frac{1}{6} \sum_{-p \leq q \leq p \wedge p \geq 0} [1 + 2 \cos(\frac{2\pi q}{3})] \langle v' | V_{pq}(\alpha) | v \rangle (-1)^{J-k+\ell'+l} [(2\ell' + 1)(2\ell + 1)(2j' + 1)(2j + 1)]^{\frac{1}{2}} \times \\ & \begin{pmatrix} \ell & p & \ell' \\ 0 & 0 & 0 \end{pmatrix} \left[\begin{pmatrix} j' & p & j \\ k' & q & -k \end{pmatrix} + (-1)^q \begin{pmatrix} j' & p & j \\ k' & -q & -k \end{pmatrix} \right] \begin{Bmatrix} \ell' & j' & J \\ j & \ell & p \end{Bmatrix} \end{aligned} \quad (9.8)$$

Note that these matrix elements vanish for $q \neq 0, 3, 6, \dots$ and that for $(p - q)$ even, $(v' - v)$ must be even, while for $(p - q)$ odd, $(v' - v)$ must be odd.

The Hamiltonian matrix which results can be symmetry factored into A_1' , A_1'' , A_2' , A_2'' , E' and E'' blocks in $D_{3h}(M)$, with the E' and E'' blocks being of interest here since only these rovibronic species can result from Ar + NH₃ ($j=1, |k|=1$). For the E' and E'' states, the symmetry adapted wavefunctions take the following form,

$$\begin{aligned} E' & \begin{cases} |JM_j k l v\rangle & \ell + v \text{ odd}, & k = 6n \pm 1 \\ |JM_j k l v\rangle & \ell + v \text{ even}, & k = 6n \pm 2 \end{cases} \\ E'' & \begin{cases} |JM_j k l v\rangle & \ell + v \text{ odd}, & k = 6n \pm 2 \\ |JM_j k l v\rangle & \ell + v \text{ even}, & k = 6n \pm 1 \end{cases} \end{aligned} \quad (9.9)$$

where $n = 0, \pm 1, \pm 2, \dots$

The Hamiltonian matrix H was set up in the $|JM_j k \ell v\rangle$ basis set including interactions from $j = 1 \dots 8$, $k = \pm 1$, and $v = 0, 1$, and diagonalized to determine energies. States with

$v > 1$ correspond to excited vibrational states of NH_3 , and were not included here since the ν_2 vibrational frequency of approximately 950 cm^{-1} is expected to be substantially greater than the $\langle v = 2, 3 | V_{pq} | v' = 0, 1 \rangle$ matrix elements coupling the ground state to the excited state. Values for $\langle v | V_{pq} | v' \rangle$ were determined iteratively from fitting the experimental data to the energies obtained from the diagonalization of H , as discussed later. Terms up to $\langle v' | V_{20} | v \rangle$ in Eq. 8 were considered. We have not considered higher-order terms since these are expected to be much smaller and the present experimental data are not sufficient to examine these in detail. This allows us to limit our basis set to states with $|k| = 1$.

The electric-dipole selection rules are $E' \leftrightarrow E''$. The dipole moment matrix elements necessary to calculate transition intensities are obtained from

$$\begin{aligned} & \langle J' M' j' k' \ell' v' | \mu_Z | J M j k \ell v \rangle = \\ & \delta_{MM'} \delta_{\ell \ell'} \mu_{vv'} (-1)^{J+J'-k} [(2J+1)(2J'+1)(2j+1)(2j'+1)]^{\frac{1}{2}} \begin{pmatrix} j & 1 & j' \\ -k & 0 & k' \end{pmatrix} \times \\ & \sum_{m=-j}^j (-1)^m \begin{pmatrix} j & \ell & J \\ m & M-m & -M \end{pmatrix} \begin{pmatrix} j' & \ell & J' \\ m & M-m & -M \end{pmatrix} \begin{pmatrix} j & 1 & j' \\ -m & 0 & m \end{pmatrix} \quad (9.10) \end{aligned}$$

where $\mu_Z = \mu(\alpha) \cos(\beta)$ is the projection of the NH_3 dipole moment onto the space-fixed Z -axis along which M is quantized. We define $\mu_{vv'} \equiv \langle v | \mu(\alpha) | v' \rangle$, where $\mu_{01} = 1.47 \text{ D}$ is the ground state dipole moment of free NH_3 . Note that $\mu_{vv'} = 0$ for $(v - v')$ even.

Following Fraser et al. for $\text{Ar-H}_2\text{O}$ [27], effective quadrupole coupling constants, eqQ_{eff} , are calculated for each rotation internal-rotation tunneling state via first-order perturbation theory using the zeroth-order diagonal in J matrix elements of the electric quadrupole interaction,

$$\begin{aligned} & \langle F M_F J j' k' \ell' v' | H_Q | F M_F J j k \ell v \rangle = \\ & \langle v' | eqQ_{cc}(\alpha) | v \rangle \delta_{\ell \ell'} (-1)^{J+\ell'+J'+j-k} [(2j'+1)(2j+1)]^{\frac{1}{2}} f(I, J, F) \times \\ & \left(\frac{(2J-1)(2J+1)(2J+3)}{J(J+1)} \right)^{\frac{1}{2}} \begin{Bmatrix} J & J & 2 \\ j & j' & \ell' \end{Bmatrix} \begin{pmatrix} j' & 2 & j \\ k' & 0 & -k \end{pmatrix} \quad (9.11) \end{aligned}$$

and the eigenvectors from the diagonalization of H . Here, $\vec{F} = \vec{I} + \vec{J}$, where $I = 1$ is the ^{14}N nuclear spin, $f(I, J, F)$ is, as before, Casimir's function, and $eqQ_{cc}(\alpha)$ is the c -axis (i.e. symmetry axis) component of the quadrupole coupling tensor of free NH_3 as a function of the tunneling coordinate. Note that $\langle v' | eqQ_{cc}(\alpha) | v \rangle = 0$ for $(v' - v)$ odd and $\langle 1 | eqQ_{cc}(\alpha) | 1 \rangle \approx \langle 0 | eqQ_{cc}(\alpha) | 0 \rangle \equiv eqQ^{\text{NH}_3}$ the quadrupole coupling constant of free NH_3 . We use $eqQ^{\text{NH}_3} = -4.08983 \text{ MHz}$, as determined by Marshall and Muentner [28].

9.6 Determination of the potential energy surface

As discussed in the previous section, the Hamiltonian is diagonalized using potential parameters V_{00} , V_{10} , and V_{20} . For B_d in Eqs. 3 and 7 the mean value of the six B_i 's has been used. This average $B = 2872.4 \text{ MHz}$ has no first-order Coriolis or angular-radial coupling effects, and is close to the B value of 2876.8 MHz found by Nelson et al. [5] for the $\Sigma(j=0, k=0)$ state of Ar-NH_3 . As an aside, we note that the mean D value of 0.0881 MHz determined

Table 5. Ar-NH₃ potential parameters (in cm⁻¹).

	Case 1	Case 2
	$\langle 0 V_{20} 0\rangle = \langle 1 V_{20} 1\rangle$	$\langle 0 V_{00} 0\rangle = \langle 1 V_{00} 1\rangle$
$(\langle 1 V_{00} 1\rangle - \langle 0 V_{00} 0\rangle)/2$	-0.0111	0 ^{a)}
$ \langle 0 V_{10} 1\rangle $	9.6709	9.6682
$(\langle 1 V_{20} 1\rangle - \langle 0 V_{20} 0\rangle)/2$	0 ^{a)}	0.0469
$(\langle 1 V_{20} 1\rangle + \langle 0 V_{20} 0\rangle)/2$	20.3797	20.3797
B_d	2872.4 MHz ^{a)}	2872.4 MHz ^{a)}

^{a)} Constrained in the fit

here is also nearly identical to that found for the $\Sigma(j=0, k=0)$ state where $D = 0.0887$ MHz. With the B_d constraint above, the energy level positions E_i of Table 3a are only functions of the potential matrix elements $\langle v'|V_{pq}|v\rangle$, and these matrix elements can consequently be iteratively determined. The maximum number of independent matrix elements, corresponding to the number of available band origins, is three. The potential matrix elements are not constrained by symmetry to be identical for the two tunneling states. Since we do not have sufficient data to determine all the V_{i0} , one of the constraints $\langle 0|V_{00}|0\rangle = \langle 1|V_{00}|1\rangle$ or $\langle 0|V_{20}|0\rangle = \langle 1|V_{20}|1\rangle$ has been used in the calculations. The potential matrix elements were then determined by fitting the experimental $J=0$ Σ levels and the $J=1$ Π levels to the V_{i0} . For the $J=1$ Π levels the average of the two ℓ -doublet split levels were fit. The potential matrix elements determined from the model are listed in Table 5.

The potential matrix elements from Table 5 can be used to calculate transition intensities and quadrupole coupling constants to compare with experiment. This will further test the model used and the validity of truncating the potential expansion at V_{20} , which is equivalent to assuming free internal rotation of the NH₃ about its symmetry axis.

The quadrupole coupling constants for some of the lower J states are known from the microwave measurements. As in Ref. [27], for every J level an effective quadrupole constant eqQ_{eff} can be defined by

$$E_Q = eqQ_{eff}f(I, J, F) \quad (9.12)$$

where eqQ_{eff} is the coefficient of $f(I, J, F)$ in Eq. 11. The eqQ_{eff} are calculated from Eq. 12 using the wavefunctions obtained from the diagonalization of the Hamiltonian with the potential matrix elements from Table 5. The results, which are given in Table 6, show good agreement with experiment. Moreover, the eqQ_{eff} do not differ appreciably for the two sets of potential parameters of Table 5.

The wavefunctions obtained by diagonalization of the H together with the dipole moment matrix elements of Eq. 10, can be used to estimate intensities for the submillimeter bands. Fig. 4 shows the calculated spectrum for the $\Pi_a \leftarrow \Sigma_s$, $\Pi_a \leftarrow \Sigma_a$ and $\Pi_a \leftarrow \Pi_s$ bands. The simulations were done using a rotational temperature of 5 K, which approximately

Table 6. Comparison of observed and calculated effective quadrupole coupling constants, eqQ_{eff} , (in MHz) for Ar-NH₃ states correlating with Ar + NH₃ ($j=1, |k|=1$). Calculations were done using the potential parameters of Case 1 in Table 5 and a maximum j of 7 in the free-rotor basis set.

State	$J = 1$	2	3	4	5
Σ_s	-1.1328	-1.1166	-1.0987	-1.0824	-1.0694
Σ_a	-1.2100	-1.1248	-1.0539	-1.0038	-0.9713
observed		[-1.114(18)]	[-1.037(20)]	[-1.044(24)]	[-0.9999(43)]
$\Pi_{s,lower}$	-0.0148	-0.0287	-0.0398	-0.0465	-0.0472
$\Pi_{s,upper}$	0.4352	0.3523	0.2882	0.2477	0.2273
observed	[0.444(12)]	[0.388(17)]	[0.250(26)]	[0.2076(50)]	
$\Pi_{a,lower}$	0.4476	-0.0625	-0.1962	-0.2564	-0.2938
$\Pi_{a,upper}$	0.0800	-0.4301	-0.5638	-0.6240	-0.6613

reproduces the observed intensity profiles. As seen in the figure, the $\Pi_a \leftarrow \Sigma_s$ band is calculated to be 9 times stronger than the $\Pi_a \leftarrow \Pi_s$ band, as obtained by comparing the ratios of the strongest lines from the two bands. Experimentally we find an intensity ratio of approximately 10, in good agreement with the calculations.

The intensities also show a number of interesting anomalies resulting from the $\Sigma - \Pi$ Coriolis interactions. The most striking of these is that experimentally the $\Pi - \Pi$ sub-millimeter bands possess Q branches with intensity profiles which resemble those expected for a perpendicular band, whereas a parallel $K = 1 \leftarrow 1$ type branch structure might be expected. The theoretical calculations however agree with the experimental results and, in fact, show that most of the intensity for the $\Pi \leftarrow \Pi$ band comes from the $\Sigma - \Pi$ Coriolis interaction, giving substantial $\Pi \leftarrow \Sigma$ or $K = 1 \leftarrow 0$ character to the $\Pi \leftarrow \Pi$ band.

Another interesting effect which is reproduced by the calculations is that experimentally several of the P branches are found to be weaker than their R branch partners. For the $\Pi \leftarrow \Sigma$ bands this type of effect is expected from consideration of the Hönl-London factors for a $K = 1 \leftarrow 0$ type band. Here, we see for the $\Pi \leftarrow \Sigma$ bands that the difference in intensity between P and R branches is 2 - 3 in the experiments and 1.9 - 2.6 in the calculations (see Fig. 4). We have estimated the strength of a branch by the intensity of the strongest lines from the branch. For $\Pi \leftarrow \Pi$ bands this effect is also observed. For transitions between $\Pi_{s,lower}$ and $\Pi_{a,lower}$ the R branch is calculated to be approximately 5 times stronger than the P branch. For transitions between $\Pi_{s,upper}$ and $\Pi_{a,upper}$ there are no large differences and the intensities are comparable. In both cases experiment and theory are in good agreement.

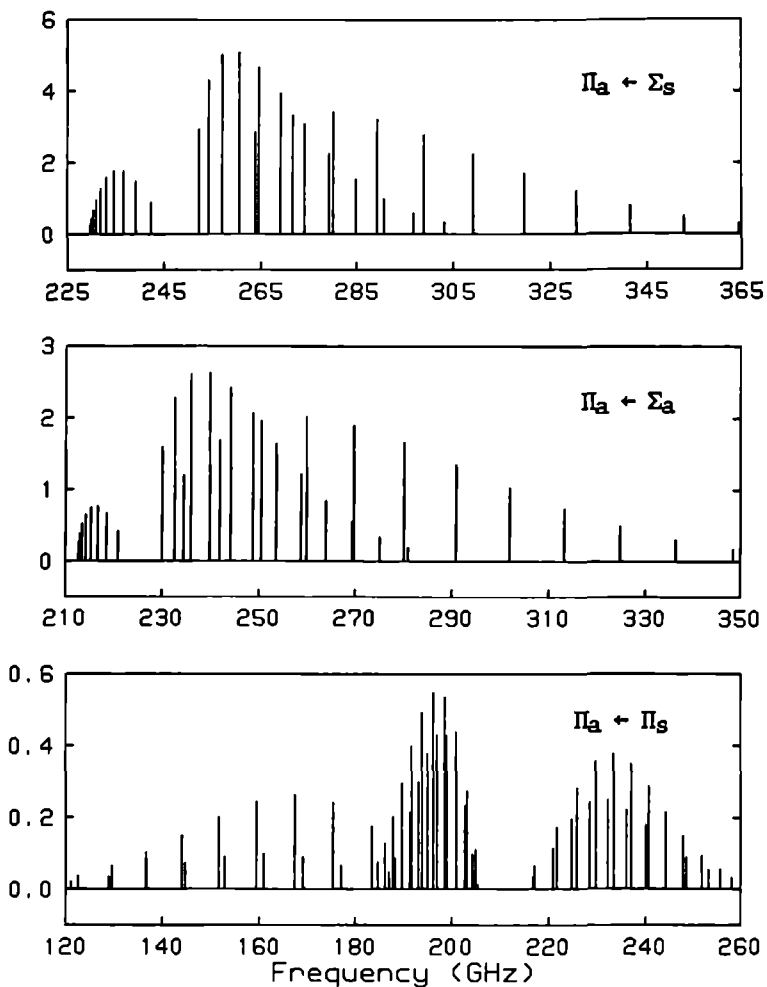


Figure 4. Calculated intensities for the observed submillimeter bands for $J=0,12$. The calculations use the potential constants from Case 1 in Table 5, a maximum j of 6 in the angular basis set and a rotational temperature of 5 K. The arbitrary intensity scale is the same for the three bands.

9.7 Discussion

The present results on the potential energy surface of Ar-NH₃ can be compared with recent dynamical calculations by van Bladel et al. [13, 14] on an ab initio surface [12]. They found that by scaling the V_{33} -type term in the ab initio potential they obtained energy levels and intensities in reasonable agreement with the present measurements on the para Ar-NH₃ states and with previous measurements on the ortho Ar-NH₃ states. It must be noted that in the calculations of [13, 14] the radial coordinate R is included. In our calculations an effective center of mass separation R_{cm} is used. The most striking difference between the calculations of van Bladel et al. and our results is that van Bladel et al. find that V_{10} and $V_{33} = -V_{3-3}$ are the most important terms in the interaction potential, whereas we have used V_{10} and V_{20} and have assumed that V_{33} is negligible. The observation that the data can be fitted to a small V_{20} term is not too surprising since the θ dependencies of the V_{20} and V_{33} terms are quite similar. The main difference between the two terms is that V_{33} is also dependent on ϕ , the angle associated with the rotation of the NH₃ unit around its symmetry axis.

To test the sensitivity of our data to V_{33} we have fitted the experimental energy levels to V_{10} and V_{33} and find $|\langle 0|V_{10}|1\rangle| = 11.9803 \text{ cm}^{-1}$, $\langle 0|V_{33}|0\rangle = -\langle 0|V_{3-3}|0\rangle = -46.8449 \text{ cm}^{-1}$ (or 46.8449 cm^{-1}), and $\langle 1|V_{33}|1\rangle = -\langle 1|V_{3-3}|1\rangle = -46.8855 \text{ cm}^{-1}$ (or 46.8855 cm^{-1}). We could probably have equally fitted our data to $|\langle 0|V_{10}|1\rangle|$, $\langle 0|V_{\nu_j}|0\rangle = (-1)^j \langle 0|V_{\nu_j}|0\rangle$, $\langle 1|V_{\nu_j}|1\rangle = (-1)^j \langle 1|V_{\nu_j}|1\rangle$, where $\nu+j$ is even. With increasing $\nu+j$, though, the potential constants must become increasingly large to obtain the observed energy level pattern. In fact, the V_{33} -type terms are already quite appreciable. For instance, at the T-shaped $\theta=90^\circ$ minimum-energy configuration, the fitted V_{33} terms imply a barrier of $\sqrt{5}|\langle 2|V_{33}|2\rangle| \approx 100 \text{ cm}^{-1}$ for threefold rotation of the NH₃ unit about its symmetry axis. This barrier term is extremely large and not easily reconcilable with the $< 20 \text{ cm}^{-1}$ barrier found for the 'T-shaped' Ar-CH₃Cl [29].

The spectroscopic consequence of the large V_{33} term in Ar-NH₃ is to reduce the Coriolis interaction between the Π and Σ states. For instance, for the V_{10} , V_{20} fit we find a predicted ℓ -type doubling splitting of 413 MHz for the $J=1$ Π_e state, compared with the observed value of 376 MHz. These can be compared with the V_{10} , V_{33} fit where we calculate an ℓ -type doubling splitting of only 213 MHz. Future measurements on other internal-rotor states of the complex, as well as a direct fit of a potential to the rotation internal-rotation states of the complex, should allow us to probe more fully the balance between the V_{20} and V_{33} terms in the interaction potential.

9.8 Conclusion

In the present work we have presented a detailed investigation of the spectroscopy and dynamics of the $j=1, |k|=1$ states of Ar-NH₃. The investigation of this species has permitted the examination of a popular problem [30], the coupling of a two-level tunneling system to a larger system consisting of many degrees of freedom. In the present system a rich variety of behaviour is found with only a few degrees of freedom. These include a strong orientation dependence to the tunneling leading to near quenching of the tunneling splitting in the Π states and giving rise to a nominally forbidden $\Sigma - \Sigma$ Q branch and rotationally-induced

tunneling in the Π states. The present system now analyzed should serve as a convenient model for the investigation of the coupling of a tunneling mode to other degrees of freedom.

Acknowledgement

The authors from Nijmegen wish to thank Prof. J. Reuss for many stimulating discussions and Prof. A. v.d. Avoird, J. v. Bladel and Dr. P. Wormer for their interest in the experiments and for making their results available prior to publication. We would like to thank T.A. Fisher for assistance with the MBER measurements.

References

- [1] S. Urban, D. Papousek, J. Kauppinen, K. Yamada, and G. Winnewisser, *J. Mol. Spectrosc.* 101, 1 (1983).
- [2] D.D. Nelson, Jr., G.T. Fraser, and W. Klemperer, *Science* 238, 1670 (1987).
- [3] G.T. Fraser, D.D. Nelson, Jr., A. Charo, and W. Klemperer, *J. Chem. Phys.* 82, 2535 (1985).
- [4] A. Bizzarri, B. Heijmen, S. Stolte, and J. Reuss, *Z. Phys. D* 10, 291 (1988).
- [5] D. D. Nelson, Jr., G.T. Fraser, K.I. Peterson, K. Zhao, W. Klemperer, F.J. Lovas, and R.D. Suenram, *J. Chem. Phys.* 85, 5512 (1986).
- [6] D.H. Gwo, M. Havenith, K.L. Busarow, R.C. Cohen, C.A. Schmuttenmaer, and R.J. Saykally, *Mol. Phys.* 71, 453 (1990).
- [7] C.A. Schmuttenmaer, R.C. Cohen, and R.J. Saykally, 45th Ohio State Symposium on Molecular Spectroscopy, Columbus, Ohio, June 1990.
- [8] E. Zwart and W.L. Meerts, in preparation.
- [9] B.J. Howard, Symposium on 'Atomic and Molecular Clusters: Spectroscopy, Structures, and Dynamics', ACS National Meeting; Miami, Florida, Sept. 1989.
- [10] G.T. Fraser, A.S. Pine and W.A. Kreiner, in preparation.
- [11] G. Chałasiński, S.M. Cybulski, M.M. Szcześniak and S. Scheiner, *J. Chem. Phys.* 91, 7809 (1989).
- [12] M. Bulski, P.E.S. Wormer and A. van der Avoird, *J. Chem. Phys.*, accepted.
- [13] J.W.I. van Bladel, A. van der Avoird and P.E.S. Wormer. *J. Chem. Phys.*, accepted.
- [14] J.W.I. van Bladel, A. van der Avoird and P.E.S. Wormer, to be published.
- [15] F.J. Lovas and R.D. Suenram, *J. Chem. Phys.* 87, 2010 (1987).

- [16] R.D. Suenram, F.J. Lovas, G.T. Fraser, J.Z. Gillies, C.W. Gillies, and M. Onda, *J. Mol. Spectrosc.* 137, 127 (1989).
- [17] G.T. Fraser, R.D. Suenram, and L.H. Coudert, *J. Chem. Phys.* 90, 6077 (1989).
- [18] G.T. Fraser, R.D. Suenram, L.H. Coudert, and R.S. Frye, *J. Mol. Spectrosc.* 137, 244 (1989).
- [19] E.Zwart, J.J. ter Meulen, and W.L. Meerts, *Chem. Phys. Lett.* 166, 500 (1990).
- [20] K.L. Busarow, G.A. Blake, K.B. Laughlin, R.C. Cohen, Y.T. Lee, and R.J. Saykally, *J. Chem. Phys.* 89, 1268 (1988).
- [21] J.M. Hutson, *J. Chem. Phys.* 92, 157 (1990).
- [22] R.C. Cohen, K.L. Busarow, K.B. Laughlin, G.A. Blake, M. Havenith, Y.T. Lee, and R.J. Saykally, *J. Chem. Phys.* 89, 4494 (1988).
- [23] R.C. Cohen, K.L. Busarow, Y.T. Lee, R.J. Saykally, *J. Chem. Phys.* 92, 169 (1990).
- [24] P.R. Bunker. *Molecular Symmetry and Spectroscopy*, (Academic Press, New York, 1979).
- [25] see for example, J.M. Hutson, in *Dynamics of Van Der Waals Complexes: Beyond Atom-Diatom Systems*, ed. N. Halberstadt and K.C. Janda, (Plenum, New York, 1990); J.M. Hutson, in *Advances in Molecular Vibrations and Collision Dynamics*.
- [26] D.M. Brink and G.R. Satchler, *Angular Momentum*, (Clarendon Press, Oxford, 1968).
- [27] G.T. Fraser, F.J. Lovas, R.D. Suenram, and K. Matsumura, *J. Mol. Spectrosc.* 143, 000 (1990).
- [28] M.D. Marshall and J.S. Muenter, *J. Mol. Spectrosc.* 85, 322 (1981).
- [29] G.T. Fraser, R.D. Suenram and F.J. Lovas, *J. Chem. Phys.* 86, 3107 (1987).
- [30] see, for instance : N. Makri and W.H. Miller, *J. Chem. Phys.* 86, 1451 (1987). P.E. Parris and R. Silbey, *J. Chem. Phys.* 86, 6381 (1987).

Samenvatting

Submillimeter spectroscopie aan moleculaire complexen en ionen.

Veel interessante eigenschappen van molekulen kunnen met behulp van spectroscopie worden onderzocht. Het spectrale gebied dat in dit proefschrift is onderzocht is het submillimeter of ver infrarood gebied. De spectra zijn opgemeten met verstembare smalbandige (< 0.1 MHz) straling en de directe absorptie methode. Het voordeel van deze aanpak is de hoge gevoeligheid en de nauwkeurigheid in de gemeten frequenties en een nadeel is dat het "zoeken" naar spectra veel tijd kost.

In het eerste deel worden experimenten aan geladen molekulen, ionen, beschreven. De ionen zijn geproduceerd in een gasontlading. De frequenties van enkele overgangen tussen verschillende rotatietoestanden van D_2H^+ , H_2D^+ , KrH^+ en KrD^+ zijn bepaald (hoofdstuk 2). De overgangen zijn om verschillende redenen interessant. De ionen zijn relatief eenvoudig en ab initio berekeningen kunnen zeer goede voorspellingen van energieniveaus geven. Door overgangen tussen verschillende energieniveaus te meten kunnen de berekeningen getest worden. Verder blijken ionen een belangrijke rol te spelen in chemische reacties in interstellaire wolken. Deze ionen zenden straling uit die op aarde of buiten de dampkring opgevangen kan worden. De frequentie van deze straling is dezelfde als de frequentie die we in een laboratorium kunnen meten. Hierdoor kunnen laboratoriumspectra als identificatie dienen.

Een ander experiment aan ionen is de bepaling van het permanente dipoolmoment van N_2H^+ . Het dipoolmoment bepaalt mede de intensiteit van de straling die op aarde opgevangen wordt van ionen in de interstellaire ruimte. Dit experiment is beschreven in hoofdstuk 3.

In de rest van dit proefschrift worden experimenten aan complexen beschreven. Een complex bestaat uit twee of meer molekulen die zwak gebonden zijn. Doordat deze molekulen zo zwak gebonden zijn, is het complex niet als "star" te beschouwen, zoals de aparte molekulen. De molekulen in een complex kunnen ten opzichte van elkaar bewegen. Deze bewegingen geven aanleiding tot een gecompliceerd spectrum. Uit zo'n spectrum kan interessante informatie verkregen worden over de krachten die tussen de twee molekulen werken.

In de hoofdstukken 4, 5 en 6 worden de resultaten beschreven die zijn verkregen voor $(H_2O)_2$, het complex bestaande uit twee watermolekulen. Het rotatiespectrum van $(H_2O)_2$ en $(D_2O)_2$ in het submillimeter frequentie gebied is onderzocht. Dit rotatiespectrum is gecompliceerd ten gevolge van tunnelbewegingen in het complex. Dit zijn dezelfde tunnelbewegingen als in het NH_3 molekuul, waarin het N atoom door het vlak van de H atomen kan "tunnelen" en opsplitsingen in het spectrum veroorzaakt. In $(H_2O)_2$ zijn vier tunnelbewegingen belangrijk en als gevolg hiervan splitst ieder rotatieniveau op in zes niveaus. Zowel voor $(H_2O)_2$ als voor $(D_2O)_2$ is nieuwe informatie over de tunnelbewegingen verkregen.

In hoofdstuk 7 worden metingen aan $(\text{NH}_3)_2$, het complex van twee ammoniak molekulen, beschreven. Het spectrum van dit complex is gecompliceerder dan dat van $(\text{H}_2\text{O})_2$ en is op dit moment nog niet helemaal begrepen. Het is mogelijk dat de NH_3 molekulen in $(\text{NH}_3)_2$ vrij makkelijk ten opzichte van elkaar kunnen bewegen. Als dit het geval is zal het spectrum niet met het $(\text{H}_2\text{O})_2$ model verklaard kunnen worden.

In hoofdstuk 8 worden metingen aan $\text{Ar-D}_2\text{O}$ en Ar-NH_3 beschreven. Omdat Ar een edelgasatoom is, is de binding tussen een Ar atoom en een D_2O of NH_3 molekuul zeer zwak. Als gevolg hiervan kan een D_2O of NH_3 molekuul bijna vrij roteren in zo'n complex. Deze bijna vrije rotatie heeft als resultaat dat het spectrum een groot deel reflecteert van de potentiaal die het D_2O of NH_3 molekuul "voelt" als het zich beweegt ten opzichte van het Ar atoom. $\text{Ar-D}_2\text{O}$ energieniveaus die correleren met $\text{Ar} + \text{D}_2\text{O}(j_{k_a k_c}=1_{01})$ en $\text{Ar} + \text{D}_2\text{O}(j_{k_a k_c}=1_{10})$ en Ar-NH_3 energieniveaus die correleren met $\text{Ar} + \text{NH}_3(j=0, k=0)$ en $\text{Ar} + \text{NH}_3(j=1, k=0)$ zijn onderzocht. De quantumgetallen $j_{k_a k_c}$, j en k zijn rotatiequantumgetallen van het D_2O of NH_3 molekuul.

In hoofdstuk 9 worden metingen aan Ar-NH_3 toestanden beschreven die correleren met $\text{Ar} + \text{NH}_3(j=1, |k|=1)$. In tegenstelling tot de Ar-NH_3 toestanden beschreven in hoofdstuk 8 is de NH_3 inversie te bestuderen in deze toestanden. Het is gebleken dat er toestanden bestaan waarin de NH_3 inversie vrijwel gelijk is aan die in vrij NH_3 en dat er ook toestanden bestaan waarin de inversie vrijwel 0 is.

Curriculum vitae

Ik ben op 1 april 1963 geboren in Helden Panningen. De lagere school heb ik doorlopen in Ulestraten (gem. Meerssen). Daarna is van 1975 tot 1981 op het Sint Maartenscollege te Maastricht het VWO bezocht. In 1981 ben ik begonnen met de studie Natuurkunde aan de Katholieke Universiteit Nijmegen. In 1983 werd het kandidaatsexamen behaald en in 1986 het doctoraalexamen. De laatste anderhalf jaar van de doctoraalfase bestond uit een stage op de experimentele afdeling Molekuul- en Laserfysica. In 1986 ben ik op deze afdeling begonnen met een promotie onder leiding van Prof. Dr. J. Reuss, Dr. W.L. Meerts and Dr. J.J. ter Meulen. De resultaten van het promotieonderzoek zijn in dit proefschrift beschreven.

